A PARAMETRIC STUDY ON CATALYST DEVELOPMENT FOR GLYCEROL DRY REFORMING

by

Selin Baç Bilgi

B.S., Chemical Engineering, Boğaziçi University, 2016

Submitted to the Institute for Graduate Studies in
Science and Engineering in partial fulfillment of
the requirements for the degree of
Master of Science

Graduate Program in Chemical Engineering

Boğaziçi University

2018

A PARAMETRIC STUDY ON CATALYST DEVELOPMENT FOR GLYCEROL DRY REFORMING

APPROVED BY:

Prof. Ahmet Kerim Avcı (Thesis Supervisor)	.....
Prof. Ahmet Erhan Aksoylu	.....
Prof. Ayşe Nilgün Akın	.....

DATE OF APPROVAL: 23.07.2018

ACKNOWLEDGEMENTS

I would like to express my sincere thanks and gratitude to my thesis supervisor, Prof. Ahmet Kerim Avcı for his endless support, motivation and patience. His encouragement and wise guidance helped me through my undergraduate and graduate studies. Under his guidance, I successfully overcame many difficulties and learned a lot. I will always remember his contributions to me while building an academic career and consider myself fortunate to have such a concerning mentor.

I would like to thank my thesis committee, Prof. Ahmet Erhan Aksoylu and Prof. Ayşe Nilgün Akın for devoting their time to read, listen and comment on my study. I would also like to express my appreciations to Prof. Aksoylu for his constant support, motivation and sharing his advanced knowledge.

I would also like to thank Assoc. Prof. Emrah Özensoy and Dr. Zafer Say for their collaboration and valuable contributions to my thesis and kind appreciations to Prof. A. Neren Ökte for devoting her time to develop my thesis.

Completing this work would have been more difficult without the members of KB-404. Special thanks to Pelin Su Bulutoğlu for always being available no matter how far see is. Thanks Sinan Koç for being always there for me whenever I need help. It has been a joyful graduate time with Semih Altınsoy, Mert Özden, Furkan Öztürk, Özge Selçuk, Uğurcan Tozar as well as former members Talha Ayar and Merve Can. Thank you so much 'KB-404 En Muhteşem Lab' especially for endless laughter and coffee.

I would like to mention my deepest thanks for Elif Esvap, Müge Kasım and Furkan Öztürk for bringing me joy not only in Boğaziçi but also at my home. Thank you Dilara Göreke, Aysun Urhan and Ece Mutlu for keeping company and sharing coffee although you are far from ChE territory. Thank you Begum Yağcı, Özlem Özbek, Merve Yüce,

İlke Kaykanat, Ezgi Öztürk, Feyza Öner and Ayşegül Karakuş for cheerful times in our gossip corner.

Thanks to CATREL team, recently the other side of KB-404, Cihat Öztepe, Serhat Erşahin, Merve Eropak, Ali Uzun, Aysun İpek Paksoy and Olcay Türkmen for their help and guidance.

I appreciate the kindness of the departmental support staff Yakup Bal, Melike Gürbüz, Başak Ünen, Murat Düzgünoğlu, Şükrü Ordu and Belgin Balkan.

The most special thanks to my mother, father, brothers, little nephew and grandmother, for supporting and comforting me. It would have been impossible for me to made so far without my loving family.

Last but definitely not least, thanks to my husband for always supporting, helping and loving me. No words can explain the gratitude I have for having him by my side. Your love enlightened me and will always keep me going.

Finally, financial support provided by TÜBİTAK BİDEB 2210-A and TÜBİTAK 117M163 and BAP-13880 are acknowledged.

ABSTRACT

A PARAMETRIC STUDY ON CATALYST DEVELOPMENT FOR GLYCEROL DRY REFORMING

Glycerol reforming to hydrogen and synthesis gas has drawn much attention recently due to increased glycerol production related with the global biodiesel demand. Among several reforming techniques, dry reforming is more promising since it involves consumption of a major greenhouse gas, CO_2. Regarding the lack of information especially about catalysis in the literature, this study aims to develop active and stable catalysts to be used in glycerol dry reforming systems. Furthermore, effects of operational parameters, namely reaction temperature, carbon dioxide-to-glycerol (CO_2/G) molar feed ratio and residence time, on reactant conversions and production distributions were investigated. Rh and Co based single oxide (ZrO_2 and CeO_2) catalysts were tested under glycerol dry reforming conditions for 72 hours to comprehend the stability of the catalysts. Catalyst characterization methods (TEM-EDX, *in-situ* FTIR and *ex-situ* Raman spectroscopic measurements) together with longevity studies suggested that Rh and Co based single oxide catalysts were not stable due to severe coke formation and sintering. Based on the knowledge obtained from the experiments and the literature, Rh, Ni and Co based catalysts were prepared with ZrO_2-TiO_2 (ZT) and Al_2O_3-ZrO_2-TiO_2 (AZT). 1 wt.% Rh/AZT and Rh/ZT together with 5 wt.% Ni/AZT and Co/AZT were tested under varying temperatures between 600 and 750 °C, CO_2/G ratios between 1 and 4 and residence time between 0.5 and 3.75 mg_{cat} min NmL^{-1}. At studied conditions, the highest activity was found over Rh/AZT catalyst followed by Ni/AZT, Rh/ZT and Co/AZT in decreasing order. Increasing temperature and decreasing CO_2/G ratio had positive effect on reactant conversion as well as desired product yields, namely H_2 and CO. Stability tests and BET, TEM-EDX and *in-situ* FTIR spectroscopic analyses were revealed the good stability of Rh/AZT and Ni/AZT.

ÖZET

GLİSEROLÜN KURU REFORMLANMASI İÇİN GELİŞTİRİLEN KATALİZÖRLERİN PARAMETRİK İNCELENMESİ

Gliserolün reformlaması, küresel biyodizel talebi nedeniyle artan gliserol üretimine bağlı olarak son zamanlarda dikkat çekmektedir. Diğer reformlama teknolojileri arasında kuru reformlama reaksiyonu, aynı zamanda bir sera gazını (CO_2) katalize ettiği icin daha ümit vericidir. Literatürdeki özellikle kataliz alanındaki eksiklik dikkate alınarak, bu çalışma gliserolün kuru reformlama sistemlerinde kullanılacak aktif ve stabil katalizörleri geliştirmeyi amaçlamaktadır. Ayrıca, sıcaklık, karbondioksit-gliserol (CO_2/G) molar besleme oranı ve etkileşim süresi gibi operasyonel parametrelerin reaktant dönüşümleri ve ürün dağılımları üzerindeki etkileri araştırılmıştır. Rh ve Co bazlı tek oksit katalizörler, stabiliteleri kavranmak üzere, 72 saat boyunca gliserol kuru reformlama koşulları altında test edilmiştir. Katalizör karakterizasyon yöntemleri, TEM-EDX, *yerinde* FTIR ve Raman spektroskopik ölçümler, uzun süreli deneylerle birlikte, Rh ve Co bazlı tek oksit katalizörlerinin ciddi kok oluşumuna ve sinterlemeye bağlı olarak stabil olmadığını ortaya koymuştur. Deneylerden ve literatürden elde edilen bilgilere dayanarak, Rh, Ni ve Co bazlı katalizörler ZrO_2-TiO_2 (ZT) ve Al_2O_3-ZrO_2-TiO_2 (AZT) ile hazırlanmıştır. Ağırlıkça %1 oranında Rh/AZT ve Rh/ZT ve %5 oranında Ni/AZT ve Co/AZT, 600 ile 750 °C arasında değişen sıcaklıklarda, 1 ile 4 arasındaki CO_2/G oranlarında ve 0,5–3,75 mg dk NmL^{-1} etkileşim süresi arasında test edilmiştir. Çalışılan koşullarda, katalizörlerin aktivesi sırasıyla Rh/AZT>Ni/AZT>Rh/ZT>Co/AZT olarak bulunmustur. Artan sıcaklık ve azalan CO_2/G oranı, H_2 ve CO verimleri ve reaktant dönüşümleri üzerinde olumlu etkiye sahiptir. Stabilite testleri ve BET, TEM-EDX ve *yerinde* FTIR spektroskopik analizleri Rh/AZT ve Ni/AZT katalistlerinin iyi stabilitesini ortaya çıkarmıştır.

TABLE OF CONTENTS

ACKNOWLEDGEMENTS . . . iii
ABSTRACT . . . v
ÖZET . . . vi
LIST OF FIGURES . . . x
LIST OF TABLES . . . xvi
LIST OF SYMBOLS . . . xviii
LIST OF ACRONYMS/ABBREVIATIONS . . . xix
1. INTRODUCTION . . . 1
2. LITERATURE SURVEY . . . 5
2.1. Ethanol Dry Reforming . . . 6
2.1.1. Thermodynamics . . . 6
2.1.2. Catalysis . . . 8
2.2. Glycerol Dry Reforming . . . 13
2.2.1. Thermodynamics . . . 17
2.2.2. Catalysis . . . 20
2.3. Mixed Oxide Supports . . . 25
3. EXPERIMENTAL WORK . . . 28
3.1. Materials . . . 28
3.1.1. Chemicals . . . 28
3.1.2. Gases and Liquids . . . 28
3.2. Experimental System . . . 28
3.2.1. Catalyst Preparation System . . . 31
3.2.2. Catalyst Characterization System . . . 31
3.2.2.1. BET Surface Analysis . . . 31
3.2.2.2. TEM/EDX Analyses . . . 32
3.2.2.3. *Ex-situ* Raman Spectroscopic Analysis . . . 33
3.2.2.4. *In-situ* FTIR Spectroscopic Analysis . . . 33
3.2.3. Catalytic Reaction System . . . 33

3.2.3.1. Feed Section 35
3.2.3.2. Reaction Section 37
3.2.3.3. Product Analysis Section 38
3.2.4. Product Analysis System 38
3.3. Catalyst Preparation and Pretreatment 40
3.3.1. Preparation of Support 40
3.3.1.1. Preparation of ZrO_2 40
3.3.1.2. Preparation of CeO_2 40
3.3.1.3. Preparation of ZrO_2–TiO_2 40
3.3.1.4. Preparation of Al_2O_3–ZrO_2–TiO_2 40
3.3.2. Preparation of Active Catalysts 41
3.3.2.1. Preparation of Rh/ZrO_2 41
3.3.2.2. Preparation of Rh/CeO_2 41
3.3.2.3. Preparation of Co/ZrO_2 41
3.3.2.4. Preparation of Co/CeO_2 42
3.3.2.5. Preparation of Rh/AZT 42
3.3.2.6. Preparation of Ni/AZT 42
3.3.2.7. Preparation of Co/AZT 42
3.3.2.8. Preparation of Rh/ZT 42
3.3.3. Pretreatment of Catalysts 42
3.4. Reactions Tests 43
3.4.1. Activity Tests 44
3.4.2. Blank Tests 44
3.4.3. Stability Tests 45
3.4.4. Experimental Procedure 45
3.4.5. Measurement of Catalytic Activities 46
4. RESULTS AND DISCUSSION 48
4.1. Catalysts with Single Support 48
4.1.1. Stability Tests 48
4.1.2. Catalyst Characterizations 53
4.1.2.1. TEM and EDX Measurements 53

4.1.2.2. *In-situ* FTIR Spectroscopic Measurements 57
4.1.2.3. *Ex-situ* Raman spectroscopic experiments 61
4.2. Catalysts with Binary and Ternary Supports 64
4.2.1. Effect of Reaction Temperature 64
4.2.1.1. Thermodynamic Analysis 64
4.2.1.2. Activity Tests 66
4.2.2. Effect of CO_2/G Ratio 73
4.2.2.1. Thermodynamic Analysis 74
4.2.2.2. Activity Tests 75
4.2.3. Effect of Active Metal 80
4.2.4. Effect of Support 83
4.2.5. Effect of Residence Time 86
4.2.6. Stability Tests 89
4.2.7. Catalyst Characterizations 95
4.2.7.1. BET Analysis 95
4.2.7.2. TEM and EDX Measurements 96
4.2.7.3. *In-situ* FTIR Spectroscopic Measurements 103
5. CONCLUSION 105
5.1. Conclusions from Rh and Co Catalysts Supported on Single Oxides . . 105
5.2. Conclusions from Rh, Ni and Co Based Binary and Ternary Oxides . . 106
5.3. Recommendations 107
REFERENCES 109
APPENDIX A: CALIBRATION OF MASS FLOW CONTROLLERS 126
APPENDIX B: CALIBRATION OF GAS CHROMATOGRAPHS 128
B.1. Calibration Curves for Schimadzu GC-2014 128
B.2. Calibration Curves for Agilent GC-6850 130

LIST OF FIGURES

Figure 1.1. Biodiesel production in key countries in 2016 (adapted from UFOP Report on Global Market Supply 2017/2018 [2]). 1

Figure 1.2. Worldwide feedstock use in biodiesel production in 2016 (reproduced from UFOP Report on Global Market Supply 2017/2018 [2]). 2

Figure 1.3. Biodiesel production in the US between 2016 and 2018 [4]. 3

Figure 2.1. Glycerol decomposition scheme obtained from Valliyappan *et al.* [88]. 15

Figure 3.1. Illustration of catalyst impregnation system *via* incipient-to-wetness impregnation [105, 127]. 1. Ultrasonic Mixer, 2. Buchner Flask, 3. Vacuum Pump, 4. Peristaltic Pump, 5. Precursor Solution, 6. Silicon Tubing. 32

Figure 3.2. Schematic representation of the experimental system. 34

Figure 3.3. Glycerol dry reforming experimental system. 35

Figure 3.4. Detailed illustration of reactor inlet. 36

Figure 3.5. Illustration of packed bed reactor. 37

Figure 3.6. Packed middle part of the quartz reactor. 43

Figure 4.1. 72 h ToS CO_2 conversion of single support catalysts (T=750 °C and CO_2/G=4). 49

Figure 4.2. 72 h ToS glycerol conversion of single support catalysts (T=750 °C and CO_2/G=4). 49

Figure 4.3. TEM (a) and HR-TEM (b) of fresh Rh/ZrO_2 catalyst. 54

Figure 4.4. STEM-EDX analysis of fresh Rh/ZrO_2 catalyst. 54

Figure 4.5. TEM (a) and HR-TEM (b) of 5 h spent Rh/ZrO_2 catalyst. 54

Figure 4.6. STEM-EDX analysis of 5 h spent Rh/ZrO_2 catalyst. 55

Figure 4.7. TEM (a) and HR-TEM (b) of fresh Rh/CeO_2 catalyst. 55

Figure 4.8. STEM-EDX analysis of fresh Rh/CeO_2 catalyst. 56

Figure 4.9. TEM (a) and HR-TEM (b) of 5 h spent Rh/CeO_2 catalyst. 56

Figure 4.10. STEM-EDX analysis of 5 h spent Rh/CeO_2 catalyst. 56

Figure 4.11. *In-situ* FTIR spectra corresponding to 10 Torr CO(g) adsorption at 25 °C for 10 min on fresh, 5 h and 72 h spent RhZr and RhCe. 57

Figure 4.12. *In-situ* FTIR spectra of 5 h spent RhZr and RhCe catalysts obtained after treatment with 10 Torr H_2(g) at 300 °C for 10 min followed by cooling to 25 °C and evacuation. 60

Figure 4.13. *Ex-situ* Raman spectra for fresh (black), 5 h spent (red) and 5 h spent and successively photobleached (blue) RhZr. 62

Figure 4.14. *Ex-situ* Raman spectra for fresh (black) and 5 h spent (red) RhCe. 63

Figure 4.15. Thermodynamic limits of solid carbon formation with respect to reaction temperature (CO_2/G=4). 66

Figure 4.16. Thermodynamic and experimental CO_2 conversions with respect to temperature at CO_2/G=4. 67

Figure 4.17. Thermodynamic and experimental glycerol conversions with respect to temperature at CO_2/G=4. 68

Figure 4.18. Thermodynamic and experimental H_2 yields with respect to temperature (CO_2/G=4). 71

Figure 4.19. Thermodynamic and experimental CO yields with respect to temperature (CO_2/G=4). 71

Figure 4.20. Thermodynamic and experimental CO_2 conversions with respect to CO_2/G ratios (T=750 °C). 77

Figure 4.21. Thermodynamic and experimental glycerol conversions with respect to CO_2/G ratios (T=750 °C). 77

Figure 4.22. Thermodynamic and experimental H_2 yields with respect to CO_2/G ratios at 750 °C. 80

Figure 4.23. Thermodynamic and experimental CO yields with respect to CO_2/G ratios at 750 °C. 81

Figure 4.24. Carbon dioxide and glycerol conversions over different active metals supported on AZT (T=750 °C and CO_2/G=4). 82

Figure 4.25. Carbon dioxide and glycerol conversions over Rh supported on single, binary and mixed supports (T=750 °C and CO_2/G=4). 85

Figure 4.26. Carbon dioxide and glycerol conversions obtained with different amounts of Ni/AZT (T=750 °C and CO_2/G=4). 87

Figure 4.27. Effect of catalyst weight on CO_2 conversion over mixed support catalysts and blank AZT (T=750 °C and CO_2/G=4). 88

Figure 4.28. Effect of catalyst weight on glycerol conversion over mixed support catalysts and blank AZT (T=750 °C and CO_2/G=4). 89

Figure 4.29. 72 h ToS CO_2 conversion of single mixed catalysts (T=750 °C and CO_2/G=4). 91

Figure 4.30. 72 h ToS glycerol conversion of mixed support catalysts (T=750 °C and CO_2/G=4). 92

Figure 4.31. HR-TEM images of fresh Rh/AZT with 50 nm (a) and 2 nm (b) resolution. 97

Figure 4.32. STEM-EDX analysis of fresh Rh/AZT. 97

Figure 4.33. HR-TEM images of 5 h spent Rh/AZT with 5 nm (a) and 2 nm (b) resolution. 97

Figure 4.34. STEM-EDX analysis of 5 h spent Rh/AZT. 98

Figure 4.35. HR-TEM images of fresh Ni/AZT with 20 nm (a) and 2 nm (b) resolution. 98

Figure 4.36. STEM-EDX analysis of fresh Ni/AZT. 99

Figure 4.37. HR-TEM images of 5 h spent Ni/AZT with 20 nm (a) and 2 nm (b) resolution. 99

Figure 4.38. STEM-EDX analysis of 5 h spent Ni/AZT. 99

Figure 4.39. STEM-EDX analysis of 72 h spent Ni/AZT used in stability analysis.100

Figure 4.40. TEM images of fresh Co/AZT with 100 nm (a) and 50 nm (b) resolution. 100

Figure 4.41. STEM-EDX analysis of fresh Co/AZT. 101

Figure 4.42. TEM images of 5 h spent Co/AZT with 100 nm (a) and 50 nm (b) resolution. 101

Figure 4.43. TEM images of 72 h spent Co/AZT with 20 nm (a) and 10 nm (b) resolution. 101

Figure 4.44. TEM result indicating lattice spacing of graphitic carbon over 72 h spent Co/AZT. 102

Figure 4.45. STEM-EDX analysis of 72 h spent Co/AZT used in stability analysis.102

Figure 4.46. *In-situ* FTIR spectra of fresh and 72 h spent Rh/AZT. 104

Figure A.1. Calibration curve of MFC for N_2 126

Figure A.2. Calibration curve of MFC for H_2 126

Figure A.3. Calibration curve of MFC for CO_2 127

Figure B.1. GC1 calibration curve for N_2 128

Figure B.2. GC1 calibration curve for H_2 128

Figure B.3. GC1 calibration curve for CO 129

Figure B.4. GC1 calibration curve for CH_4 129

Figure B.5. GC2 calibration curve for N_2 130

Figure B.6. GC2 calibration curve for CO_2 130

Figure B.7. GC2 calibration curve for C_2H_4 131

Figure B.8. GC2 calibration curve for C_2H_6 131

LIST OF TABLES

Table 2.1. Estimated model parameters for ethanol dry reforming [85]. 13

Table 3.1. Chemicals used for catalyst preparation 29

Table 3.2. Gases used in the experimental system 30

Table 3.3. Liquids used in the experimental system 30

Table 3.4. Operating parameters of gas chromatographs. 39

Table 3.5. Reaction conditions for catalytic tests (Default values are shown in boldface). 44

Table 4.1. Product yields over single support catalysts. 51

Table 4.2. Product selectivities over single support catalysts. 52

Table 4.3. Thermodynamic product yields at different temperatures. 65

Table 4.4. Thermodynamic product selectivity values at different temperatures. 65

Table 4.5. Product yields over mixed support catalysts at different temperatures (CO_2/G=4). 70

Table 4.6. Product selectivity values over mixed support catalysts at different temperatures (CO_2/G=4). 72

Table 4.7. Thermodynamic product yields at carbon dioxide-to-glycerol ratios (T=750 °C). 75

Table 4.8. Thermodynamic product selectivities at carbon dioxide-to-glycerol ratios (T=750 °C). 75

Table 4.9. Product yields over mixed support catalysts at different CO_2/G ratios (T=750 °C). 78

Table 4.10. Product selectivity values over mixed support catalysts at different CO_2/G ratios (T=750 °C). 79

Table 4.11. Product yields over AZT catalysts (T=750 °C and CO_2/G=4). . . 83

Table 4.12. Product yields over Rh impregnated single and binary support catalysts (T=750 °C and CO_2/G=4). 86

Table 4.13. Product yields over mixed support catalysts. 93

Table 4.14. Product selectivity values over mixed support catalysts. 94

Table 4.15. BET specific surface area of binary and ternary oxide supports. . . 95

Table 4.16. BET analysis results for mixed oxide and its catalysts. 96

LIST OF SYMBOLS

A	Exponential factor
$d_{particle}$	Diameter of particle (mm)
d_{tube}	Diameter of tube (mm)
E_a	Activation energy (kJ mol^{-1})
F	Total volumetric flow rate (NmL min^{-1})
$F_{i,in}$	Molar flow rate of species in feed (mol min^{-1})
$F_{i,out}$	Molar flow rate of species i in the product stream (mol min^{-1})
L_{bed}	Lenth of bed (mm)
r_g	Glycerol consumption rate (mol g^{-1} s^{-1})
S_i	Selectivity of species i
T	Temperature (°C)
V	Volume (μL)
W	Catalyst weight (mg)
x_i	Conversion with respect to reactant i
Y_i	Yield of species i
α	Reaction order with respect to ethanol
β	Reaction order with respect to CO_2
γ	Reaction order with respect to glycerol
ΔH^o	Standard enthalpy of reaction (kJ mol^{-1})
ν_i	Volumetric flow rate of species i (NmL min^{-1})
ϕ	Reaction order with respect to CO_2

LIST OF ACRONYMS/ABBREVIATIONS

AZT	Alumina-Zirconia-Titania
BET	Brauner-Emmett-Teller
BJH	Barrett-Joyner-Halenda
CC	Cement clinker
CEG	Carbon dioxide to ethanol-glycerol ratio
CNF	Carbon nanofilament
DMR	Dry methane reforming
DRE	Dry reforming of ethanol
EDS	Energy dispersive spectroscopy
EDX	Energy-dispersive X-ray spectroscopy
EtOH	Ethanol
FESEM	Field emission scanning electron microscopy
FTIR	Fourier transform infrared spectroscopy
G	Glycerol
GC	Gas chromatograph
GDR	Glycerol dry reforming
GSR	Glycerol steam reforming
HAADF	High angle annular dark field
HPLC	High performance liquid chromatograph
HR-TEM	High-resolution transmission electron microscopy
ID	Inner diameter
MCT	Mercury Cadmium Telluride
MFC	Mass flow controller
MW	Molecular weight
MWNT	Multi-wall nanotube
PID	Proportional integral derivative
RWGS	Reverse water gas shift
SEM	Scanning electron microscopy

SMR	Steam methane reforming
SMSI	Strong metal support interaction
SR	Steam reforming
SRE	Steam reforming of ethanol
STEM	Scanning transmission electron microscopy
TEM	Transmission electron microscopy
TGA	Thermogravimetric analysis
ToS	Time on stream
TPD	Temperature programmed desorption
TPR	Temperature programmed reduction
TPO	Temperature programmed oxidation
WGS	Water-gas shift
XRD	X-ray diffraction
XRF	X-ray fluorescence
ZT	Zirconia-Titania

1. INTRODUCTION

High energy demand of the current world lead to search for alternative energy sources due to drastic shortage of the commercialized fossil fuels. Renewable energy commercialization become an important issue not only to supply the energy demand but also to reduce the environmentally hazardous emissions such as CO_2 to the atmosphere. Nowadays, biomass that is produced by living organisms draws great attention due to its clean nature, sustainability and applicability to production of chemicals and fuels. Only 19% of the total energy consumption worldwide comes from renewable energy, while only 4% of energy consumption for transport is supplied by bio-fuels [1]. Some estimations indicate that bio-fuels could replace almost 10 times the global demand for transport fuels in 2016, which is equivalent to 1%, by 2025 [1].

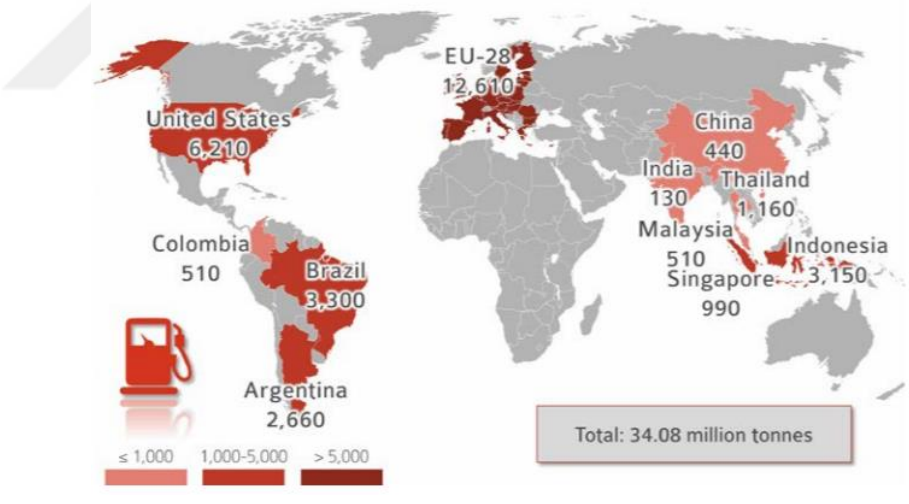

Figure 1.1. Biodiesel production in key countries in 2016 (adapted from UFOP Report on Global Market Supply 2017/2018 [2]).

Biodiesel, being one of the major bio-fuel, become a consistently growing market worldwide, from 25 million gallons in 2000s [3] to 34.08 million tonnes [2] in 2016. biodiesel production in the key manufacturing countries and amounts of feedstock used to produce the biodiesel can bee seen in Figures 1.1 and 1.2, respectively. Biodiesel production in the United States, available in Figure 1.3, shows a growing trend [4]. The

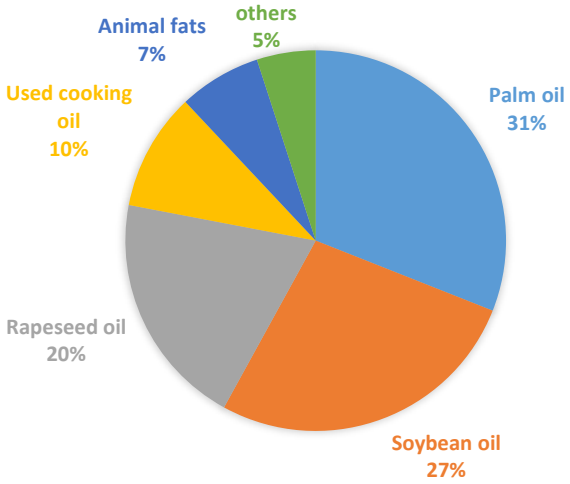

Figure 1.2. Worldwide feedstock use in biodiesel production in 2016 (reproduced from UFOP Report on Global Market Supply 2017/2018 [2]).

increase in production of biodiesel directly causes increase in glycerol, a by-product of biodiesel synthesis *via* transesterification (Equation 1.1) [5]:

$$C_3H_5(OOC)_3(R_n)_3 + R'OH \rightleftharpoons 3R_nCOOR' + C_3H_5(OH)_3 \tag{1.1}$$

Glycerol is found in the product stream at about 10 wt.% of the total biodiesel [6]. Thus, in order to decrease the cost of making biodiesel, glycerol, which is presently produced more than demanded, should be valorized into useful products [7]. The bio-derived glycerol can be converted to hydrogen for fuel cell applications or synthesis gas (syngas) for Fischer-Tropsch synthesis (FTS) [8].

Glycerol (propane-1,2,3-triol or glycerin) is a colorless, viscous liquid whose boiling point is 290 °C under normal conditions [9]. More than 1500 uses of this compound have been already reported and yet there are lots of developments [10]. One of the most important use of crude bio-derived glycerol from transesterification of vegetable oils/fats is its use in hydrogen and syngas production [11].

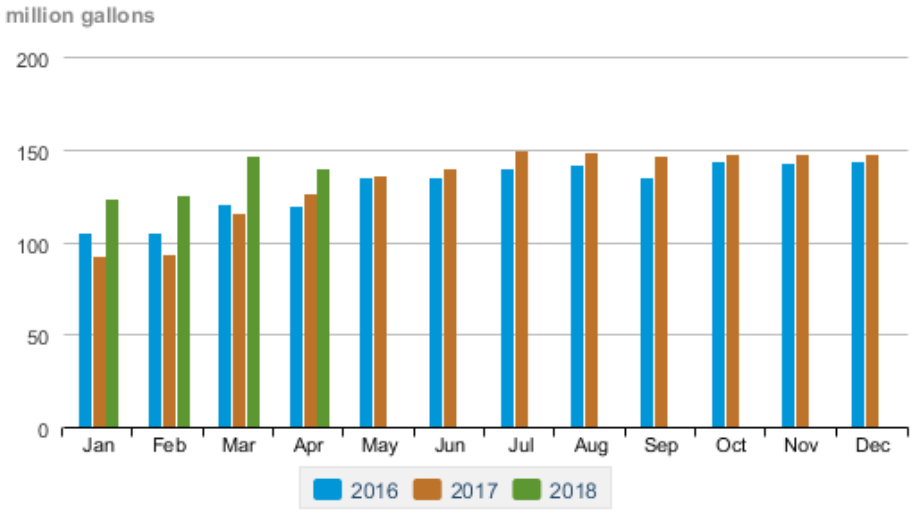

Figure 1.3. Biodiesel production in the US between 2016 and 2018 [4].

Hydrogen economy is growing readily as a result of zero emission from its combustion. However, due to the lack of its distribution and infrastructure, it should be produced on-board for fuel cell applications [12]. Additionally, CO which is poisonous to the fuel cell catalyst should be removed from the product stream and almost pure hydrogen should be fed to the cell for electricity generation. On the other hand, syngas (H_2+CO and sometimes little amount of CO_2) can be used to produce large variety of hydrocarbons from light hydrocarbons to heavy wax, depending on syngas ratio (H_2/CO ratio). Thus, more fuel can be obtained with the byproduct of the biodiesel and due to widespread distribution of those fuels there are no limitations for transmitting them to the consumer [8].

H_2 or syngas production from glycerol can be achieved by several processes, the most common ones being steam reforming (SR), dry reforming, partial oxidation and autothermal reforming, which is the combination of non-catalytic partial oxidation with catalytic steam reforming. Dry reforming or CO_2 reforming of glycerol (GDR) includes an additional benefit to the reforming processes, consumption of greenhouse gas carbon dioxide. The process is more suitable to produce syngas rather than hydrogen since CO production is relatively higher than that involved in other methods such as steam

reforming [13]. The theoretical syngas ratio for GDR is 0.75 which is suitable for FTS for long chain hydrocarbons, carbonyls and carboxylic acid production [14].

Dry reforming of glycerol is not studied extensively in the literature. Existing studies generally focused on Ni based catalysts [15–28] with an only exception that utilized nobel metal catalysts [29]. Support materials used in the Ni-based catalysts are very scarce, namely cement clinker (CC), Al_2O_3, CeO_2, ZrO_2 and SiO_2. Most of the catalysts reported in the literature suffer from deactivation due to sintering and coke formation. Thus, the main aim of this study is to design catalysts that are resistant to coke formation and sintering under GDR conditions. In the first part of the study, stability of Rh and Co catalysts supported on single oxides (ZrO_2 and CeO_2) are investigated and catalyst characterization methods are performed to understand major deactivation mechanisms. Then, mixed oxides, namely ZrO_2-TiO_2 (ZT) and Al_2O_3-ZrO_2-TiO_2 (AZT), are used to support Rh, Ni and Co metals whose catalytic activities, stabilities as well as characterizations are then investigated. Effects of temperature, CO_2/G feed ratio and residence time are explored to find the most suitable operation conditions for GDR.

The present work consists of 5 main chapters, including Introduction. In Chapter 2, an extensive literature survey on ethanol and glycerol dry reforming has been provided with a narrow-scoped survey on mixed oxide supports. In Chapter 3, catalyst preparation of catalysts, experimental system with operational parameters and catalyst characterization systems have been presented. In Chapter 4, results of catalytic activity and stability tests together with catalysts characterizations have been reported including interpretations. Finally, in Chapter 5, conclusions from the study have been prepared and recommendations for further improvements have been made.

2. LITERATURE SURVEY

Synthesis gas (syngas) is a mixture of H_2, CO and CO_2 that is commonly used in fuel cell applications and well-established Fischer-Tropsch syntheses for the production of valuable compounds [30]. Different H_2/CO ratios (or syngas ratio) obtained with different routes are used to produce different type of hydrocarbons [31]. These methods include steam reforming, dry reforming, autothermal reforming and partial oxidation of various fuels, mostly methane (major component in natural gas), followed by ethanol and glycerol [13, 32–34]. Among all those processes, steam reforming is the most studied, especially for methane [35].

Steam reforming of hydrocarbons is well-established in the industry and there are variety of research done and ongoing [36]. There are many studies on steam methane reforming (SMR) with different catalysts at different operating conditions in the literature since the optimum conditions are sought for high methane conversions with desired H_2/CO ratios [37–42]. In addition to SMR, steam reforming of ethanol and glycerol are also studied [43–53]. The most common active metals used in SMR catalysts are Ni (62%) followed by Pt (12%), Rh (9%), Pd (8%), Ru (6%) and Ir (3%) [42].

In recent years, CO_2 reforming of methane (DMR) drew attention by researchers [54–63]. Compared to steam, autothermal reforming and partial oxidation; DMR offers up to 20% reduction in operating costs, making it attractive among the other conversion routes [64]. Highly endothermic DMR reaction requires temperatures between 800 and 1000 °C in order to obtain high conversions and syngas yields. The most common catalysts are Ni based, which, however, are prone to deactivation by coke deposition [65]. Nobel metal catalysts are more resistant to coke formation but they are expensive [54]. Apart from methane; biogas, ethane, methanol, ethanol and glycerol are other hydrocarbons used in reforming techniques. Due to deficiency in glycerol literature, ethanol dry reforming studies are also provided in this section considering the resemblance of the oxygenated hydrocarbons.

2.1. Ethanol Dry Reforming

Ethanol (EtOH), especially bio-ethanol, is a convenient renewable energy carrier mainly produced from biomass fermentation from sugar based feedstock like corn, potatoe, sugarcane, sweet sorghum, sugar beets and molasses [66]. Its convenience as an energy carrier arises from its non-toxic and biodegradable nature. On top of it, it does not contain any catalyst poisons such as sulphur [43]. High heating value and high H atom content of ethanol also makes its utilization in dry reforming preferable. Dry reforming of ethanol (DRE) occurs according to following reaction:

$$C_2H_5OH + CO_2 \rightleftharpoons 3CO + 3H_2 \qquad \Delta H^0 = 297 \text{ kJ mol}^{-1} \tag{2.1}$$

In this study, research focused on ethanol dry reforming is categorized into two sections, namely thermodynamic analysis (Section 2.1.1) and catalysis for experimental studies (Section 2.1.2).

2.1.1. Thermodynamics

There are several studies on thermodynamic analysis of dry reforming on ethanol in the literature starting from 2001 up to 2017. The first analysis was made by Tsiakaras and Demin [67] in 2001 for solid oxide fuel cell (SOFC) which was considered to be fed with the equilibrium ethanol products from steam reforming, dry reforming, or partial oxidation with air. Results suggested that carbon formation was not thermodynamically possible in the temperature range between 527 and 927 °C. SOFC system efficiency of 83.6 - 89.9% was found to be highest for temperatures between 677 and 827 °C when dry reforming was performed. Partial oxidation with air provided the lowest efficient while steam reforming gave the highest system efficiency at temperatures lower than 677 °C or higher than 827 °C.

Later, Wang and Wang [68] studied on Gibbs free energy minimization method between a temperature range of 227 and 1227 °C, pressures between 1-20 bar and

CO_2/EtOH ratio between 0 and 5. The optimum conditions were suggested as temperatures between 927 and 1027 °C and CO_2/EtOH ratios of 1.2 - 1.3 at atmospheric pressure. These conditions allowed complete conversion of ethanol with high H_2 and CO yields of 95% and 97%, respectively. Increase in inert amount had positive effect to H_2 yield but its cost should be also considered according to this study. Fortunately, no carbon formation was observed. Thermodynamically, product stream contained H_2, CO, CO_2, H_2O but did not include C_2H_4, C_2H_6, CH_3CHO, $C_2H_5OC_2H_5$ and CH_3COCH_3.

In 2010, Kale and Kulkarni [69] investigated the thermoneutral point of dry autothermal reforming of ethanol in which they also referred to carbon nanofilament (CNF) formation which is valuable when compared to other carbon formations that deactivate the catalyst. The maximum syngas yield with ratio of 2.01 was obtained at 604 °C and 1 bar with CO_2/EtOH and O_2/EtOH ratios 1 and 0.5, respectively. In those conditions, 2.58 moles of syngas was produced along with 0.82 moles of C(s), 0.20 moles of CH_4 and 0.89 moles of H_2O. Syngas ratio increased with decreasing pressure and ranged between 1.30 and 7.34. Thus, increasing pressure regulated syngas ratio to desirable values for FTS and increases CO_2 conversions but suppressed H_2 production.

Another study that utilized Gibbs free energy minimization method was conducted by Kale and Gaikwad [70] where the effect of combined variables like temperature, pressure and CO_2/C ratio were investigated. They observed a temperature range of 300 to 900 °C, pressure range of 1 - 10 bar and CO_2/C ratio of 1 to 5. Conditions for obtaining syngas ratio of 1-3, maximized carbon (CNF) or H_2 were tabulated with their corresponding operating conditions and values.

Very similar results to findings in previous study [69] of Kale and Kulkarni [69] wss reported in a research article. The difference between previous and current studies is the exclusion of O_2 which characterize the autothermicity. They reported complete conversion of ethanol *via* dry reforming at different thermoneutral (net ΔH=0) temperatures between 496 - 545 °C with CO_2/EtOH ratio between 1 and 5. The best operating temperature was set as 545 °C.

Ortiz *et al.* [71] investigated dry reforming of ethanol using calcium carbonate ($CaCO_3$) as a source of CO_2. Their results suggested that at temperatures above 750 °C and $CaCO_3$/EtOH ratios above 2.2 carbon formation was eliminated. The highest H_2 yield was obtained at 790 °C which was 2.95 kmol H_2 per 1 kmol EtOH fed. They also compared their computational results obtained *via* ASPEN-Plus software with experimental data obtained from literature [72]. The highest fit was obtained at 900 °C with $CaCO_3$/EtOH of 2.

Finally, a recent study by Kumar *et al.* [73] was focused on different additives used to increase hydrogen yield and decrease the carbon formation. Those additives; glycine, hydrazine, urea and ammonia, were observed at atmospheric pressure and temperatures between 27 and 927 °C. Hydrazine was found to be most suitable additive in increasing hydrogen production and significantly suppressing the carbon formation so that catalyst lifetime was extended. Complete removal of solid carbon was observed by adding 6 mol or above value of hydrazine per mole of ethanol where H_2/CO ratio close to 2 was reported.

2.1.2. Catalysis

Apart from thermodynamic analysis there are also significant amount of experimental studies available in the literature. The first work was performed by De Oliveira-Vigier *et al.* [74] They utilized 316 stainless steel (Fe<61%, C<0.03%, Cr:16 - 18.5%, Ni:10 - 14%, Mo: 2 - 3%, Mn<2, Si<1, S<0.03 and P<0.045) as a catalyst and achieved a H_2 yield 98% close to its thermodynamic value. They also mentioned CNF formation which is valuable. They reported that their catalyst was recyclable with stable activity and selectivity. In their study, they investigated the effect of temperature, EtOH/CO_2 ratio as well as pretreatment (800 °C under N_2 flow) on EtOH conversion and selectivities towards H_2 and carbon. They performed SEM imaging to observe catalyst surface and carbon formations onto it. Pretreating the catalyst improved ethanol conversion from 13 to 43%, H_2 and carbon yielded from 4 to 22% and from 0.05 to 19%, respectively. Highest H_2 yield of 45% was obtained at EtOH/CO_2 ratio of 3.2 (range: 0.8 -

4.1). Along the temperature range investigated (400 - 600 °C), 600 °C yielded highest H_2 of 98% with whisker type of C(s) formation which was then characterized. EDX performed on whisker carbon showed iron traces (C: 98.3%, Fe: 0.85%, Ni: 0.43% and Cr: 0.17%).

Another experiment on carbon steel catalyst was performed by Jankhah *et al.* [75] with varying temperature and CO_2/EtOH ratios. They investigated the rates of thermal and catalytic reforming and cracking reactions and performed SEM and EDX for catalyst characterization. Highest H_2 and carbon (especially CNF) was obtained at 550 °C with CO_2/EtOH ratio of 1. They also determined thermodynamic limits which resulted lower H_2 and CO yields but higher CNF formation than experimental results. Blank tests without carbon steel yielded no carbon and showed ethanol thermal reforming and cracking reactions and also, ethanol catalytic cracking reaction was occurred. On the other hand, when experiments conducted with both carbon steel reactor and CO_2 and ethanol both in feed, all four reactions were observed to occur simultaneously.

In a conference proceeding by Abatzoglou *et al.* [76] CO_2 sequestration was observed under dry reforming conditions with activated carbon steel 1008. They reported that energetic efficiency of dry reforming process is 50% lower but valuable by-product MWNT (multi wall nanotubes) formation at low temperatures and atmospheric pressure offset this advantage. Afterwards, a journal article about this work was published by Blanchard *et al.* [77] where carbon steel was proposed to activate by micro- and nano-magnetite formation on it. They reported that minimum rate of reforming to cracking ratio of 0.25 was necessary to obtain high value CNFs.The overall reaction sought was as follows *via* Equation 2.2:

$$3C_2H_5OH + CO_2 \rightleftharpoons 5CO + 9H_2 + 2C(s) \tag{2.2}$$

By 2009, supported non-precious metals were started to be used in DRE where focus was on the dry reforming rather than CNF formation. Bellido *et al.* [78] performed

experiments on Ni/Y_2O_3–ZrO_2 (NiYZ) catalyst prepared by two different methods (polymerization and wet impregnation) and with two different metal loadings (5 and 10 wt.%). Polymerization method was found to be better due to less agglomeration and better Ni dispersion on support. The highest CO_2 conversion of 61% was achieved at 5 wt.% NiYZ prepared by polymerization at 800 °C where no carbon deposition observed.

In the same year Hu and Lu [72] worked on 30 wt.% Ni/Al_2O_3 catalyst and found that syngas ratio about 1 can be achieved with this catalyst above 700 °C and therefore the catalyst was suitable for FTS. Effect of temperature between 500 and 800 °C and CO_2/EtOH ratio between 1 and 5 was observed. They reported that at lowest temperature investigated, ethanol conversion was 80% but CO_2 conversion was low at 5.2%. Thus they reported dehydrogenation of ethanol to acetaldehyde (Equation 2.3), decomposition of acetaldehyde (Equation 2.4) or direct ethanol decomposition (Equation 2.5) reactions dominated as follows:

$$C_2H_5OH \rightleftharpoons C_2H_4O + H_2 \qquad \Delta H^0 = 68.5 \text{ kJ mol}^{-1} \tag{2.3}$$

$$C_2H_4O+ \rightleftharpoons CO + CH_4 \qquad \Delta H^0 = -18.9 \text{ kJ mol}^{-1} \tag{2.4}$$

$$C_2H_5OH+ \rightleftharpoons CH_4 + H_2 + CO \qquad \Delta H^0 = 49.6 \text{ kJ mol}^{-1} \tag{2.5}$$

On the other hand, increasing temperatures to 700 °C suppressed methane and acetaldehyde formation. At this stage, CO_2 up to 33.3% (equivalent to stoichiometric conversion according to DRE, Equation 2.1) were achieved with H_2 yield of 96% at H_2/CO ratio close to 1. Unfortunately, they observed coke formation in all the experiments which decreased with increasing temperature and CO_2/EtOH ratio. Moreover, they performed BET surface area investigation and observed that surface area of Ni/Al_2O_3 (previously 87.9 m^2 g^{-1}) was drastically reduced probably due to blockage of pores with carbon [72].

In another study, da Silva *et al.* [79] observed both steam and dry reforming of ethanol on Rh/CeO_2 catalyst. It was the first time precious metals were investigated over dry reforming of ethanol. Two different catalysts were prepared with low and high surface areas of 14 and 275 m^2 g^{-1}, respectively. DRE was experimented at atmospheric pressure and 500 °C with CO_2/EtOH ratio of unity. Significant deactivation was observed probably due to low temperature of operation. The deactivation of catalyst led to a decrease in the conversion from 90 to 50% within 6 hours of operation which indicated the existence of ethanol decomposition (Equation 2.5) and was in agreement with previous study [72]. At a higher temperature of 800 °C over Rh/CeO_2, CO_2 conversion of 88% is achieved with H_2/CO ratio of 0.6. Additionally, carbon deposition was observed for all cases except for high surface area catalyst when steam reforming was performed.

5 wt.% Nickel catalyst supported on single-oxides like Al_2O_3, CeO_2, MgO and ZrO_2 were prepared by Zawadzki *et al.* [80] and their performances at different operating conditions were investigated. Fine dispersion of Ni over CeO_2 was validated by XRD analysis, in which no peaks characterizing Ni was observed. The best performance was obtained with Ni/CeO_2 catalyst at 750 °C. Coke deposition occured but was less compared to that occured at 650 °C. Mostly filamentous type carbon formation was hindered by elevating temperature from 700 to 750 °C. Thus, authors concluded that higher temperatures should be employed for eliminating deactivation of catalyst due to coke formation.

In 2015, two different groups worked on ethanol dry reforming. Hou *et al.* [81] used Ir/CeO_2 catalyst and they performed some characterization techniques to investigate the properties of the catalyst. Temperature range of 450 to 700 °C was investigated at atmospheric pressure. Although some undesired by-products observed, performed 70 h stability tests showed no deactivation which was explained with the strong metal-support interaction (SMSI) *via* TEM and XRD analyses. Additionally, 100% ethanol conversion was obtained with syngas ratio around 1 at 700 °C. In the study of Drif *et al.* [82] dry reforming of methane and ethanol was investigated over Rh catalyst

on different metal oxides (CeO_2, La_2O_3, MgO, NiO and ZrO_2) doped on Al_2O_3. The activity of the catalyst for ethanol dry reforming at 800 °C was ranked as follows: Rh/NiO–Al_2O_3 ≥ Rh/Al_2O_3 ≈ Rh/MgO–Al_2O_3 ≈ Rh/CeO_2–Al_2O_3 >Rh/ZrO_2–Al_2O_3 ≈ Rh/La_2O_3–Al_2O_3, which was similar to the findings for methane dry reforming when the reaction temperature was 700 °C. Although the best catalyst suggested here was Rh/NiO–Al_2O_3, it deactivated during reaction.

In 2016, Bahari and co-workers worked on two different catalysts in two different studies [83,84]. In the first one, La-doped Ni/Al_2O_3 catalyst with different La loadings were used and optimal loading was suggested to be 3%. By changing the CO_2 partial pressure, a parametric study was also included to the work and syngas yield was found to increase with increasing CO_2 partial pressure [84]. In the second work, Ce was used instead of La at different temperatures and feed ratios. It was suggested that Ce addition increased EtOH and CO_2 conversions rather than the unpromoted catalyst. Also, they draw attention to the coke deposition on the spent catalyst which consisted of mostly CNFs and least amount of graphitic carbon [83].

Finally, Bej *et al.* [85] utilized nano-NiO/SiO_2 catalyst supported on Al_2O_3, which differentiated their work from the previous ones. Catalyst activity experiments were performed at different temperatures, feed ratios and space times where the catalyst was found to be active at atmospheric pressure. The most favorable conditions that gave almost complete EtOH conversion, 76% CO_2 conversion and 100% H_2 yield was obtained at 750 °C, CO_2/EtOH feed ratio of 1.4 and 24.9 kg_{cat} h $kmol^{-1}$ space time. The data also used for determining a kinetic rate (Equation 2.6) as follows:

$$-r = 6.78 \times 10^5 e^{-97.87/RT} (p_{EtOH})^{\alpha} (p_{CO_2})^{\beta} \tag{2.6}$$

where α and β values represent orders of reaction with respect to ethanol and CO_2, respectively. Estimated values for those parameter are presented in Table 2.1 with respect to temperature values.

Table 2.1. Estimated model parameters for ethanol dry reforming [85].

Temperature (°C)	**k**	$\boldsymbol{\alpha}$	$\boldsymbol{\beta}$
500	0.1607	0.233	4.02
550	0.441	1.17	3.56
600	0.9165	1.48	4.24

2.2. Glycerol Dry Reforming

Glycerol is a major by-product of biodiesel production that has been considered as an alternative to coal based fuels. Increase in energy demand cause an increase in biodiesel production which cause surplus of glycerol in the market (see Section 1). This makes glycerol basically a waste, thus its conversion to valuable products like hydrogen or synthesis gas draws attention.

Glycerol steam reforming (GSR) is one of the main routes preferred for the production of hydrogen due to high H_2/CO ratio in the product stream. Hydrogen produced *via* this method is aimed to be used in fuel cell applications. Most common catalysts used in GSR for H_2 production are Ni,Rh and Ru based [44]. On the other hand, glycerol dry reforming (GDR) has been drawing attention due to the consumption of CO_2, a well-known greenhouse gas. GDR can be represented by the reaction of one mole of glycerol and and one mole of CO_2 to produce 4 moles of CO, 3 moles of H_2 and one mole of H_2O, as shown in Equation 2.7.

$$C_3H_8O_3 + CO_2 \rightleftharpoons 4CO + 3H_2 + H_2O \qquad \Delta H^0 = 293.2 \text{ kJ mol}^{-1} \tag{2.7}$$

Glycerol steam reforming is defined as combination of glycerol decomposition (Equation 2.8) and WGS (Reverse of Equation 2.9) by Lin *et al.* [86] due to presence of H_2O in the feed. In GDR where CO_2 instead of H_2O is present in the feed it is possible to state that RWGS (Equation 2.9) is more significant than WGS. Thus, dry

reforming of glycerol can be defined as the combination of glycerol decomposition and RWGS reactions as shown below.

$$C_3H_8O_3 \rightleftharpoons 3CO + 4H_2 \qquad \Delta H^0 = 251.2 \text{ kJ mol}^{-1} \tag{2.8}$$

$$CO_2 + H_2 \rightleftharpoons CO + H_2O \qquad \Delta H^0 = 41.2 \text{ kJ mol}^{-1} \tag{2.9}$$

Thermal unstability of glycerol as well as its high atom content complicates the dry reforming system and cause many side reactions. In addition to complete decomposition reaction (Equation 2.8), glycerol can decompose to several other components as can be seen in Figure 2.1. Three of those pathways are glycerol dehydration to give acetol (Equation 2.10), dehydrogenation to give glyceraldehyde (Equation 2.11) and decomposition to ethylene (Equation 2.12) [87]:

$$C_3H_8O_3 \rightleftharpoons C_3H_6O_2 + H_2O \qquad \Delta H^0 = 450 \text{ kJ mol}^{-1} \tag{2.10}$$

$$C_3H_8O_3 \rightleftharpoons C_3H_6O_3 + H_2 \qquad \Delta H^0 = -15 \text{ kJ mol}^{-1} \tag{2.11}$$

$$C_3H_8O_3 \rightleftharpoons C_2H_4 + CO + 2H_2O \tag{2.12}$$

Glyceraldehyde can be then decompose to 2-oxopropanal *via* Equation 2.13 and produced 2-oxopropanal can further decompose to acetaldehyde (Equation 2.14) at high temperatures. Finally, at elevated temperatures produced acetaldehyde decomposes to methane and CO *via* Equation 2.15.

$$C_3H_6O_3 \rightleftharpoons C_3H_4O_2 + H_2O \tag{2.13}$$

$$C_3H_4O_2 \rightleftharpoons CH_3CHO + CO \tag{2.14}$$

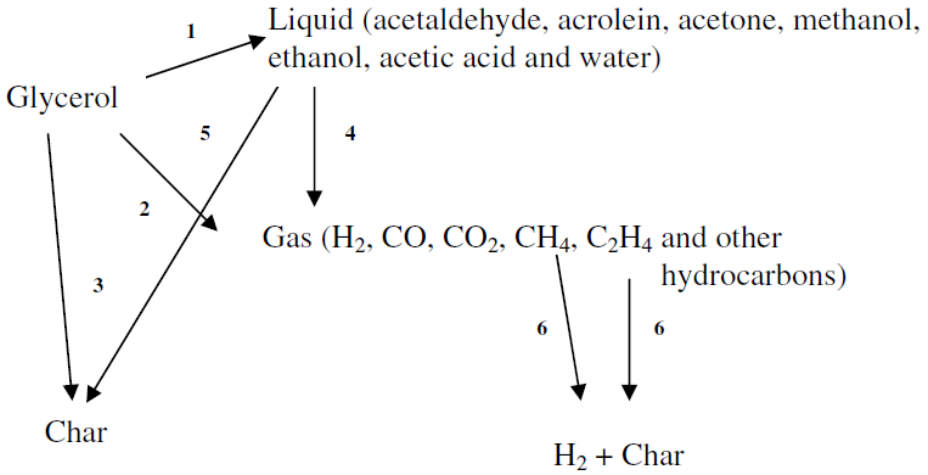

Figure 2.1. Glycerol decomposition scheme obtained from Valliyappan *et al.* [88].

$$CH_3CHO \rightleftharpoons CH_4 + CO \tag{2.15}$$

On the other hand, acetol can decompose to acrolein *via* Equation 2.16 which can then produce ethylene, ethane, hydrogen, carbon monoxide and propanal at elevated temperatures [89].

$$C_3H_6O_2 \rightleftharpoons C_3H_4O + H_2O \qquad \Delta H^0 = -36 \text{ kJ mol}^{-1} \tag{2.16}$$

Catalyst deactivation occurs due to coke deposition and methane formation in dry reforming [90]. Methane steam reforming (SMR - Equation 2.17) as well as dry reforming (DMR - Equation 2.18) and methanation (Equation 2.19 are major reactions producing or consuming methane [91].

$$CH_4 + H_2O \rightleftharpoons CO + 3H_2 \qquad \Delta H^0 = 206.1 \text{ kJ mol}^{-1} \tag{2.17}$$

$$CH_4 + CO_2 \rightleftharpoons 2CO + 2H_2 \qquad \Delta H^0 = 247.3 \text{ kJ mol}^{-1} \tag{2.18}$$

$$CO_2 + 4H_2 \rightleftharpoons CH_4 + 2H_2O \qquad \Delta H^0 = -165 \text{ kJ mol}^{-1} \tag{2.19}$$

Carbon may be formed *via* Boudouard reaction (Equation 2.20), coke gasification (Equations 2.21 and 2.22) or methane decomposition (Equation 2.23) [91].

$$2CO \rightleftharpoons C_{(s)} + CO_2 \qquad \Delta H^0 = -172.4 \text{ kJ mol}^{-1} \tag{2.20}$$

$$C_{(s)} + H_2O \rightleftharpoons H_2 + CO \qquad \Delta H^0 = 131 \text{ kJ mol}^{-1} \tag{2.21}$$

$$C_{(s)} + 2H_2O \rightleftharpoons 2H_2 + CO_2 \qquad \Delta H^0 = 90 \text{ kJ mol}^{-1} \tag{2.22}$$

$$CH_4 \rightleftharpoons 2H_2 + C_{(s)} \qquad \Delta H^0 = 74 \text{ kJ mol}^{-1} \tag{2.23}$$

Advantage of glycerol dry reforming to steam reforming is that GDR produces lower H_2/CO ratios close to unity. Thus, this makes GDR product stream unsuitable for fuel cell applications but rather a good fit to Fischer-Tropsch synthesis forthe production of long chain hydrocarbons *via* Equation 2.24 [64, 92–94].

$$nCO + (2n+1)H_2 \rightleftharpoons C_nH_{2n+2} + nH_2O \tag{2.24}$$

In case of Fe-based catalyst driven FTS, necessary syngas ratio may be adjusted by combining Equation 2.24 with WGS reaction:

$$2nCO + (n+1)H_2 \rightleftharpoons C_nH_{2n+2} + nCO_2 \tag{2.25}$$

Thus, total stoichiometry for H_2:CO becomes $(n+1) : 2n$ which is less than 1 for n>2 [54]. In addition to long chain hydrocarbons, syngas with ratio close to unity can be used in production of carbonyls (Equation 2.26) or carboxylic acids (Equation 2.27) [14].

$$nCO + (2n-1)H_2 \rightleftharpoons (CH_2)_nO + (n-1)H_2O \tag{2.26}$$

$$nCO + (2n-2)H_2 \rightleftharpoons (CH_2)_nO_2 + (n-2)H_2O \tag{2.27}$$

2.2.1. Thermodynamics

The very first article about glycerol dry reforming was published by Wang *et al.* [95] in 2009. In their work, Wang *et al.* used Gibbs free energy minimization method and investigated the effect of CO_2/G feed ratio, temperature and pressure on H_2 yield. They calculated the equilibrium compositions of the prodcut stream *via* Lagrange's undetermined multiplier method in MATLAB. Ideal gas assumption was made through the study. They found that the optimum H_2 yield was obtained at 727 °C and atmospheric pressure when CO_2/G ratio is unity. At these conditions, CO_2 conversion was equivalent to stoichiometric conversion of 33.3% dictated by Equation 2.7 and 6.4 moles of syngas with ratio of 1 is produced per mole of glycerol. Wang *et al.* [95] reported 100% glycerol conversion but it is important to mention here that their glycerol conversion is different than that used in this study which is glycerol conversion to gaseous products (see Section 3.4.5). Pressure was found to have negative effect on GDR. Methane formation was hindered with increasing temperature and CO_2/G ratios but increasing feed ratio of CO_2 to glycerol promoted carbon formation which is poisonous to catalysts. Additionally, increasing temperature showed promoting effect on H_2 yield when CO_2/G ratio was smaller than 1. On the other hand, when the feed ratio was above 1, increasing temperature first promoted then hindered H_2 yield. Moreover, in the study H_2/CO ratios lower than unity were found at elevated temperatures and high CO_2/G ratios. It is worth noting that the use of syngas ratios below 1 in FTS are demonstrated in the literature [96, 97].

Later, thermodynamic analysis of glycerol dry autothermal reforming was investigated by Kale *et al.* [98]. This study combined dry reforming with partial oxidation and provided the energy necessary to drive the endothermic dry reforming from oxidation reaction to produce synthesis gas rich product. Addition of O_2 to the system triggered the partial oxidation reaction and eliminated the external energy demand of the dry reforming process. Dry autothermal reforming of glycerol was also reported to be better than dry reforming in the sense of less carbon formation which is desirable since carbon deactivates the catalysts and causes higher pressure drops in the reactors.

Increase in the CO_2/G ratio increased the carbon formation whereas addition of oxygen decreased it. Another undesired product was methane, but its formation was predicted at negligible amounts. Four different parameters were investigated in the study, with three of them, namely temperature, pressure and CO_2/G ratio, being the same with the study of Wang *et al.* [95]. The additional parameter was O_2/C ratio where C comes from glycerol only. The results show that increase in all parameters except pressure decreased the syngas ratio. Maximum syngas ratio of 1.33 was obtained with O_2/C ratio of 0.5 and CO_2/G ratio of 1 at 677 °C whereas minimum syngas ratio of 0.63 was obtained with O_2/C and CO_2/G ratios of 0.1 and 5, respectively. Finally, the best thermoneutral point was reported to be at 653.3 °C and atmospheric pressure while O_2/C and CO_2/G ratios of 0.3 and 1, respectively. At this thermoneutral point negligble amounts of CH_4 and C(s) were reported with 4.8 moles of syngas (2.67 moles from H_2) yield.

In 2014, Freitas and Guirardello [13] studied on different glycerol reforming technologies, namely steam reforming, dry reforming, autothermal reforming, partial oxidation and supercritical water gasification, by employing Gibbs free energy minimization method together with Virial equation of state. The methods were compared in the context of product composition and coke formation and the effect of temperature, pressure and as well as feed compositions were investigated. Higher temperatures together with lower pressures should be preferred since syngas yield was maximized and all the methods were found suitable for FTS. The results showed that highest syngas amount was obtained at 750 °C for all methods, while steam reforming gave the highest value of 88.4 mol% with H_2/CO ratio 2.34 with no carbon formation. Syngas ratios at the given temperature varied between 0.67 and 2.34, where dry reforming gave the lowest ratio. Specifically for dry reforming, increasing temperature increased the molar fraction of CO and syngas while resulted in a first increasing then decreasing trend in H_2 mole fraction. Thus, increase in temperature from 600 to 750 °C decreased the H_2/CO ratio from 1.17 to 0.67. Pressure was found to have negative effect on GDR which was in accordance with previous thermodynamic results [95, 98]. Additionally, carbon formation was only observed in dry reforming and partial oxidation of glycerol. Finally, CO

yield was found to the highest in GDR due to increased amount of carbon and oxygen atoms in the feed from carbon dioxide.

In 2017, Wang *et al.* [91] studied on dry autothermal reforming of glycerol with *in-situ* H_2 separation. They investigated the effect of H_2 separation on product distributions and reaction heat. It is found that separation of H_2 promoted its yield and decreased methane formation. Increasing temperature from 577 to 627 °C required increasing O_2/G ratio from 0.15 to 0.4. They also observed the impurity effect, which showed that increasing purity (*i.e.* methanol) decreased syngas yield while promoted attainment of thermoneutral point.

There are also studies that investigated thermodynamics of dry reforming of mixtures including glycerol. Zakaria *et al.* [99, 100] performed two different studies on dry reforming of ethanol-glycerol mixtures with Gibbs free energy minimization method. In the first study [99], three different parameters, namely temperature (300-1000 °C), pressure (1-50 bar) and CO_2/ethanol-glycerol ratio (CEG, 1-12) where ethanol/glycerol ratio is 1 were investigated. The optimum pressure was found to be 1 bar and temperatures higher than 800 °C gave good syngas yield with CEG of 1. It was stated that increasing CEG or pressure did not favor syngas production. Later in 2015, Zakaria *et al.* [100] compared the dry reforming of ethanol-glycerol mixture to SR. The same parameters with same values in former work were investigated together with the effect of H_2O/ethanol-glycerol ratio (1-12) and production of H_2, CO, CO_2 and C(s) were sought. Steam reforming at 900 °C gave the highest H_2 amount. Amounts of CO and CO_2 formed were higher in dry reforming, thus resulted in lower syngas ratios than steam reforming. Another advantage of SR was that it inhibited carbon formation better than dry reforming. Finally, in 2017, Saimon *et al.* [101] performed thermodynamic investigation for dry reforming of methanol-ethanol-glycerol mixture vie Gibbs free energy minimization method. They kept mixture ratio methanol:ethanol:glycerol always at 1:1:1 and observed product yields while changing CO_2/mixture ratio from 1/6 to 6/1 and temperature from 300 to 1000 °C. The optimal parameters for hydrogen yield were reported as CO_2/mixture ratio of 1/6 at 1000 °C and atmospheric pressure.

Hydrogen yield was improved by increasing temperature and decreasing pressure and CO_2/mixture ratio. Moreover, they compared methanol-ethanol-glycerol mixture with ethanol-glycerol and found that ethanol-glycerol mixture yielded more H_2 due to higher hydrogen availability when utilized in dry reforming condition.

2.2.2. Catalysis

Although literature lacks information about glycerol dry reforming, there are several experimental studies concerned with GDR. The first experimental journal article was published in 2010 by Fernandez *et al.* [102]. In their study, three different processes, namely pyrolysis, steam reforming and dry reforming of glycerol were investigated with two different heating systems consisting of electrical (conventional heating system) and microwave heating. The idea was originated from their previous study in which they were able to show microwave pyrolysis of glycerol can be used for syngas production [103]. The catalyst used in both studies was commercial activated carbon which was found to be effective in producing H_2/CO ratios around 1 and low CO_2 emissions. The results showed that dry reforming integrated with microwave heating resulted in higher syngas yields and less methane formation than conventional heating system. Nevertheless, steam reforming with microwave heating gave the higher syngas amounts than dry reforming processes with similar methane and much less CO_2 formations.

Lee *et al.* [15–17] performed dry reforming of glycerol with cement clinkers (CC composed of 62% CaO and 17% SiO_2) and reported experimental results of different catalysts in three different articles. In 2013, they prepared CC with Ni with four different loadings (5, 10, 15 and 20 wt.%) and analyzed the catalysts with TGA, XRF, XRD, FESEM-EDS and BET surface area analyses [15]. The results showed although BET surface area of CC is low (0.55 m^2 g^{-1}) impregnation of Ni significantly increased the area to the range of 7.73 - 17.83 m^2 g^{-1} depending on the Ni loading. XRF was used to determine the composition of of the catalysts whereas FESEM images proved the fine dispersion of Ni on CC for 15 wt.% Ni/CC. Later, in 2014 they performed experiments

on those catalysts loaded with Ni [17]. The best loading for Ni/CC was suggested as 20 wt.% Ni onto cement clinker which gave the highest glycerol conversion and hydrogen yield. Increase in metal loading increased glycerol conversion to hydrogen and methane as well as hydrogen yields but CO amount was decreased. When the feed ratio of CO_2/G was about 1 the H_2/CO ratio was between 0.6 and 1.5, always lower than 2.0 which makes this process and reaction suitable for Fischer-Tropsch synthesis. Whisker and graphitic types of carbon were reported to be deposited on the catalyst. On the other hand, 5 wt.% Ni/CC showed better stability over reaction time (equals to 4 h) than 10 wt.% Ni/CC due to smaller Ni particles that were better dispersed on the support. Activity tests on 5 wt.% Ni/CC showed an increasing glycerol conversion (defined by H balance between H_2, CH_4 and glycerol) from 24.7 to 53.4% and H_2 yield from 13.6 to 28.6% between the first and fourth hours of operation, respectively. Later, the best candidate, 20% Ni loaded into cement clinker catalyst was further investigated in another study [16]. The effect of CO_2/G ratio that was varied between 0.6-5.0 was investigated at different temperatures (650-750 °C) which yielded in glycerol conversions between 70 and 80% when the CO_2/G was between 1-1.67. The results showed that chemisorption of carbon dioxide and glycerol are at different active sites and therefore the pathway of reaction was primarily determined by glycerol decomposition (Equation 2.8). Additionally, carbon deposited on the catalyst was whisker type which can be easily removed by O_2.

La-promoted Ni/Al_2O_3 catalyst was used in glycerol dry reforming processes and investigated extensively by Siew and co-workers in four different articles [18, 19, 21, 22]. In all of their works, it was found that 3% La-promoted catalyst gave the highest activity due to increased BET surface area and addition of La decreased the carbon deposition on the catalyst. With the catalyst characterization methods (EDX, XRD and TPR), it was shown that metal dispersion was increased due to decreased crystalline size with La-promotion. But in some different La loadings, the decreased crystalline size blocked the pores and therefore resulted in lower surface areas [18]. In the second paper, they reported highest glycerol conversion to gaseous products over 3 wt.% La promoted on Ni/Al_2O_3 whereas La promotion at other loadings decreased the activ-

ity of the catalyst [19]. In other words, 1,2,4 and 5 wt.% La promotion on Ni/Al_2O_3 resulted in lower glycerol conversions then non-promoted Ni/Al_2O_3. The syngas ratio (H_2/CO) was found between 0.8 and 2.0 with non-promoted and 1-5 wt.% La-promoted catalysts. After determination of the promising catalyst, parameter investigation was done over 3 wt.% La doped Ni/Al_2O_3 and the catalyst was found to be stable under 4 h of GDR conditions. In 2015, they reported that decrease in the carbon decomposition with La-promotion was related with the redox property of La [21]. The 3 wt.% La-promoted Ni/Al_2O_3 catalyst was investigated at atmospheric pressure between temperatures 650-850 °C and CO_2/G ratios 0-5. H_2/CO ratio was found to be less than 2 in all of the experiments whereas the maximum glycerol conversion achieved was 96% at ratio of 1.67. Kinetics of GDR (Equation 2.28) was determined by the power law as follows:

$$r_g = 2.6 \times 10^{-4} e^{\frac{-E_a}{RT}} (P_{C_3H_8O_3})^{\gamma} (P_{CO_2})^{\phi} \tag{2.28}$$

where reaction order of glycerol and CO_2 were calculated as 0.72 and 0.14, respectively and activation energy was 34.9 kJ mol^{-1}. With the suitable syngas ratio and high yields, the catalyst and the process were found to be suitable for providing synthesis gas to Fischer-Tropsch synthesis. Finally again in 2015, longevity of the catalyst was investigated for continuous 72 hours of operation [22]. The catalyst was found to be stable and coke formations were reported to be filamentous type.

Kumar *et al.* [20] worked on tri-reforming (steam and dry reforming coupled with oxygen) of glycerol in 2014 for 10 wt.% Ni supported on three different supports: CeO_2, ZrO_2 and CeO_2-ZrO_2. Mixed support showed increased surface area in BET analysis when compared to both single oxide supports. Addition of Ni decreased the surface area as expected. The authors reported their reason for selecting Ni as an active metal which was the high capacity of Ni towards C–C bond breakage. The activity reactions were carried out at atmospheric pressure ad temperatures between 400-800 °C. The highest thermodynamic limit for hydrogen yield was found to be 95% with mixed support at 600 °C, where glycerol conversion was 100%. This Ni/CeO_2-ZrO_2

catalyst had additional advantages of catalyzing WGS reaction (Equation 2.9) and it improved stability.

Arif *et al.* [23] used different weight percent Ni (5, 10 and 15 wt.%) supported on ZrO_2 and CaO to investigate the dry reforming of glycerol at atmospheric pressure and 700 °C when CO_2/G is 1. The highest glycerol conversion of 30.3% and hydrogen yield of 24.6% was achieved on 15 wt.% Ni/CaO which was verified with some catalyst characterization methods (BET, SEM, XRD, TGA, TPR). The characterizations showed the good dispersion of Ni on the catalyst and high BET surface area of 44.9 m^2 g^{-1}. Therefore, it is possible to draw attention to the strong interaction between Ni metal and CaO support. The same authors published another article in 2017 [25], reporting GDR over 15 wt.% Ni supported on CaO or ZrO_2 or La_2O_3. They performed their experiments under atmospheric pressure at 700 °C, similar to their previous work. BET surface area of the supports were reported in decreasing order as follows: La_2O_3 >CaO >ZrO_2. The highest glycerol conversions were achieved over CaO ($\sim$ 30%) followed by La_2O_3 ($\sim$ 20%) and ZrO_2 ($\sim$ 13%).

In 2016, Harun *et al.* [24] investigated the properties of Ag-promoted (0-5 wt.%) Ni/SiO_2 catalyst for dry reforming of glycerol. The experiments were conducted with CO_2/G ratio of 1 at atmospheric pressure and 700 °C. All experiments ended up with syngas ratios below 1.0, with 5 wt.% Ag-promoted catalyst giving the best results of 32.6% glycerol conversion and 27.4% hydrogen yield. Through some catalyst characterization methods (BET, SEM, XRD, TGA), it was found that this catalyst gave the highest dispersion of metals and highest BET surface area which explained the superiority of this catalyst among other Ag-Ni/SiO_2 catalysts. In 2018, they supported Ni on α-Al_2O_3 and SiO_2 [26]. Ni/Al_2O_3 gave the highest glycerol conversion of 14.4% and H_2 yield of 9.9% at atmospheric pressure and 700 °C. The higher activity of Ni supported on alumina was attributed to its higher surface area and smaller cyrstallite size. Structure of alumina improved the activity and stability of catalyst thus carbon deposition was decreased. Types of coke formation on Ni/Al_2O_3 and Ni/SiO_2 were encapsulating and filamentous, respectively. The authors published another study in 2018, in which

they promoted Ni/Al_2O_3 catalyst with different amounts of Ag (1, 3 and 5 wt.%) [27]. They investigated the temperature range of 600 - 900 °C and gas hourly space velocity range of 14.4 - 72 L g_{cat}^{-1} h^{-1} at CO_2/G ratio of 0.5. Highest glycerol conversion of 40.7% and H_2 yield of 32% were obtained at 800 °C and gas hourly velocity of 36 L g_{cat}^{-1} h^{-1} over 3 wt.% Ag-Ni/Al_2O_3. Although BET surface area of Ni/Al_2O_3 decreased with Ag promotion, the high activity of 3 wt.% Ag-Ni/Al_2O_3 was based on small metal crystallite size. 72 h stability of the best performance catalyst showed significant decrease in glycerol conversion due to whisker type of carbon formation which can be easily removed *via* oxygen treatment.

The most recent study was published by Tavanarad *et al.* [28]. In their study, they loaded different amounts on Ni (5, 10, 15 and 20 wt.%) onto mesoporous γ-Al_3O_3. BET surface area of the support decreased when Ni is impregnated and increasing metal loading decreased the surface area further. 15 wt.% Ni showed the best catalytic activity but 20 h stability showed significant decrease in the activity. Increasing temperature from 600 to 750 °C and CO_2/G ratio from 0 to 3 increased glycerol conversion while H_2/CO ratio was decreased but always higher than 1. Finally, whisker type of carbon was found to be deposited on the catalyst surface. In their another study, Tavanarad *et al.* [29] impregnated noble metals (Rh, Ru, Ir, Pd and Pt) on Al_2O_3 stabilized MgO. BET analysis showed higher surface area for Rh, Ru and Pd catalysts while TEM imaging revealed the good dispersion of metal particles with sizes smaller than 5 nm. H_2S chemisorption analysis showed crystallite sizes between 1.28 and 4.2 nm. Increasing temperature (from 600 to 750 °C) and CO_2/G ratio (from 0 to 3), increased catalytic activity and carbon deposition. For instance, increase of temperature from 600 to 750 °C increased glycerol conversion from $\sim$ 50% to $\sim$ 90% for the most active catalyst, $Rh/MgAl_2O_4$. The activity of the noble metals were given in the following order: Rh>Ru>Ir>Pd >Pt. 20 h stability over the most active catalyst (Rh/MgO-Al_2O_3) were performed at 700 °C and CO_2/G ratio of 1 which stated that catalytic activity severely reduced until 14_{th} hour and then stabilized. The deactivation of the catalyst was grounded on the carbon formation of whisker type.

2.3. Mixed Oxide Supports

Mixed oxide supports are commonly used in reforming reactions due to their advanced characteristics [104]. Dry reforming catalysts should be durable against coke formation due to the nature of the reaction conditions. In order to obtain high active and stable catalyst with good selectivity, binary or ternary oxide supports can be prepared from most commonly used metal oxide supports (MgO, Al_2O_3, TiO_2, CC, ZrO_2 and CeO_2) [23].

ZrO_2 has been used in dry reforming of glycerol in various studies [20, 23] as well as an M.S. thesis that this study is based on [105]. Its main drawback as a catalyst is its thermal unstability [106]. It has three phases, namely monoclinic, tetragonal and cubic. Monoclinic phase is stable under 1000 °C whereas tetragonal phase is stable between 1000 and 2300 °C and cubic phase stable over 2300 °C [106]. ZrO_2 has high oxygen storage capacity which makes it a very promising support in reforming applications [107,108]. Although, its is more active than CeO_2, its stability (see Section 4.1.1) [105] is below acceptable limits. Thus, this support could be further improved *via* addition of another metal oxide.

TiO_2 has been commonly used in dry methane reforming reactions [109–113] since it is a reducible metal oxide [114]. Ti can exist in variety of oxidation states [114] and its oxide, TiO_2 have three crystalline modifications, namely anatase, brookite and rutile [115]. Anatase is stable below 700 °C where phase transition to rutile occurs between 700 and 800 °C. Strong metal-support interaction between TiO_2 and other metals, especially Ni, was reported by several researchers [110, 112–115]. Strong Ti-support interaction results in reduction in H_2 and CO adsorption on the catalyst. [116] Moreover, large particle clusters can be destroyed by TiO_x which can serve as active sites later [114]. Additionally, TiO_2 was reported to decrease coke formation [114].

Tada *et al.* [117] observed CO_2 methanation at low temperatures over 10 wt.%Ni catalysts supported on CeO_2, α-Al_2O_3, TiO_2 and MgO. Although Ni supported on

CeO_2 and Al_2O_3 showed higher catalytic activities, almost complete methane conversion was obtained with Ni/CeO_2 and Ni/TiO_2. Although Ni/TiO_2 showed high activity and stability for DMR, it was severely deactivated the in partial oxidation of methane. Ruckenstein and Wang [109] attributed this deactivation to partial migration of TiO_x onto metal (Rh or Ni in their case) sites.

Kumar *et al.* [118] performed dry methane reforming reactions on binary oxide catalysts supported Ni. Those binary oxide supports include CeO_2-ZrO_2, CeO_2-Al_2O_3 and La_2O_3-Al_2O_3. All of the binary oxide supports used in the experiments were said to enhance the reducibility of Ni. Finally, authors suggested that Al_2O_3 did not affect the stability of catalyst.

Kim *et al.* [110] experimented the effect of Ce/Ti ratio in Ni/CeO_2-TiO_2 catalyst on the activity and stability of DMR. 5 different Ce:Ti ratio was selected, 100:0, 80:20, 50:50, 20:80 and 0:100. Ni/TiO_2 showed higher catalytic activity at the beginning but Ni/CeO_2 was reported to be more stable. Better dispersion on Ni particles on the support was correlated with higher catalytic activity, stability and reducibility of the catalysts. The authors emphasized the importance of RWGS reaction. Increase in the rate of RWGS decreased the syngas ratio. Additionally, increasing CeO_2 loading increased the reducibility of the catalyst thus increased the rate of RWGS which was directly correlated with the activity of the catalyst.

TiO_2 has also been used commonly together with other metal oxides for NO_x storage and reduction due to its acidic nature [119–122]. The acidic sites made the catalyst durable against sulphur poisoning which is a major drawback of NO_x storage and reduction. In their work, Say *et al.* [119, 123] investigated Pt catalyst supported on ZT and AZT. They reported that there was a strong interaction between ZrO_2 and TiO_2 which resulted in low specific surface areas ($\sim$ 26 m^2 g^{-1}) due to formation of highly ordered $ZrTiO_4$ crystalline phase [104]. Addition of Al_2O_3 to ZT prevented the formation this phase, thus resulted in greater surface are of approximately 264 m^2 g^{-1}. Thermal stability of AZT found to be higher than ZT and addition of Pt

improved storage capacity in both supports. The best compositions for ZT and AZT were reported as Z:T=70:30 and A:Z:T=50:35:15, respectively.

γ-Al_2O_3 is a commonly used as catalyst support in petroleum industries due to its surface (*i.e.* surface area, pore volume and its distribution) and acidic/basic characteristics [124]. It was found to appear at temperatures between 350 and 1000 °C depending on its precursor and it is stable up to 1200 °C. γ-Al_2O_3 is amphoteric with higher H_2O content than its another form η-Al_2O_3 [125]. Highly porous γ-Al_2O_3 has BET specific surface area of 204 m^2 g^{-1} when dried at 500 °C with rather uniform pore size of $\sim$ 95% of the pore radius between 20-40 Å [125].

Abate *et al.* [126] tested the performance of Ni/γ-Al_2O_3-ZrO_2-TiO_2-CeO_2 catalyst under CO_2 methanation reaction (Equation 2.19) conditions. Under operating conditions (250-400 °C) RWGS (Equation 2.9) and CO methanation (Equation 2.17) occurred. Higher surface area was observed over Ni supported on quarternary oxide than Ni/γ-Al_2O_3 and better Ni dispersion occurred with increasing amount in additional metal oxides. The better dispersion promoted the catalytic activity as well. But authors revealed that catalytic activity was not directly related with the surface area (thus physical properties), but more related with the reduction properties.

3. EXPERIMENTAL WORK

3.1. Materials

3.1.1. Chemicals

Table 3.1 contains all chemicals used in catalyst preparation. Supports were used to prepare ZrO_2 (Zr), CeO_2 (Ce), ZrO_2-TiO_2 (ZT) and Al_2O_3-ZrO_2-TiO_2 (AZT) and active metals were used to prepare RhZr, RhCe, CoZr, CoCe, Rh/AZT, Ni/AZT, Co/AZT and Rh/ZT catalysts. Zeneer Water Purification System was used for producing deionized water with a conductivity less than 0.1 μS cm^{-1}.

3.1.2. Gases and Liquids

All gaseous and liquid feeds used in experimental system are listed in Table 3.2 and Table 3.3, respectively. Ar and He are used as gas chromatograph (GC) carrier gases and all of the rest were used in GC calibration. H_2 was also used for reducing the catalyst and CO_2 and N_2 were used directly in experiments as reactant and inert, respectively. Glycerol was the liquid reactant with specifications listed in Table 3.3. Other liquids listed in the aforementioned table was used for cleaning the experimental system following an order with respect to their volatilities which is distilled water, ethanol and finally acetone.

3.2. Experimental System

In this study an experimental system consisting of 4 main parts is used:

- Catalyst Preparation System: The incipient-to-wetness impregnation system is comprised of an ultrasonic mixing valve and a Buchner flask in which precursor solution is added drop-wise to support *via* silicon tubes by peristaltic pump.

Table 3.1. Chemicals used for catalyst preparation.

Chemicals	**Formula**	**Supplier**	**MW (g/mol)**	**Purity**	**Usage**
Co (II) nitrate hexahydrate	$Co(NO_3)_2{\cdot}6H_2O$	Sigma-Aldrich	291.03	> 99.0%	Active Metal
Ni (II) nitrate hexahydrate	$Ni(NO_3)_2{\cdot}6H_2O$	Sigma-Aldrich	290.79	> 97.0%	Active Metal
Rh (III) nitrate solution	$Rh(NO_3)_3$	Sigma-Aldrich	288.92	10% in HNO_3	Active Metal
Aluminum tri-sec-butoxide	$Al[OCH(CH_3)C_2H_5]_3$	Sigma-Aldrich	246.32	97%	Support
Ce (III) nitrate hexahydrate	$Ce(NO_3)_3{\cdot}6H_2O$	Sigma-Aldrich	434.22	> 99.9%	Support
Titanium (IV) isopropoxide	$Ti[OCH(CH_3)_2]_4$	Sigma-Aldrich	284.22	97%	Support
Zirconium oxide	ZrO_2	Alfa-Aesar	123.22		Support
Zirconium (IV) propoxide	$Zr(OCH_2CH_2CH_3)_4$	Sigma-Aldrich	327.57	70% in propanol	Support
Aluminum oxide	α-Al_2O_3 3/16" spheres	Alfa-Asear	101.96	> 99.0%	Diluent
2-propanol	$(CH_3)_2CHOH$	Sigma-Aldrich	60.10	> 99.5%	Solvent
Nitric acid solution	0.5 M HNO_3	Sigma-Aldrich	63.01	65%	Solvent
Deionized water	H_2O	-	18.02	-	Solvent

Table 3.2. Gases used in the experimental system.

Gas	**Specifications**	**Application**
Argon	99.998%	GC carrier gas
Carbon dioxide	99.995%	GC calibration, reactant
Carbon monoxide	99.90%	GC calibration
C_2 mixture	2% C_2H_6, 2% C_2H_4, 5% CH_4, balance N_2	GC calibration
Helium	99.99%	GC carrier gas
Hydrogen	99.99%	GC calibration, reducing agent
Methane	99.50%	GC calibration
Nitrogen	99.998%	GC calibration, inert

Table 3.3. Liquids used in the experimental system.

Liquid	**Formula**	**Supplier**	**MW (g/mol)**	**Purity**	**Usage**
Glycerol	$C_3H_8O_3$	Sigma-Aldrich	92.09	$> 99.5\%$	Reactant
Ethanol	C_2H_5OH	Merck	46.07	$> 99.9\%$	Cleaning
Acetone	C_3H_6O	Merck	58.08	$> 99.8\%$	Cleaning
Distilled Water	H_2O	-	18.02	-	Cleaning

- Catalyst Characterization System: Catalysts used in this study were analyzed *via* different characterization methods. These methods are namely transmission electron microscopy (TEM), energy dispersive X-ray Spectroscopy (EDX), *ex-situ* Raman and *in-situ* FTIR spectroscopic analysis and finally BET surface analysis.
- Catalytic Reaction System: The reaction takes place through a packed-bed reactor where mass flow controllers arrange the gas feed and an HPLC pump leads the liquid feed. Desired temperature was adjusted by a furnace with three controllable chambers.
- Product Analysis System: The exit stream of reactor was analyzed by two distinct gas chromatography (GC) devices each analyzing different gaseous products.

3.2.1. Catalyst Preparation System

Mixed oxide supports and catalysts used in this study were prepared by conventional sol-gel and incipient-to-wetness impregnation methods, respectively. The representative system for the latter method is given in Figure 3.1. Retsch UR1 ultrasonic mixer was used for mixing the support-precursor solution continuously through impregnation, KNF diaphragm vacuum pump was used to evacuate air from the pores of the support and Masterflex peristaltic pump was used for drop-wise addition of precursor to catalyst support. Detailed explanation of the catalyst preparation will be provided in Section 3.3.

3.2.2. Catalyst Characterization System

In this study, TEM, EDX, *ex-situ* Raman and *in-situ* FTIR analyses were used to determine characterization of Rh/ZrO_2 and Rh/CeO_2 catalyst while BET and TEM, EDX and *in-situ* FTIR analyses were used for Rh/AZT, Ni/AZT and Co/AZT catalysts. Finally, surface analysis *via* BET was done for AZT sample.

3.2.2.1. BET Surface Analysis. The nitrogen adsorption/desorption isotherm was obtained *via* Quantachrome Nova 2200e automated gas adsorption system available in

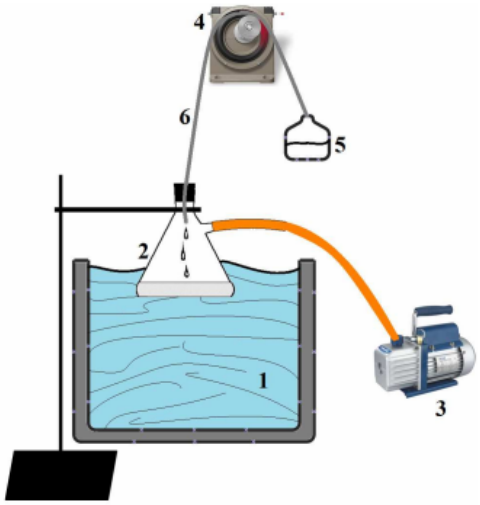

Figure 3.1. Illustration of catalyst impregnation system *via* incipient-to-wetness impregnation [105, 127]. 1. Ultrasonic Mixer, 2. Buchner Flask, 3. Vacuum Pump, 4. Peristaltic Pump, 5. Precursor Solution, 6. Silicon Tubing.

Boğaziçi University. Liquid nitrogen at -196 °C was utilized. The specific surface areas of AZT samples were determined by using multi-point BET analysis. Pore volumes and diameters were calculated by the BJH method.

3.2.2.2. TEM/EDX Analyses. TEM imaging and EDX analysis of catalysts were performed in Bilkent University OzensoyLab *via* an FEI, Tecnai G2 F30 microscope utilizing an electron beam voltage of 300 kV. Before the analysis, each sample was dispersed in EtOH and sonicated for 5 minutes. The suspension was then transferred on a copper TEM grid *via* help of a micropipette. The excess solution was dried in the fume hood at ambient temperature overnight. For HR-TEM, bright field imaging mode was used while for EDX analysis, high angle annular dark field scanning transmission electron microscopy (HAADF-STEM) was utilized. Average particle size was determined by ImageJ digital image processing software.

3.2.2.3. *Ex-situ* Raman Spectroscopic Analysis. *Ex-situ* Raman spectroscopic experiments were carried out in Bilkent University OzensoyLab using a Renishaw inVia-Reflex confocal Raman microscope/spectrometer. A 532 nm laser with an adjustable power was utilized. The maximum output laser power at the end of the fiber was 50 mW.

3.2.2.4. *In-situ* FTIR Spectroscopic Analysis. *In-situ* FTIR measurements were performed at Bilkent University OzensoyLab in a batch-type catalytic reactor coupled to an FTIR spectrometer (Bruker Tensor 27). FTIR spectra were recorded using a MCT detector at 50 °C, where each spectrum was acquired by averaging 32 scans with 4 cm^{-1} resolution. Approximately 20 mg grounded catalysts were pressed onto a lithographically etched W-grid sample holder.Details of experimental setup can be found elsewhere [128].

In-situ CO adsorption experiments were performed using FTIR technique. In these experiments, the catalyst surfaces were exposed to 0.013 bar (equivalent to 10.0 Torr) of CO(g) for 10 minutes at 50 °C. Then, spectroscopic chamber was evacuated to approximately 10^{-2} Torr at the same temperature. Here, FTIR spectras were obtained. Prior to each analysis, background spectrum was collected. Only 72 h spent catalysts were treated with 10.0 Torr of H_2 (purity >99.999%, Linde GmbH) for 10 minutes at 300 °C before CO adsorption experiments since their surfaces were covered with carbon. FTIR spectra of the spent catalysts, either 5 h or 72 h, were directly used as the background spectra. *In-situ* FTIR spectra of the spent catalysts were obtained after exposing them to 10.0 Torr of H_2 for 10 minutes at 300 °C, then evacuation and cooling to bach to ambient temperature.

3.2.3. Catalytic Reaction System

The catalytic reaction system is composed of three major parts namely, feed, reaction and product analysis systems all which illustrated in Figure 3.2. The latter section is detailed in Section 3.2.4. The actual system can also be seen in Figure 3.3.

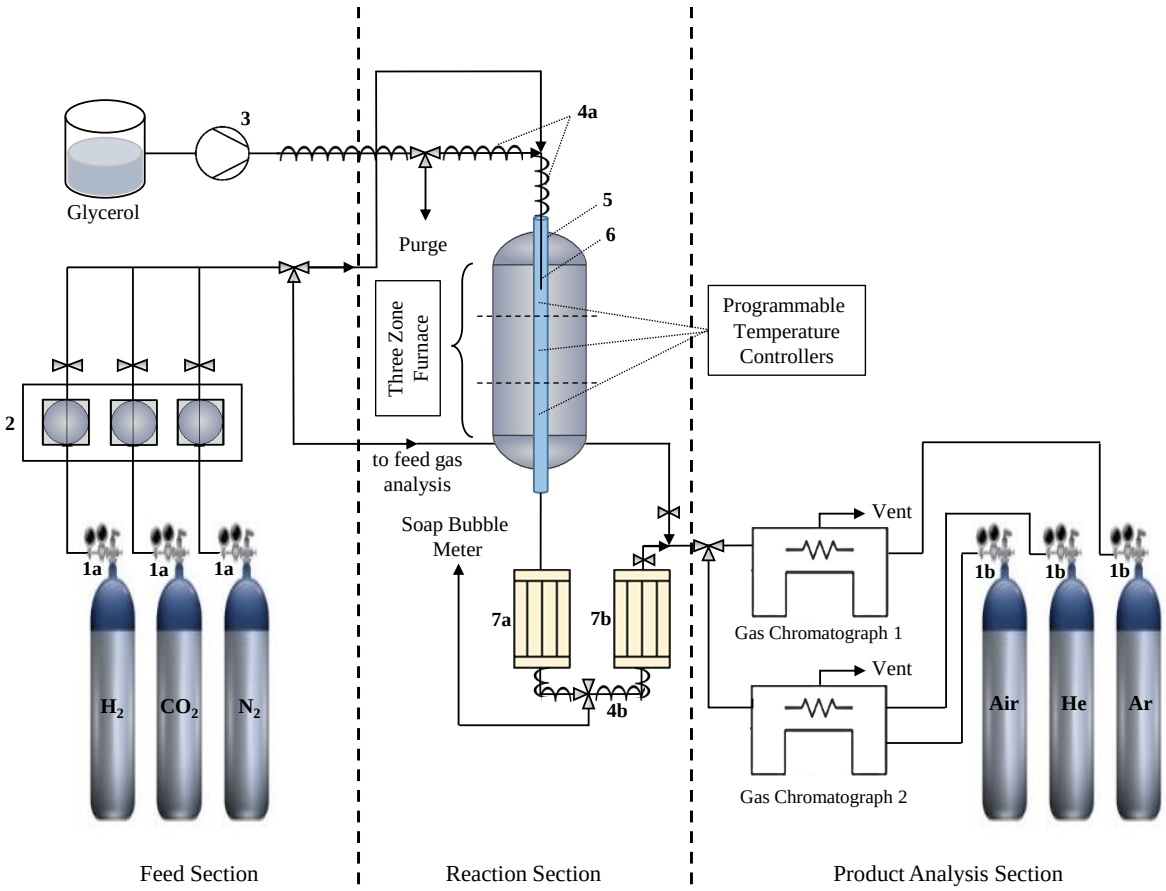

Figure 3.2. Schematic representation of the experimental system.



Figure 3.3. Glycerol dry reforming experimental system.

3.2.3.1. Feed Section. The feed section seen in Figure 3.2 is consisted of glycerol feed connected to s Schimadzu LC-20AT high-performance liquid chromatography (HPLC) pump (marked as 3 in Figure 3.2), pressurized H_2, N_2 and CO_2 storage tanks, specifications provided in Table 3.3, connected to Brooks Model 5850E series mass flow controllers (MFC) (marked as 2 in Figure 3.2) *via* regulators provided by the Linde Group (marked as 1a in Figure 3.2). Three different sizes Swagelok tubing and fitting namely 1/4", 1/2" and 1/8" are used to connect the equipment.

Outlets of H_2, N_2 and CO_2 tanks are kept at $\sim$ 2 atm *via* regulators (marked as 1a in Figure 3.2) and exit of these regulators are connected to individual MCFs by 1/8" tubing. Individual MFCs of H_2, CO_2 and N_2 are used to regulate volumetric flow rate of these components *via* separate Brooks Instruments MFC display box. They are calibrated and corresponding set points to actual flow rates can be found in Appendix A. On-off valves are inserted after each MFC *via* 1/4" tubing to prevent back flow of the reactant product mixture. Exit of these three MFC are then connected with two

1/4" Swagelok union tee, at the exit of the second union tee, tubing size is reduced to 1/8" *via* reducing union which is connected to a 3-way valve. This valve is used to direct incoming feed flow to either gas chromatographs for feed gas analysis or reactor. Reducing union is used to decrease tubing size from 1/8" to 1/16" just before the reactor inlet.

Glycerol feed from 50 mL graduated cylinder is connected to the HPLC pump with 1/16" tubing. Since glycerol is highly viscous liquid, a heating line is surrounded around the tubing connecting HPLC pump to inlet of the reactor. Temperature of this line is kept $\sim$ 100 °C with ENDA ET4420 type digital proportional integral derivative (PID) temperature controllers. The outlet pressure of glycerol from HPLC pump is generally between 2 and 3 bars.

Liquid and gaseous feeds are connected by a union tee just before the reactor and reactant mixture enters the reactor *via* 1/16" tubing. This tubing, called injector, is elongated for 10 cm along the reactor inlet (see Figure 3.4) to ensure complete vaporization of glycerol. Temperature is kept above 400 °C at the tip of this injector which allows homogeneous mixture of reactants at gaseous phase. This configuration is found to be the best to keep CO_2/G ratio in the catalyst bed by our group [105].

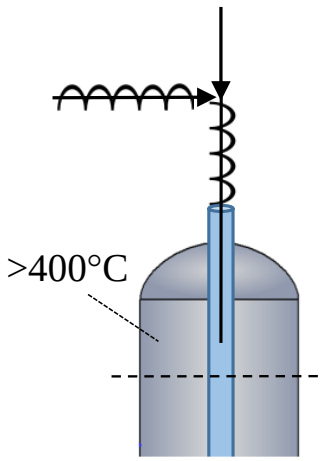

Figure 3.4. Detailed illustration of reactor inlet.

3.2.3.2. Reaction Section. The reaction section seen in Figure 3.2 is consisted of PROTHERM PZF 12/50/500 three zone furnace each zone controllable by PC442 PID temperature controller, quartz reactor and two cold traps with Dewar flasks.

80 cm long quartz reactor is a packed bed reactor which is detailed in Section 3.4. Middle zone of the furnace is kept at reaction temperature since the catalytic bed is at the middle of the reactor (see Figure 3.5). Top and bottom zones of the furnace are aimed kept above 310 °C which is the boiling point of glycerol. Due to heat dissipation from the middle zone of the furnace, top and bottom temperatures varies between the experiments but it is always above 400 °C.

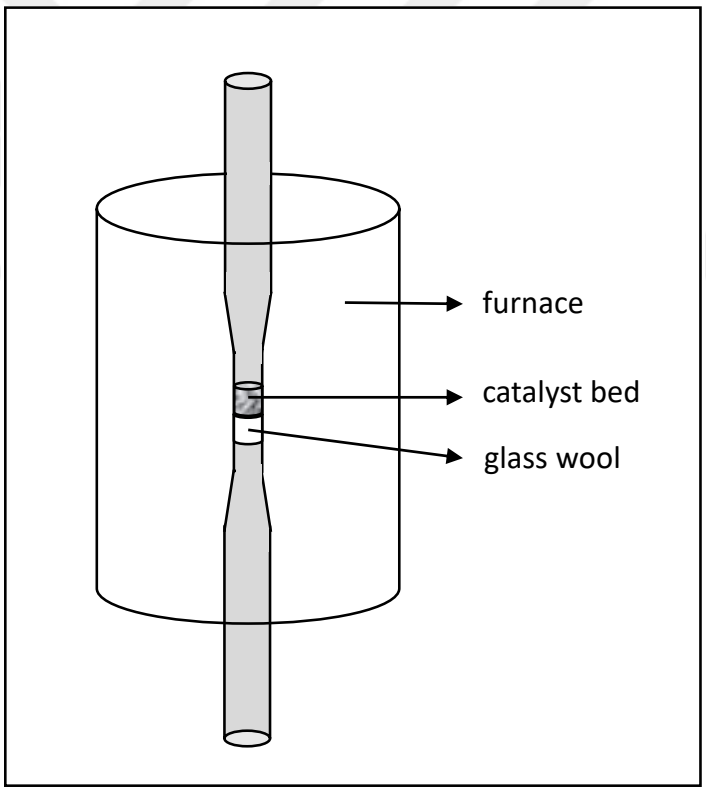

Figure 3.5. Illustration of packed bed reactor.

The exit of the reactor is connected to two consecutive cold traps containing ice which are used to condense any low boiling point hydrocarbons that may be formed by side reactions and water *via* 1/4" tubing. Exit of the first cold trap (marked as 7a in Figure 3.2) is attached to 3-way valve with is used to direct the out coming product

stream to either second cold trap (marked as 7b in Figure) or to soap bubble meter which is used to determine the actual flow rate within the system and therefore avoid any gas leak from the system. Exit of this bubble meter is connected to vent. In between two cold traps there is a heating line that keeps the temperature of the tubing at $\sim$ 120 °C (marked as 4b in Figure 3.2). This is necessary to avoid any condensation at the tubing which may lead to blockage afterwards. Finally, the exit of the second cold trap is directed to product analysis system.

3.2.3.3. Product Analysis Section. The product analysis section is consisted of two gas chromatographs detailed in the coming Section 3.2.4 and three pressurized Ar, dry air, He storage tanks. There are two inlets to this section one is from feed section directly which is used for feed gas analysis and the other from the reaction section. One of these streams is directed to GC system by 3-way valve which is connected to another valve that is used to direct the stream to one of the gas chromatographs.

3.2.4. Product Analysis System

Product analysis system is used for determining the composition of both product stream exiting the reactor and feed stream entering. In this section there are two different gas chromatographs Schimadzu GC-2014 and Agilent 6850N (marked as GC1 and GC2, respectively in Figure 3.2), each is used to detect different compounds. Properties of these two GCs can be found in Table 3.4. Calibration charts available in Appendix A are used to calculate the composition and flow rate of the product stream corresponding to each peak obtained by GC. A specific carrier gas (Ar for GC1 and He for GC2) is connected to gas chromatographs *via* 1/8" tubing and their pressure is adjusted to 6.5 atm by regulators (marked as 1b in Figure 3.2). Dry air at $\sim$ 4 atm is necessary for GC2 in order to activate the pneumatic valve used to direct the sampling loop to GC column. This is done manually in GC1 so there is no need for dry air for this system.

Table 3.4. Operating parameters of gas chromatographs.

GC Parameter	**Schimadzu GC-2014 (GC1)**	**Agilent 6850N (GC2)**
Compounds	H_2, N_2, CH_4, CO	CO_2, C_2H_6, C_2H_4
Carrier gas	Argon	Helium
Carrier gas flow rate (mL min^{-1})	25	20
Column ID (mm) and length (m)	2.1 & 2.0	2.1 & 1.82
Column oven temperature (°C)	50	40
Column packing material	Molecular Sieve 5A (60-80 mesh)	Porapak Q (80-100 mesh)
Column tubing material	Stainless steel	Stainless steel
Detector current (mA)	50	Set by GC itself
Detector temperature (°C)	150	80
Detector type	Thermal conductivity	Thermal conductivity
Injector temperature (°C)	80	90
Sampling loop volume (mL)	1.3	1

3.3. Catalyst Preparation and Pretreatment

In this study eight different catalysts, namely RhZr, RhCe, CoZr, CoCe, Rh/AZT, Ni/AZT, Co/AZT and Rh/ZT were prepared. The preparation step consisted of support preparation by sol-gel method, active catalyst preparation by incipient-to-wetness impregnation method and *in-situ* pretreatment with H_2.

3.3.1. Preparation of Support

3.3.1.1. Preparation of ZrO_2. ZrO_2 with specifications provided in Table 3.1.1 was sieved to obtain 45-60 mesh size which corresponds to particle size of 250-354 μm. Later, sieved ZrO_2 was calcined at 800 °C for 4 hours under air [105].

3.3.1.2. Preparation of CeO_2. Ce-precursor, namely cerium (III) nitrate was calcined at 600 °C for 4 hours under air. After Ce-precursor decomposes to ceria, obtained powder was again calcined at 800 °C for 4 hours under air [105].

3.3.1.3. Preparation of ZrO_2–TiO_2. In this study ZrO_2–TiO_2 (ZT) support with mass ratio Zr:Ti 70:30 was used according to the study of Say *et al.* [119, 123]. In order to prepare 6 grams ZT, 15.27 mL Zr-precursor Zirconium (IV) propoxide and 6.86 mL Ti-precursor Titanium (IV) isopropoxide were dissolved in 100 mL of 2-propanol. Then, the mixture was stirred for 40 minutes under ambient conditions. 3 mL of 0.5 M nitric acid solution was added drop-wise to mixture in order to obtain a gel. The gel was dried under ambient conditions for 48 h followed by 2.5 h calcination at 750 °C in air.

3.3.1.4. Preparation of Al_2O_3–ZrO_2–TiO_2. In this study, Al_2O_3–ZrO_2–TiO_2 (AZT) support with mass ratio Al:Zr:Ti 50:35:15 was used according to the study of Say *et al.* [119, 123]. A similar procedure to ZT was followed in preparation of this support. In order to prepare 6 grams of AZT, 14.94 mL of Al-precursor Aluminum sec-butoxide, 7.64 mL Zr-precursor and 3.44 mL Ti-precursor were added to 100 mL of 2-propanol.

The mixture was stirred for 60 minutes under ambient conditions. Gel formation was obtained by drop-wise addition of 9 mL of 0.5 M nitric acid solution to the mixture. Then, the mixture was dried under air for 48 h and calcined at 750 °C.

3.3.2. Preparation of Active Catalysts

Eight active catalysts, namely RhZr, RhCe, CoZr, CoCe, Rh/AZT, Ni/AZT, Co/AZT and Rh/ZT were all prepared by incipient-to-wetness impregnation method. Therefore, the followed procedure was approximately the same and the equipment used in preparation is explained in Section 3.2.1 in detail.

3.3.2.1. Preparation of Rh/ZrO_2. 2 grams of 1 wt.% RhZr catalyst was prepared in a batch. Firstly, 1.98 grams of ZrO_2 was weight and stirred in ultrasonic mixer under vacuum for 30 minutes (consult Figure 3.1). Meanwhile, precursor solution was prepared by dissolving 0.2 g of 10 wt.% Rh solution ($\sim$ 142 μL) in necessary amount of deionized water ($\sim$ 1.2 mL). After 30 minutes, the precursor solution was drop-wise added to ZrO_2 in Buchner flask *via* help of peristaltic pump with a speed of 0.04 m/s. Support-precursor solution was in a form of slurry and mixed for 1.5 hours under vacuum to ensure good dispersion of active metal on the support ZrO_2. Then, the catalyst was dried overnight at 110 °C and calcined in air at 800 °C for 4 hours [105].

3.3.2.2. Preparation of Rh/CeO_2. 2 grams of 1 wt.% RhCe catalyst was prepared using the same procedure explained in Section 3.3.2.1. 1.98 g CeO_2 and 0.2 g 10 wt.% Rh solution was used. Since surface area of CeO_2 is lower than ZrO_2 (refer to Section 4.2.7.1), necessary amount of deionized water for impregnation was slightly lower ($\sim$ 1.1 mL) [105].

3.3.2.3. Preparation of Co/ZrO_2. 2 grams of 5 wt.% CoZr catalyst was prepared using the same procedure explained in Section 3.3.2.1. 1.9 grams of ZrO_2 and 0.494 g Co-precursor was used. Approximately, 1.2 mL of deionized water was used [105].

3.3.2.4. Preparation of Co/CeO_2. 2 grams of 5 wt.% CoCe catalyst was prepared using the same procedure explained in Section 3.3.2.1. 0.494 g of Co-precursor dissolved in $\sim$ 1.1 mL deionized water was impregnated onto 1.9 g CeO_2 [105].

3.3.2.5. Preparation of Rh/AZT. 1 gram of 1 wt.% Rh/AZT catalyst was prepared in a batch. 0.99 grams of AZT and 0.1 g of 10 wt.% Rh solution ($\sim$ 71 μL) were dissolved in $\sim$ 1.2 g deionized water. Amount of deionized water necessary was more than twice that of ZrO_2 or CeO_2 since BET surface area of AZT is much higher than these supports (refer to Section 4.2.7.1).

3.3.2.6. Preparation of Ni/AZT. 1 gram of 5 wt.% Ni/AZT catalyst was prepared following the same procedure explained in Section 3.3.2.1. 0.95 grams of AZT and 0.2477 g Ni-precursor was used to prepare the catalyst. Amount of water necessary was slightly higher since the precursor is in solid form.

3.3.2.7. Preparation of Co/AZT. 1 gram of 5 wt.% Co/AZT was also prepared and calcined with the same procedure detailed in Section 3.3.2.1. 0.95 grams of AZT and 0.2470 grams of Co-precursor was used.

3.3.2.8. Preparation of Rh/ZT. 1 gram of 1 wt.% Rh/ZT was prepared using the steps given in Section 3.3.2.1. 0.99 grams ZT and 0.1 grams 10 wt.% Rh solution was necessary for preparation of this catalyst. Amount of deionized water necessary was slightly lower than used for Rh/AZT preparation since ZT surface area is lower than that of AZT (see Section 4.2.7.1).

3.3.3. Pretreatment of Catalysts

In heterogeneous systems, it is crucial to reduce the metal oxide sites to active metal sites *via* exposing it to H_2 at elevated temperatures. In this study, all catalysts were brought to 800 °C under N_2 flow and catalyst was reduced *in-situ* under 40 NmL

min^{-1} H_2 flow for 2 hours prior to experiments. Later, the catalyst bed temperature was allowed to cool to reaction temperature under N_2 flow.

3.4. Reactions Tests

Reactor used in experiments was a quartz tube reactor with 80 cm length and 2 cm inner diameter narrowed to 1 cm at the middle as represented in Figure 3.5. As can be seen in Figure 3.6 approximately 1 cm quartz wool was placed at the middle of the reactor and catalyst together with diluent α-Al_2O_3 which corresponds to $\sim$ 1 cm height when it is poured on top of the wool. In experiments, 20 mg of active catalyst was diluted with 700 mg of α-Al_2O_3 which was crushed to 45-60 mesh size. On the other hand, for the activity tests, 150 mg of pure active catalyst without any diluent was used. These amounts were determined to ensure bed length to particle diameter and tube to particle diameter ratios close to 35 which is adequate to assume plug flow conditions and ignore diffusion limitations [129].

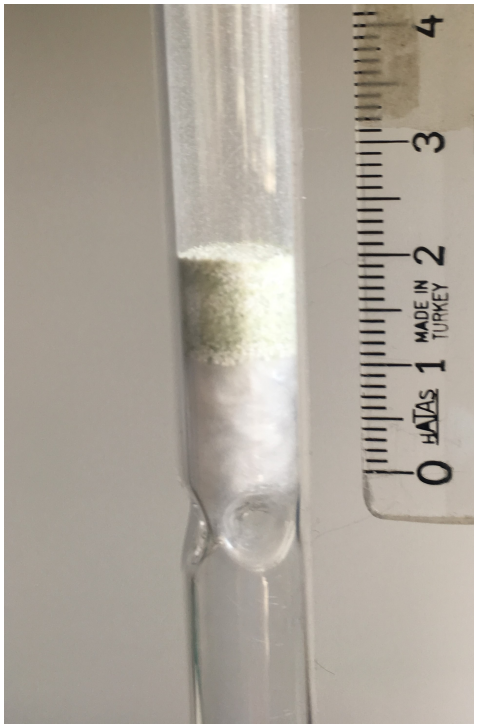

Figure 3.6. Packed middle part of the quartz reactor.

3.4.1. Activity Tests

Activity tests were performed to investigate the effect of temperature, CO_2/G and W/F ratios on CO_2 and glycerol conversions and product distributions. In all experiments, total gaseous flow rate and glycerol feed were kept constant at 40 NmL min^{-1} and 4 NmL min^{-1}, respectively. CO_2 flow rate was determined by CO_2/G ratio and flow is balanced with N_2. Parameter ranges and default values can be seen in Table 3.5. While changing a parameter, other values are kept at their default values. For instance, when temperature effect was investigated, CO_2/G ratio was kept at 4 and 20 mg of active catalyst was used. Default values are chosen so that coke formation was minimized at 750 °C and utilizing maximum amount of CO_2 at CO_2/G ratio 4. Experimental procedure followed in the tests is explained in Section 3.4.4.

Table 3.5. Reaction conditions for catalytic tests (Default values are shown in boldface).

Parameter	**Value**
Reaction Temperature (°C)	600, 650, 700, **750**
Glycerol Flow Rate (NmL min^{-1})	4
CO_2/G Feed Ratio	1, 2, 3, **4**
Catalyst Amount (mg)	**20**, 50, 100, 150
Total Flow Rate (NmL min^{-1})	40
W/F (mg min NmL^{-1})	**0.5**, 1.25, 2.5, 3.75

3.4.2. Blank Tests

Blank tests are performed in order to observe homogeneous glycerol conversions where no catalyst is packed inside the reactor. Those experiments are conducted to verify quartz reactor and wool together with catalyst diluent α-Al_2O_3 do not have catalytic activity. Blank tests are conducted at different temperatures and CO_2/G ratios (see Table 3.5) at constant total flow rate of 40 NmL min^{-1}.

3.4.3. Stability Tests

Stability tests were carried out to observe the long-term activity of the catalyst. 72 hours on-stream stability tests were conducted at 750 °C when CO_2/G and W/F ratios are 4 and 3.75 mg min NmL^{-1}, respectively. Experimental procedure detailed in Section 3.4.4 was followed and after 5 hours of operation, data was taken every 2 hours until 71st hour and last two data was taken each 30 minutes. Experiments were finalized before 72 hours if no carbon dioxide conversion was observed.

3.4.4. Experimental Procedure

Experimental procedure followed is as follows:

- Quartz reactor is loaded with quartz wool and active catalyst.
- Reactor is placed inside the furnace.
- 20 NmL min^{-1} N_2 is flowed through the reactor while leakage test with soap bubble meter and Swagelok liquid leak detector is made. Reactor effluent is directed to vent.
- Temperature controller of the furnace is adjusted to 800 °C with $\sim$ 18 °C min^{-1} ramp rate.
- For reduction, 40 NmL min^{-1} flow rate of H_2 is directed to reactor and N_2 flow is closed. Meanwhile, GC1 and GC2 are opened and they are brought to operation conditions provided in Table 3.5.
- After approximately half an hour, GC oven and detector temperatures are stabilized and therefore detectors are activated.
- When 2 h reduction is completed, N_2 flow is again allowed and H_2 flow is turned off. Reactor is allowed to cool down to reaction temperature. Meanwhile, two heating lines are turned on and N_2 flow rate necessary for the experiment is set.
- When the experimental temperature is reached, Dewar flasks are filled with ice. HPLC pump is turned on and glycerol is purged. After first drop formation, glycerol is directed to reactor. CO_2 flow rate is arranged and after 2 minutes,

CO_2 flow is allowed into the reactor. Reaction time is started and finally effluent of the reactor is directed to gas chromatographs.

- First product gas analysis is made at the 30th minute of the experiment and others are taken every 45th minute until 5 hours. Since GC2 tubing is longer the analysis is first made with GC2 then the flow is directed to GC1. Sampling is done after 2.5 minutes for each run to make sure the product is reached to GC1 sampling loop. At the end of the analysis product stream is directed back to GC2.
- After the last analysis, HPLC pump is closed and 3-way valve is turned to purge position. Temperature controller of the furnace as well as heating lines are closed. Effluent of the reactor is directed to vent. N_2 flow rate is adjusted to feed conditions and stream exiting MFCs are directed to GCs.
- After approximately 15 minutes feed data is taken from GC2. CO_2 flow is closed and N_2 is allowed through GC lines for approximately 2 minutes to sweep any impurities. Later, N_2 flow is adjusted to 20 NmL min^{-1} and directed to reactor. Reactor is allowed to cool overnight under N_2 flow.
- When the analyses in GCs are finished, their detectors are turned-off and they are allowed to cool.
- When the detector temperature is below 100 °C, GCs are turned-off together with carrier gas tanks including Ar and He.

3.4.5. Measurement of Catalytic Activities

In this study, effects of various parameters are investigated on glycerol (x_G) and carbon dioxide (x_{CO_2}) conversions, product yields and selectivities and activity loss. Carbon dioxide is one of the main reactants and its conversion is calculated using Equation 3.1.

$$x_{CO_2} = \frac{F_{CO_{2,in}} - F_{CO_{2,out}}}{F_{CO_{2,in}}} \tag{3.1}$$

Glycerol is the other reactant but calculating its conversion is relatively complicated. One of the major products in glycerol dry reforming is H_2O (consult to Equation 2.7) and there may be other side reactions that yields higher hydrocarbons that are liquid at ambient conditions. Since product analysis can only be made on gaseous species these liquid components are condensed in cold traps and therefore their compositions at the product stream cannot be detected. Thus, it is suitable to define glycerol conversion as glycerol conversion to gaseous products (x_G), but for convenience glycerol conversion is used instead of glycerol conversion to gaseous products. In calculating glycerol conversion to gaseous products, H atom balance is used considering glycerol ($C_3H_8O_3$, G) is the sole H source in the feed (others are CO_2 and N_2) [16–19, 23, 24, 102, 105]. Glycerol conversion to gaseous products can be calculated using Equation 3.2 by making balance between the flow rates H containing products that can be detected by GCs, namely H_2, CH_4, C_2H_4, C_2H_6, and glycerol feed.

$$x_G = \frac{2F_{H_2} + 4F_{CH_4} + 4F_{C_2H_4} + 6F_{C_2H_6}}{8F_{G,in}} \times 100 \tag{3.2}$$

Yield and selectivity are important indicators of catalytic activity when there is more than one reaction occurs within the system. Yield (Y_i) and selectivity (S_i) of a product are calculated using Equations 3.3 and 3.4, respectively. Yield of a species is based on moles of glycerol fed while selectivity is based on moles of glycerol converted.

$$Y_i = \frac{F_{i,out}}{F_{G,in}} \tag{3.3}$$

$$S_i = \frac{F_{i,out}}{x_G F_{G,in}} \tag{3.4}$$

4. RESULTS AND DISCUSSION

4.1. Catalysts with Single Support

Rh/ZrO_2 (RhZr), Rh/CeO_2 (RhCe), Co/ZrO_2 (CoZr) and Co/CeO_2 (CoCe) catalysts were previously investigated by our group [105]. Although 24 h stability tests were reported, all of the catalyst showed drastic decrease in catalytic activity toward the end of the tests. Therefore, in this study longer stability tests that last 72 h of these catalysts are performed and some catalyst characterization techniques are used interpret between the catalytic activities and stabilities. Stability tests are finalized for CoZr and CoCe before 72th hour since they give no carbon dioxide conversion. The results for stability tests and catalyst characterizations are reported in the Sections 4.1.1 and 4.1.2, respectively.

4.1.1. Stability Tests

Glycerol dry reforming occurs at high temperatures to overcome thermodynamic restrictions. Harsh conditions cause catalysts to deactivate especially due to metal sintering and coke formation. Specifically glycerol dry reforming conditions are prone to coke deposition onto catalyst surface than steam and/or oxidative steam reforming of glycerol [13, 52, 95, 100, 130, 131].

Thermodynamically, no solid carbon formation is observed at temperatures above 650 °C when CO_2/G ratio is equal to 4 in the calculations (see Section 4.2.1.1). Catalytic activity is another determinant factor for coke deposition since coke is more easily formed when it is already deposited onto the catalyst surface [95]. Therefore, catalyst types and properties are key factor for catalyst stability.

72 h stability tests for RhZr, RhCe, CoZr and CoCe catalysts are performed and carbon dioxide and glycerol conversions with respect to ToS are provided in Figures 4.1

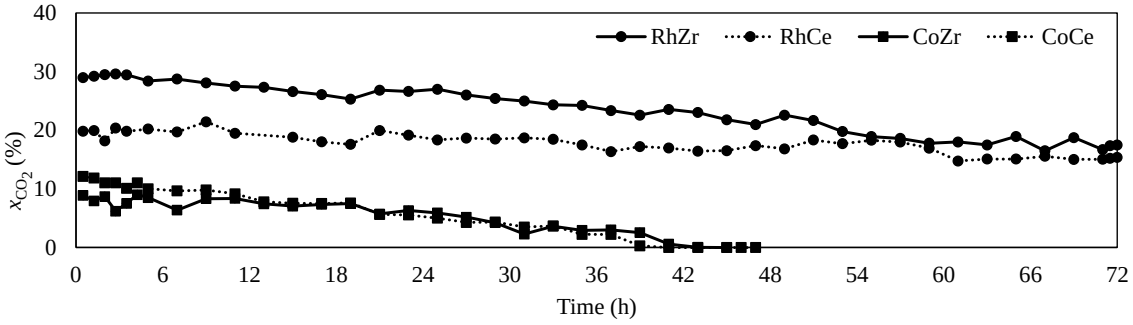

Figure 4.1. 72 h ToS CO_2 conversion of single support catalysts (T=750 °C and CO_2/G=4).

and 4.2, respectively. Although RhZr delivered high CO_2 conversions at the beginning it deactivated faster than RhCe. At the end of the longevity tests, CO_2 conversion of RhZr dropped from 29% to 17.5% corresponding to a conversion loss of 40%. On the other hand, conversion loss of RhCe is 23% from 19.8% to 15.4%. For Co samples, the deactivation was unfortunately very fast. Both CoZr and CoCe lost their catalytic activity completely before 42nd hour and the rate of deactivation seemed to be the same. This suggests that stability of glycerol dry reforming catalysts does not directly depend on active metal or support but on the interaction between them.

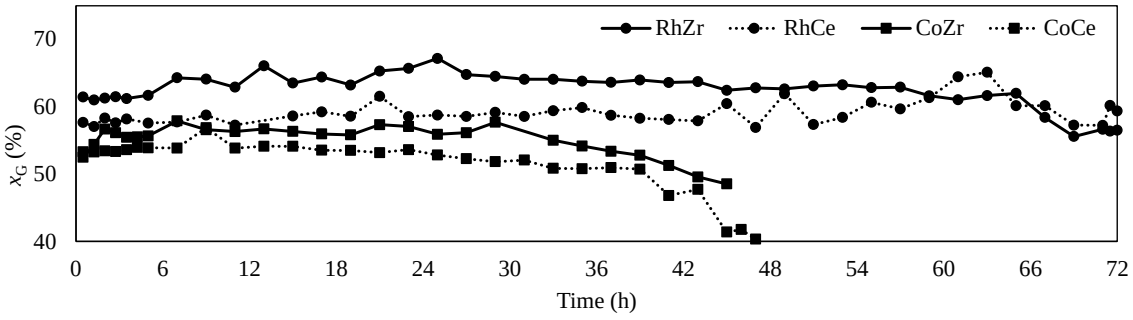

Figure 4.2. 72 h ToS glycerol conversion of single support catalysts (T=750 °C and CO_2/G=4).

Glycerol conversions of RhZr, RhCe and CoZr stayed almost constant throughout the stability tests. Glycerol conversion drops for RhZr and CoZr are 7.9% and 7.5%,

respectively; whereas glycerol conversion drops from 53.% to 40.3% that corresponds to a loss of 24.4% for CoCe. On contrary, glycerol conversion of RhCe sample increases 2.9% towards the end of the experiment from 57.7% to 59.4%. These findings reveal that CO_2 conversion, which is interestingly not reported at all in the GDR literature, is more sensitive to catalyst deactivation; and, hence a better metric to monitor catalyst stability. Higher glycerol stability suggests glycerol is rather converted by thermal decomposition reactions (Equations 2.8, 2.10, 2.11 and 2.12) rather than its dry reforming reaction (Equation 2.7). However, further decrease in CO_2 conversions cause (consult to Co catalysts in Figures 4.1 and 4.2) a significant decrease in glycerol conversion due to almost complete deactivation of catalysts into a point where they cannot catalyze high hydrocarbons (probably liquid at ambient conditions) produced by thermal decomposition of glycerol (Equations 2.10 and 2.11).

Product yields and selectivities at selected time intervals (0.5^{th}, 13th, 25th, 37th, 49th, 61st and 72nd) are present in Tables 4.1 and 4.2, respectively. H_2 and CO yields of all catalyst are monotonically diminished due to severe catalytic activity losses. Though, H_2/CO ratio is fluctuated around the same values, *i.e.* between 0.71 and 0.79 for RhZr. For RhZr and RhCe, CH_4 yields increased in time, suggesting the increasing extents of methanation reactions. Since H_2/CO ratio and glycerol conversions are approximately constant while CO_2 conversion is dropped, most possible reaction producing methane is dry methane reforming (Equation 2.18). As catalytic activity is hindered, DRM reaction cannot proceed to its extent and therefore CO_2 conversion is decreased and CH_4 yield is increased while H_2/CO ratio and glycerol conversion are kept constant. Only hydrocarbons that can be detected from gas chromatography used in experiments are CH_4 C_2H_4 and C_2H_6 which all indicate activity loss but they are not the only metrics. Although no methane, ethane or ethylene yields are observed over RhZr, its stability is significantly decreased. However, increasing yields of ethane and ethylene over Co catalysts support the extinction of CO_2 conversions.

Stability tests for Rh and Co catalyst supported ZrO_2 and CeO_2 showed significant activity losses. The most stable catalyst is found to be RhCe although it has lower

Table 4.1. Product yields over single support catalysts.

	t (h)	Y_{H_2}	Y_{CO}	Y_{CH_4}	$Y_{C_2H_4}$	$Y_{C_2H_6}$	H_2/CO	x_{CO_2}	x_G
RhZr	0.5	2.45	3.26	0.00	0	0	0.75	29.0	61.4
	13	2.60	3.33	0.02	0	0	0.78	27.3	66.1
	25	2.58	3.26	0.05	0	0	0.79	27.0	67.2
	37	2.36	3.01	0.09	0	0	0.78	23.4	63.6
	49	2.23	2.96	0.14	0	0	0.75	22.6	62.6
	61	2.08	2.84	0.18	0	0	0.73	18.0	61.0
	72	1.87	2.65	0.19	0	0	0.71	17.5	56.5
RhCe	0.5	2.01	2.87	0.15	0	0	0.70	19.8	57.7
	13	1.90	2.80	0.22	0	0	0.68	18.8	58.6
	25	1.86	2.75	0.24	0	0	0.67	18.3	58.8
	37	1.82	2.70	0.26	0	0	0.67	16.4	58.7
	49	1.89	2.74	0.28	0	0	0.69	16.8	61.9
	61	1.89	2.70	0.33	0	0.01	0.70	14.8	64.4
	72	1.74	2.58	0.30	0	0.01	0.67	15.4	59.4
CoZr	0.5	1.41	2.06	0.32	0.01	0.01	0.68	8.9	52.5
	13	1.56	2.15	0.33	0.01	0.01	0.73	7.4	56.7
	25	1.51	2.02	0.33	0.02	0.01	0.75	5.9	55.9
	37	1.35	1.80	0.34	0.03	0.01	0.75	3.0	53.4
	45	1.09	1.58	0.36	0.05	0.01	0.69	0	48.5
CoCe	0.5	1.49	2.39	0.31	0.01	0.01	0.62	12.1	53.3
	13	1.46	2.21	0.32	0.02	0.01	0.66	7.8	54.1
	25	1.38	1.99	0.32	0.03	0.01	0.69	5.0	52.8
	37	1.26	1.82	0.33	0.04	0.01	0.69	2.2	50.9
	47	0.77	1.35	0.33	0.07	0.01	0.57	0	40.3

Table 4.2. Product selectivities over single support catalysts.

	Time (h)	$\mathbf{S_{H_2}}$	$\mathbf{S_{CO}}$	$\mathbf{S_{CH_4}}$	$\mathbf{S_{C_2H_4}}$	$\mathbf{S_{C_2H_6}}$
RhZr	0.5	3.99	5.30	0.01	0	0
	13	3.93	5.04	0.04	0	0
	25	3.84	4.86	0.08	0	0
	37	3.71	4.74	0.14	0	0
	49	3.55	4.72	0.22	0	0
	61	3.40	4.65	0.29	0	0
	72	3.31	4.68	0.33	0.01	0
RhCe	0.5	3.48	4.98	0.26	0	0
	13	3.25	4.78	0.37	0	0
	25	3.16	4.68	0.41	0	0
	37	3.09	4.60	0.44	0	0.01
	49	3.06	4.43	0.46	0	0.01
	61	2.94	4.19	0.51	0.01	0.01
	72	2.93	4.35	0.51	0.01	0.01
CoZr	0.5	2.69	3.92	0.61	0.02	0.02
	13	2.75	3.79	0.58	0.02	0.01
	25	2.70	3.61	0.59	0.03	0.02
	37	2.53	3.37	0.64	0.06	0.02
	45	2.24	3.26	0.73	0.11	0.02
CoCe	0.5	2.79	4.49	0.58	0.01	0.01
	13	2.70	4.09	0.60	0.03	0.02
	25	2.61	3.77	0.62	0.05	0.02
	37	2.48	3.57	0.65	0.07	0.02
	47	1.91	3.34	0.82	0.18	0.03

catalytic activity than RhZr at the beginning. Co catalysts are completely deactivated before 72 h.

4.1.2. Catalyst Characterizations

Different catalyst characterization techniques are used to understand surface chemistry and morphology of the Rh catalysts and carbon formations on them. Fresh samples that are only reduced by H_2 at 800 °C for 2 h, 5 h spent samples that are used in activity tests and 72 h spent samples used in stability tests are investigated with TEM, EDX, FTIR and Raman techniques.

4.1.2.1. TEM and EDX Measurements. Fresh and 5h spent samples of RhZr and RhCe catalysts are investigated through TEM and EDX analyses in order to have an insight on catalyst morphology and composition.

Representative TEM and HR-TEM images of fresh RhZr sample are shown in Figure 4.3. Both images support good dispersion of distinct Rh particles on the ZrO_2 support. Average particle size of the nanoparticles are estimated to be 2.1 nm (± 0.4 nm) *via* ImageJ software. STEM-EDX results shown in Figure 4.4 for the same catalyst validate the existence of Rh and Zr atoms and absence of any other impurities. TEM and HR-TEM images for 5 h spent RhZr sample are shown in Figure 4.5. The images indicate that Rh nanoparticles are sintered and grew bigger with average particle size of 4.1 nm (± 1.1 nm). Similar to fresh sample of RhZr, 5 h spent sample is investigated in STEM-EDX shown in Figure 4.6 and results are approximately the same, supporting the existence of Rh and Zr.

Analogous to RhZr, TEM and HR-TEM and STEM-EDX results of both fresh and 5 h spent samples of RhCe are provided in the Figures 4.7, 4.8, 4.9 and 4.10, respectively. HR-TEM images of both samples indicate the geometry of Rh particles as truncated cubo-octahedal whereas CeO_2 has an ordered structure. Estimated Rh particles sizes of fresh and 5 h spent samples of RhCe are 3.5 nm (± 0.6 nm) and 3.4

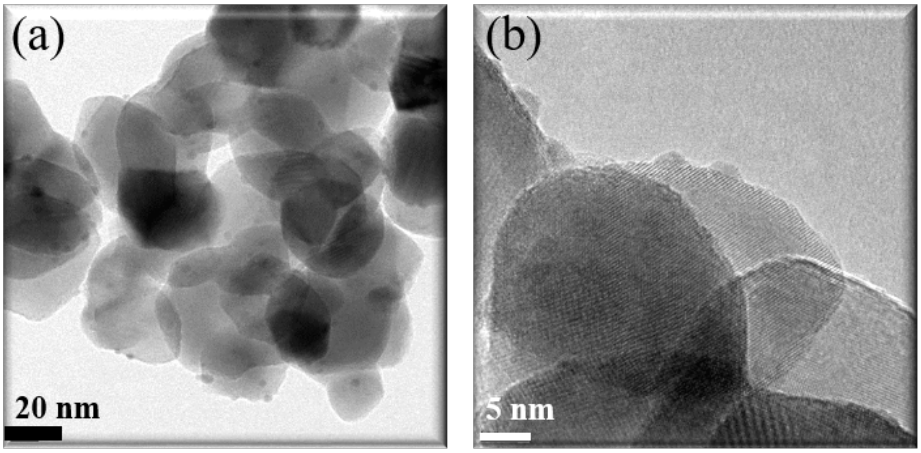

Figure 4.3. TEM (a) and HR-TEM (b) of fresh Rh/ZrO_2 catalyst.

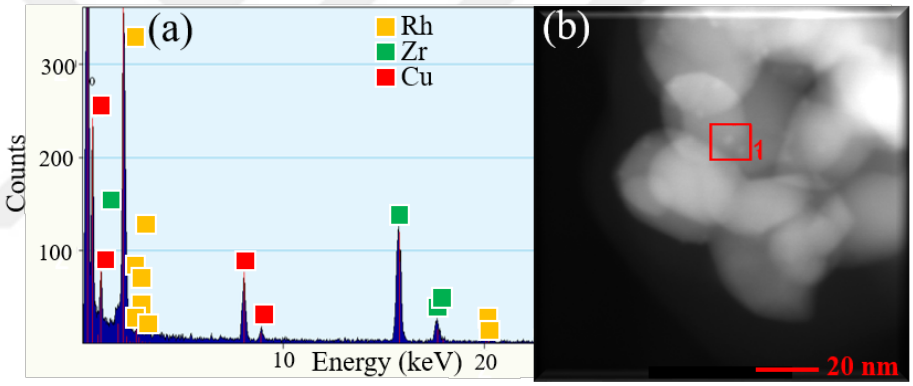

Figure 4.4. STEM-EDX analysis of fresh Rh/ZrO_2 catalyst.

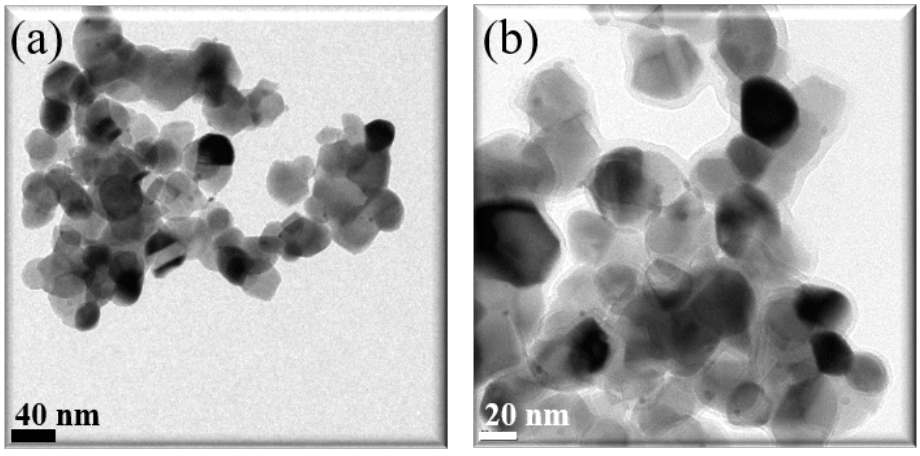

Figure 4.5. TEM (a) and HR-TEM (b) of 5 h spent Rh/ZrO_2 catalyst.

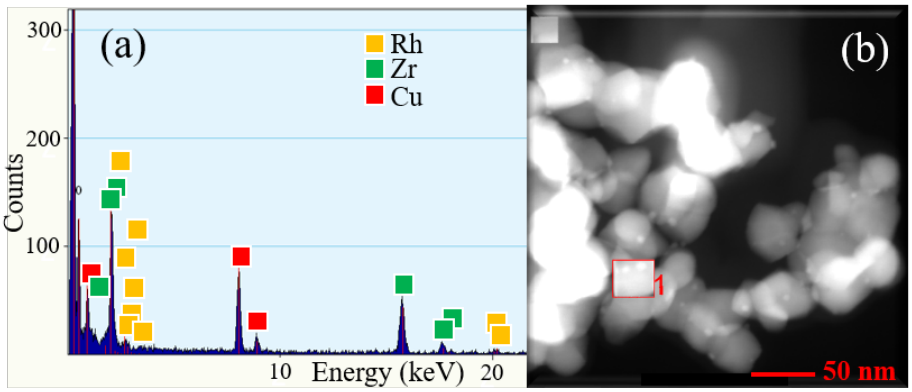

Figure 4.6. STEM-EDX analysis of 5 h spent Rh/ZrO_2 catalyst.

nm (± 1.3 nm), respectively. It is evident that Rh and Ce exists in catalyst structure as demonstrated in STEM-EDX results of both fresh and 5 h spent samples of RhCe.

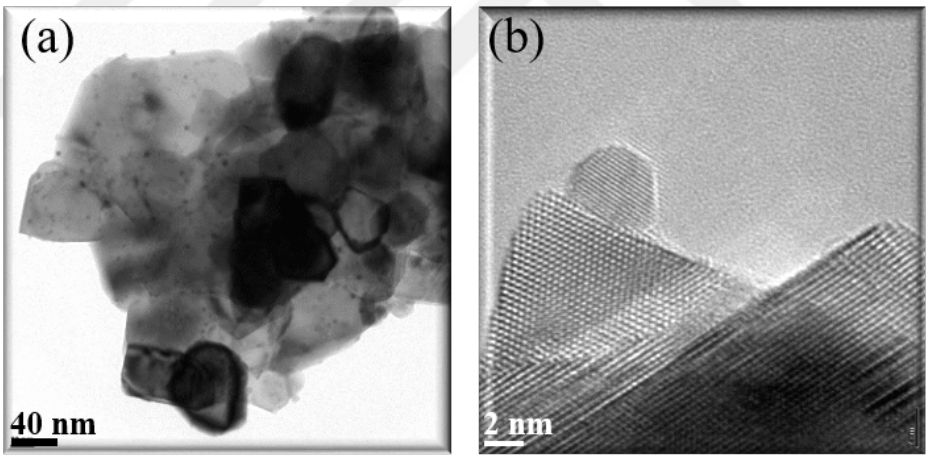

Figure 4.7. TEM (a) and HR-TEM (b) of fresh Rh/CeO_2 catalyst.

Comparing the average Rh particle sizes in each sample, it is possible to state that active metal on CeO_2 resisted sintering. Although average size of Rh particles in fresh RhZr is smaller than that of RhCe, they sintered relatively fast and after 5 hours on reaction conditions, they become bigger than Rh particles in 5 h spent RhCe catalyst. These findings indicate strong interaction between Rh and CeO_2 which hinders the mobility of Rh atoms on the support.

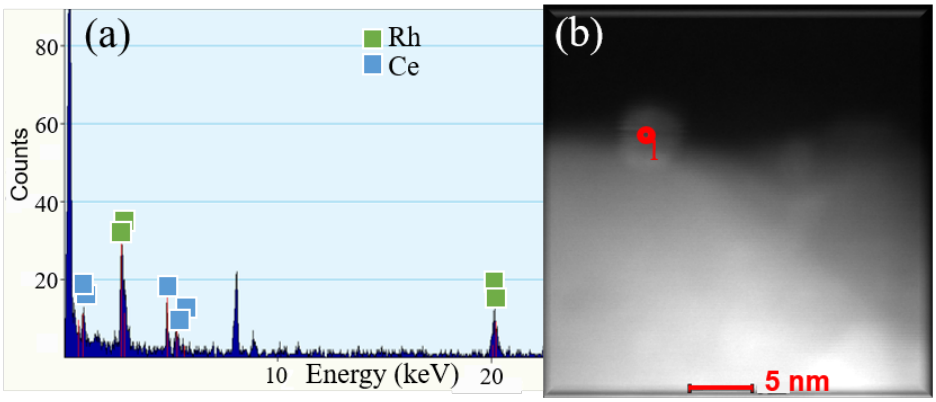

Figure 4.8. STEM-EDX analysis of fresh Rh/CeO_2 catalyst.

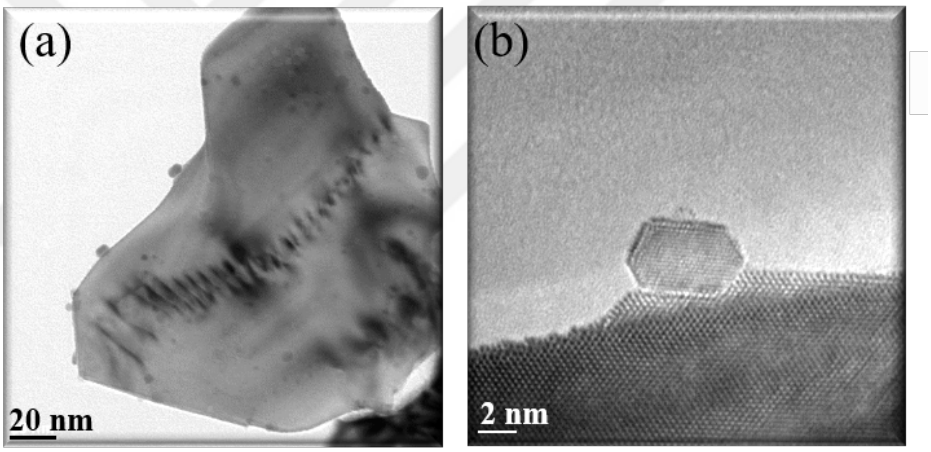

Figure 4.9. TEM (a) and HR-TEM (b) of 5 h spent Rh/CeO_2 catalyst.

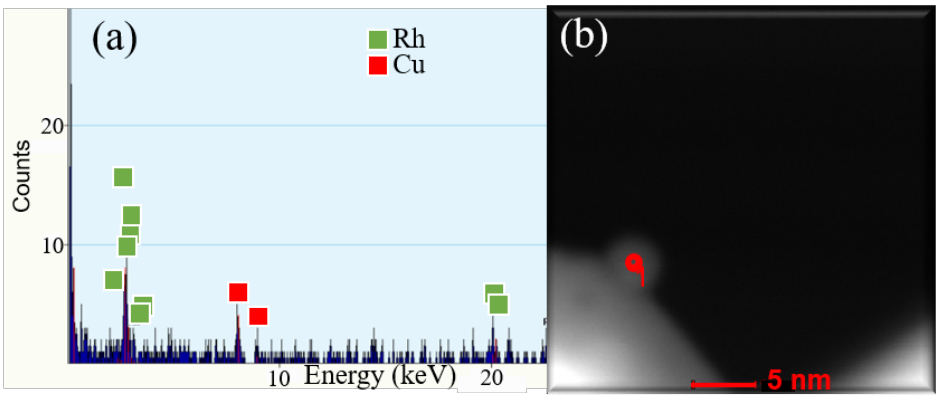

Figure 4.10. STEM-EDX analysis of 5 h spent Rh/CeO_2 catalyst.

4.1.2.2. *In-situ* FTIR Spectroscopic Measurements. *In-situ* FTIR characterizations of fresh, 5 h and 72 h spent samples of RhZr and RhCe can be seen in Figure 4.11. CO(g) is used as a probe molecule to investigate properties of Rh particles and their interaction with supports ZrO_2 and CeO_2. Before the acquisition of the 72 h spent catalyst spectra, catalysts were treated with 10 Torr H_2(g) at 300 °C for 10 min followed by cooling to 25 °C and evacuation. Three different forms of Rh, namely Rh^0, Rh^+ and Rh^{3+} can be present on supports. Rh^{3+} state is possible due to Rh(III) nitrate hexahydrate precursor used in catalyst preparation. Though, it is challenging to detect this form since during *in-situ* FTIR analysis, oxide ions coordinated to Rh^{3+} can be consumed to produce CO_2 from CO and therefore reduce Rh^{3+} to Rh^+.

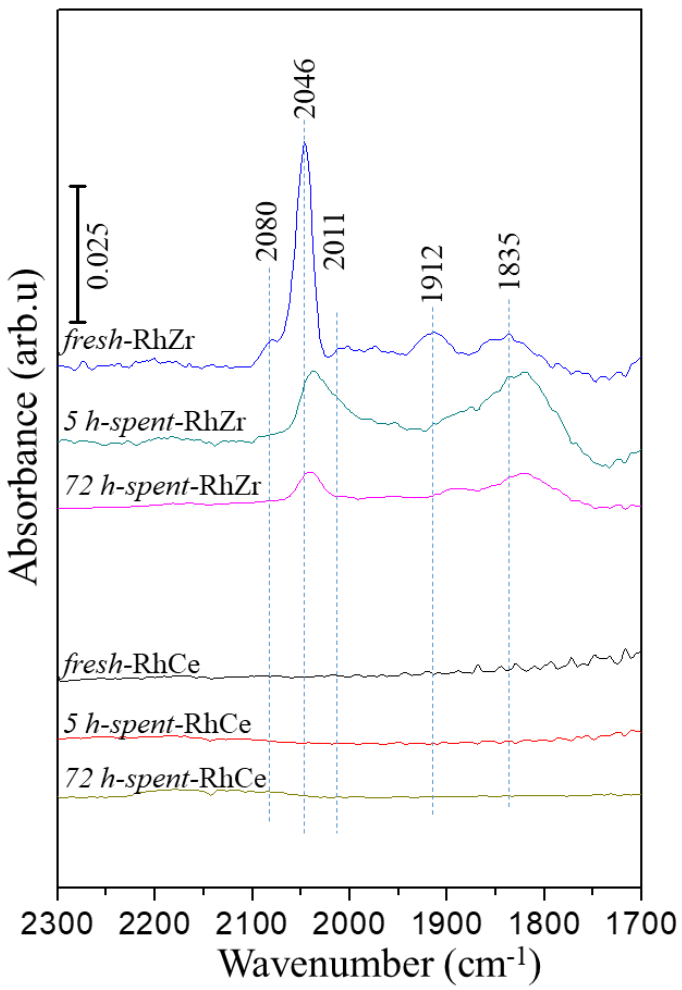

Figure 4.11. *In-situ* FTIR spectra corresponding to 10 Torr CO(g) adsorption at 25 °C for 10 min on fresh, 5 h and 72 h spent RhZr and RhCe.

Spectrum at the top of Figure 4.11 that corresponds to fresh RhZr sample, gives strong vibrational features that is related with CO(*ads*). Vibrations at 2090 and 2011 cm^{-1} are related to the symmetric and asymmetric stretching whereas steep peak at 2048 cm^{-1} is associated with CO(*ads*) on metallic Rh particles. Signals at lower frequencies, namely 1912 and 1835 cm^{-1} can be attributed to CO(*ads*) on two- and three-fold metallic Rh sites, respectively. It is also possible to conclude that both Rh and Rh^{+} corresponding to metallic and oxide Rh sites are present in fresh RhZr sample. Two possible explanations are proposed that oxygen is exchanged between ZrO_2 lattice and Rh^{+} sites and/or gas phase oxygen is generated during calcination procedure. Another information deducted from *in-situ* FTIR results is in accordance with TEM results provided in Section 4.1.2.1. IR bands at 2046, 1912 and 1835 cm^{-1} suggest high concentration of point defects that favor linear CO(*ads*) which means small Rh particles are finely dispersed on ZrO_2 support as verified with TEM analysis.

Figure 4.11 also reveals *in-situ* FTIR spectrum of 5 h spent RhZr. When compared to fresh sample result, peak at 2046 cm^{-1} is drastically reduced, while bands related to CO(*ads*) on Rh sites grew in intensity. Possible reasons for the attenuated Rh-CO feature may be carbon deposition or sintering of Rh particles to bigger sizes which support the average particle size increase of approximately 2 nm as reported in TEM results in Section 4.1.2.1.

Vibrations observed in fresh and 5 h spent samples of RhZr flattens when the catalyst is spent for 72 h due to severe deactivation and coke deposition. Therefore, catalyst was treated with H_2 at 300°C in order to gasify coke to provide Rh sites that could be used in *in-situ* FTIR analysis. The result is shown in Figure 4.11 along with other RhZr and RhCe samples. Peak intensities further decreased when compared to fresh and 5 h spent RhZr samples which indicates sintering of Rh particles as concluded from TEM results in Section 4.1.2.1.

Analogous *in-situ* FTIR spectra of fresh, 5 h and 72 h spent RhCe samples are shown in Figure 4.1.2.2. As detailed before in this section, 72 h spent sample

is pretreated for coke removal. None of the RhCe samples revealed any CO(ads) vibrational signals which is interesting for fresh sample since it cannot deposit any coke. The findings imply exposed Rh sites are not present on ceria support but rather CeO_2 covered Rh particles. Strong chemical bonds between ceria and precious metals may embed metal particles inside the ceria lattice and reaction rate can be increased 100 folds [132, 133]. Therefore, high stability of RhCe can be attributed to strong Rh-Ce interactions as proposed in Section 4.1.1. This SMSI may lead formation of Rh-O-Ce type surface species which cannot be detected by further CO(g) adsorption. Additionally, CO(g) can be adsorbed on ceria in forms of carbonates, carboxylates and formates which have vibrational features below 1800 cm^{-1}. But since carbonyl region is investigated in this study these forms of CO(g) are not reported.

Information regarding the aging and coking of spent catalysts can be obtained by comparing vibrational features by *in-situ* FTIR of 5 h spent RhZr and RhCe catalysts before and after treatment with H_2. The non-treated 5 h spent samples are used as background spectra and results obtained with treated samples are subtracted from this spectra. This difference give the loss of carbonaceous species through H_2 treatment. The results are shown in Figure 4.12. RhCe show no significant changes in the 1800-1000 cm^{-1} region where the spectrum is multiplied by 5. Coke is expected in this region whereas O–H formation is expected in 3600-3000 cm^{-1} region which is a positive feature. Thus, from Figure 4.12 5 h spent RhCe catalyst is mostly coke free and can generate atomic hydrogen adsorbed on Lewis basic sites (*i.e.* O^{-2}) of ceria.

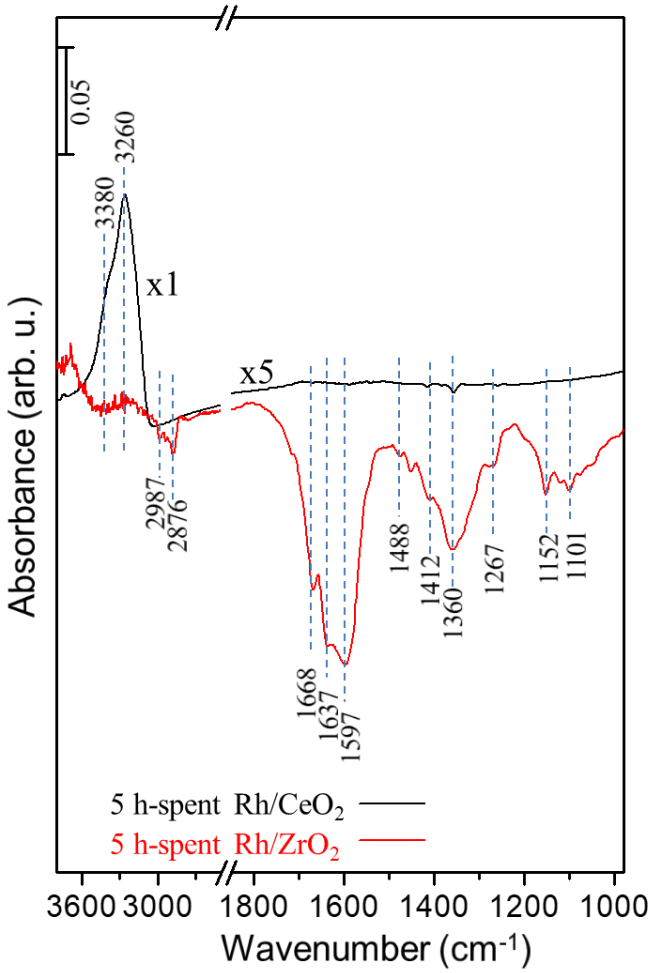

Figure 4.12. *In-situ* FTIR spectra of 5 h spent RhZr and RhCe catalysts obtained after treatment with 10 Torr H_2(g) at 300 °C for 10 min followed by cooling to 25 °C and evacuation.

On contrary to RhCe, RhZr showed strong negative vibrations within the range of 1800-1000 cm^{-1} and also 3000-2850 cm^{-1}. Due to fluctuations, it is not easy to depict the species corresponding to peaks. But it is obvious that severe amount of coke is deposited onto 5 h spent RhZr which explains the high activity loss during 72 h longevity runs explained in detail in Section 4.1.1.

Differences in CO(g) adsorption and associated vibrational features of RhZr and RhCe are related with the differences between Rh particle sizes, their dispersion and interaction with supports. SMSI within RhCe sample is found by *in-situ* FTIR analysis. Comparison between post H_2 treated and direct 5 h spent sample of RhZr revealed the severity of coke deposition within 5 h long experiments.

4.1.2.3. *Ex-situ* Raman spectroscopic experiments. *Ex-situ* Raman experiments are performed to attain further understanding about the structural properties of fresh and 5 h spent RhZr and RhCe catalysts. *Ex-situ* Raman spectra for RhZr can be seen in Figure 4.13. The feature at 173 cm^{-1} indicates RhO_x which is in line with *in-situ* FTIR investigations explained in Section 4.1.2.2 where presence of oxidic Rh^+ are mentioned [134]. Signals at 325, 468 and 611 cm^{-1} characterize tetragonal-ZrO_2 whereas signals at 211, 367 and 548 cm^{-1} indicate monoclinic-ZrO_2 [119]. Red Raman spectrum of 5 h spent RhZr sample is a clear indication of fluorescence which overwhelms most of the Raman signals due to coke deposition. Thus, photoleaching was performed to remove this coke and blue Raman spectrum is the result of this sample. High similarity between fresh Rhzr and photoleached 5 h spent RhZr shows that deposited coke can be almost completely removed *via* photoleaching.

Ex-situ Raman experiment for RhCe samples are provided in Figure 4.14. Signal at $\sim$ 462 cm^{-1} is expected the most since it characterize stoichiometric CeO_2. But *ex-situ* Raman spectra for RhCe shows a peak at 454 cm^{-1} with 9 cm^{-1} shift. This shift is related with ceria unit cell expansion due to formation of Ce^{3+} ions by reduction of Ce^{4+} in the literature [135]. Fresh RhCe showed two weaker and broader features at 240 and 571 cm^{-1} corresponding to oxygen vacancies and defects in ceria lattice. These defects

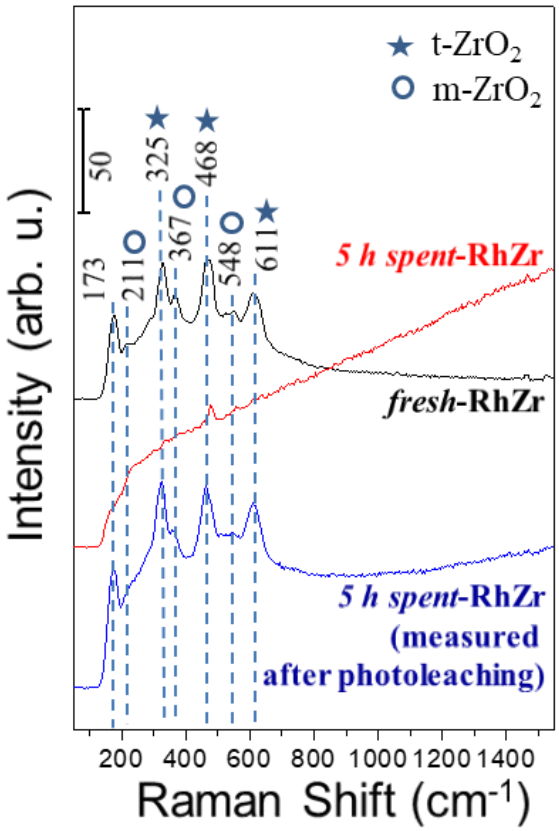

Figure 4.13. *Ex-situ* Raman spectra for fresh (black), 5 h spent (red) and 5 h spent and successively photobleached (blue) RhZr.

may be resulted due to Rh incorporation since there is strong Rh ceria interaction or due to reduction of H_2 which is a standard procedure prior to both activity and stability tests. Finally, there is a feature at 167 cm^{-1} in *ex-situ* Raman spectra of RhCe that ascribes defects in ceria lattice or Rh–O–Ce species. There are significant changes in spectra when catalyst is exposed to 5 h glycerol dry reforming conditions. This finding indicates oxygen vacancies and defects are fixed. Mars and Van Krevelen mechanism may be proposed to frequency shift towards 462 cm^{-1} [136]. The mechanisms suggests that products may leave the catalyst surface with constituents belonging to catalysts lattice. For RhCe sample, deposited carbon may be oxidized by mobile lattice oxide ions and those formation of those ions are aided by Rh corporation to ceria.

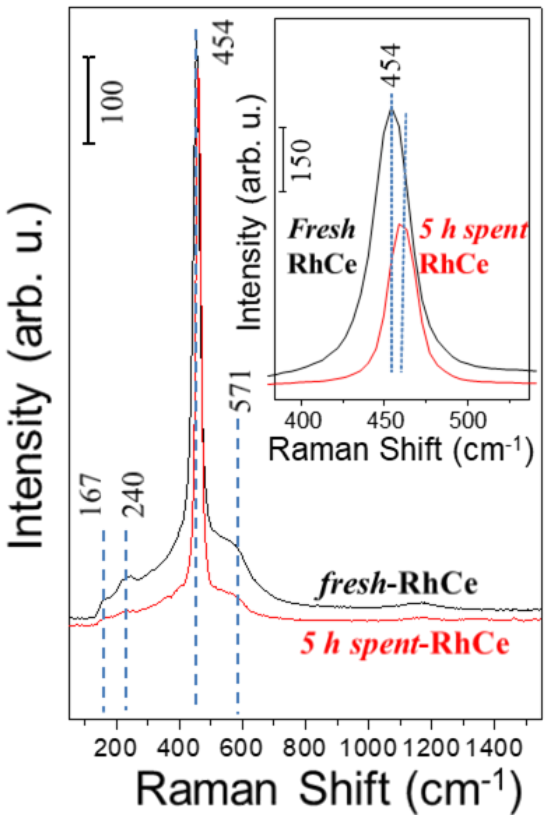

Figure 4.14. *Ex-situ* Raman spectra for fresh (black) and 5 h spent (red) RhCe.

Ex-situ Raman spectra of RhZr revealed that the catalyst is severely effected by coke deposition. While same characterization method affirms the strong metal-support interactions between Rh and ceria.

4.2. Catalysts with Binary and Ternary Supports

4.2.1. Effect of Reaction Temperature

Reaction temperature is one the most important parameter that determines the reaction rates due to kinetics and thermodynamics. Considering the fact that glycerol dry reforming is highly endothermic in nature, temperature effect should not be ignored. Therefore, temperature effect is investigated at four different values of 600, 650, 700 and 750 °C on glycerol and CO_2 conversions, as well as product yields and selectivities. In order to explore the results further, a thermodynamic study is made utilizing Gibbs free energy minimization *via* chemical process simulation software.

4.2.1.1. Thermodynamic Analysis. Thermodynamic limits at different reaction temperatures are determined *via* CHEMCAD 7.1.4 software. For this purpose, a unit named Gibbs free energy reactor (GIBS) is utilized at certain inlet conditions (CO_2/G=4, total flow rate 40 NmL min^{-1} and varying temperatures). Components taken into consideration are selected by examining possible reaction routes and reactions detailed in Section 2.2. Those are: $C_3H_8O_3$, CO_2, N_2, H_2, CO, H_2O, CH_4, C_2H_4, C_2H_6, C_3H_6O (acetol, allyl alcohol and propionaldehyde), C_3H_4O (acrolein), C_2H_4O (acetaldehyde), C_2H_6O (ethanol) and finally C(s). It is also important to state that in these investigations reactant-product mixtures are assumed to be in touch with catalyst bed for a very long time interval, in other words, W/F ratios are going to infinity.

Four different temperatures as mentioned in Section 4.2.1 are simulated and the resulting product yields and selectivity values are tabulated in Tables 4.3 and 4.4, respectively. The absence of products (except C(s), see Figure 4.15) in Tables 4.3 and 4.4 mean that their existence at the reactor effluent is not thermodynamically favored. In other words, no glycerol, acetol, allyl alcohol, propionaldehyde, acrolein, acetaldehyde or ethanol is present in the product stream, independent of temperature. Literal glycerol conversion is 100% at each temperature since glycerol is absent in downstream of the reactor, but glycerol conversion to gaseous products as defined in

this study is lower than 100% since this conversion do not take water into account. Complete consumption of glycerol was also reported in a previous study by Wang *et al.* [95] in which Gibbs free energy minimization was employed (refer to Section 2.2).

Table 4.3. Thermodynamic product yields at different temperatures.

T (°C)	$\mathbf{Y_{H_2}}$	$\mathbf{Y_{CO}}$	$\mathbf{Y_{CO_2}}$	$\mathbf{Y_{CH_4}}$	$\mathbf{Y_{H_2O}}$	$\mathbf{H_2/CO}$	$\mathbf{x_{CO_2}}$ (%)	$\mathbf{x_G}$ (%)
600	2.23	2.16	3.70	0.16	1.46	1.03	7.7	63.6
650	2.71	3.85	3.05	0.11	1.07	0.70	23.9	73.2
700	2.75	4.15	2.84	0.02	1.20	0.66	29.2	70.1
750	2.67	4.30	2.70	0.01	1.32	0.62	32.7	67.1

Table 4.4. Thermodynamic product selectivity values at different temperatures.

T (°C)	$\mathbf{S_{H_2}}$	$\mathbf{S_{CO}}$	$\mathbf{S_{CO_2}}$	$\mathbf{S_{CH_4}}$	$\mathbf{S_{H_2O}}$
600	3.51	3.40	5.83	0.25	2.29
650	3.70	5.26	4.17	0.15	1.46
700	3.93	5.92	4.05	0.04	1.71
750	3.98	6.42	4.03	0.01	1.96

Thermodynamically, increasing temperature increases both hydrogen and carbon monoxide yields while increase in latter is steeper. Thus syngas (H_2/CO) ratio decreases from 1.03 to 0.62 as temperature increases from 600 to 750 °C. This inverse relation is also reported in some of the glycerol dry reforming studies that focuses on thermodynamics [13, 95]. Additionally, increase in reaction temperature always increases CO_2 conversion, whereas glycerol conversion shows a maximum at $\sim$ 650 °C.

Solid carbon C(s) formation on the catalyst surface is critical since it significantly decreases the catalytic activity. Figure 4.15 shows decreasing moles of solid carbon at the exit of GIBS reactor simulated in CHEMCAD due to increase in temperature. No carbon is formed after $\sim$ 650 °C as extensively mentioned in the literature [13, 95].

Nevertheless, it is important to mention that amount of solid carbon determined *via* experiments is almost always higher than predictions since once a carbonaceous species is formed on the catalyst surface, it is easier to carbon to accumulate on top of it [95]. Methane is also another indicator of carbon and catalyst deactivation and its formation can be hindered by increasing temperature as demonstrated in Tables 4.3 and 4.4.

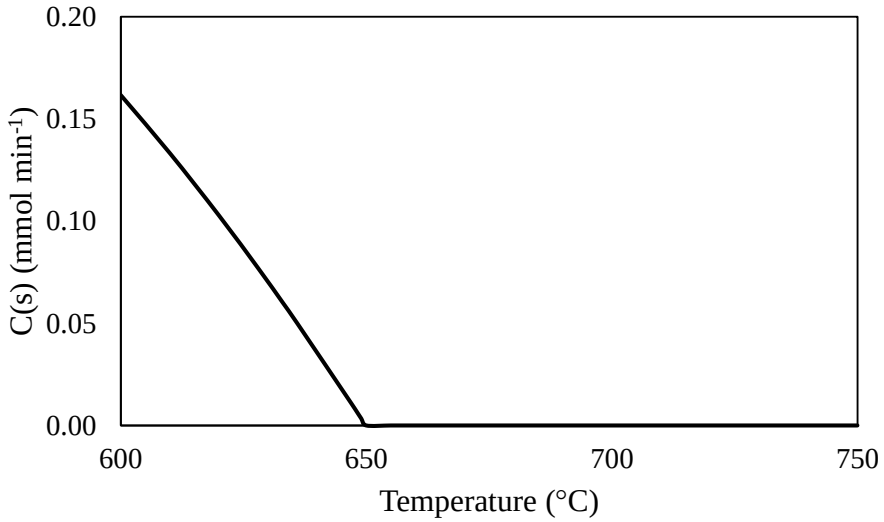

Figure 4.15. Thermodynamic limits of solid carbon formation with respect to reaction temperature (CO_2/G=4).

4.2.1.2. Activity Tests. Carbon dioxide conversions of Rh/AZT (RhAZT), Co/AZT (CoAZT), Ni/AZT (NiAZT) and Rh/ZT (RhZT) along with thermodynamic barrier (referred as equilibrium) at varying temperatures can be seen in Figure 4.16. CO_2 conversion is positively related with temperature and conversion is not observed at 600 °C regardless of catalyst. Although not represented in the corresponding figure, no CO_2 conversion is observed in blank experiments regardless of reaction temperature. There is significant increase in thermodynamic CO_2 conversion from 600 to 650 °C whereas this increase is seen between 650 and 700 °C in the experiments. A possible explanation is the severe carbon deposition onto catalyst surfaces and thermodynamics underestimates the activity loss. Highest CO_2 conversions are obtained at the highest investigated temperature, 750 °C for all catalysts where the results get closer to thermodynamic barrier. Rh/AZT seems to be the most active catalyst among oth-

ers followed by Ni/AZT and then Rh/ZT at every temperature that carbon dioxide conversion can be reported.

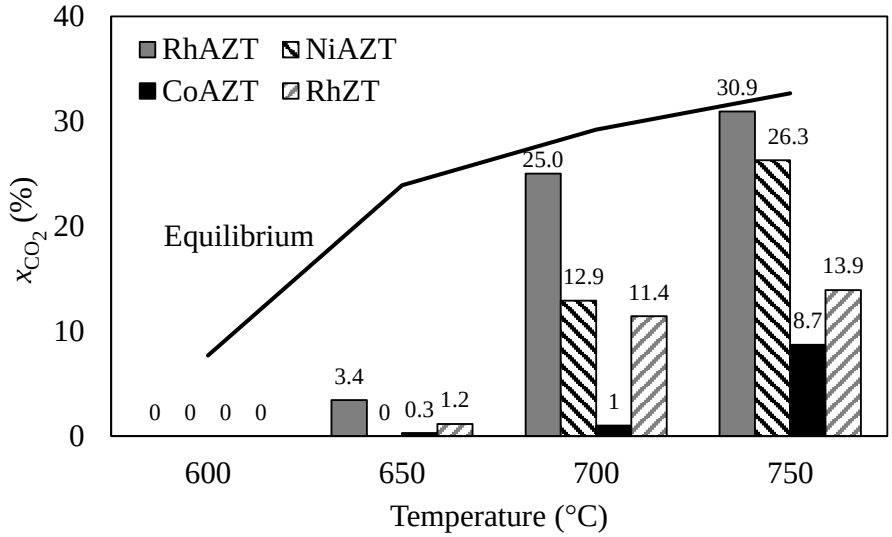

Figure 4.16. Thermodynamic and experimental CO_2 conversions with respect to temperature at CO_2/G=4.

Reactions dominating at higher temperatures are RWGS (Equation 2.9) and methane dry reforming (Equation 2.18). Apart from explaining CO_2 consumption, RWGS reaction causse an increase in CO amount while H_2 is decreased which causes H_2/CO ratio to decrease (see Table 4.6) as temperature is increased. Increase in H_2O amount due to RWGS reaction may trigger the steam reforming of hydrocarbons (*i.e.* C_2H_4 and C_2H_6) which may explain the decrease of these components as temperature is increased. At the same time, CO_2 reforming of methane explains the reduction in methane amount with temperature. At lower temperatures it is possible to state CO decomposition (Boudouard reaction - Equation 2.20) takes place which contributes to solid carbon formation as well.

Glycerol conversion to gaseous products is another indicator of catalytic activity. It is important to mention glycerol conversion can also be observed in the experiments where catalysts is not used since glycerol is a thermally unstable molecule that can

easily decompose at elevated temperatures. Thus, blank tests are performed to evaluate the homogeneous glycerol conversion values. Glycerol conversions of binary and ternary support catalysts together with blank tests can be seen in Figure 4.17. Unlike thermodynamic CO_2 conversion, glycerol conversion increases to a maximum value at temperature $\sim$ 650 °C and then starts to decrease due to increase in H_2O yield that can be seen in Table 4.3 in which thermodynamic yields of products are available. Glycerol conversion decreases as H_2O yield increases since liquid components like water are not considered in calculation of glycerol conversion (see 3.4.5). As explained previously, RWGS reaction is the major factor of the increment in water yield. Glycerol conversion to gaseous products is unaffected by methane dry reforming reaction since by definition it is calculated by hydrogen balance in gaseous stream. Homogeneous glycerol conversions obtained *via* blank tests show increasing trend with temperature, however, conversion values are always lower than glycerol conversions obtained over heterogeneous catalysts (*i.e.* with Rh/AZT, Ni/AZT, Co/AZT and Rh/ZT).

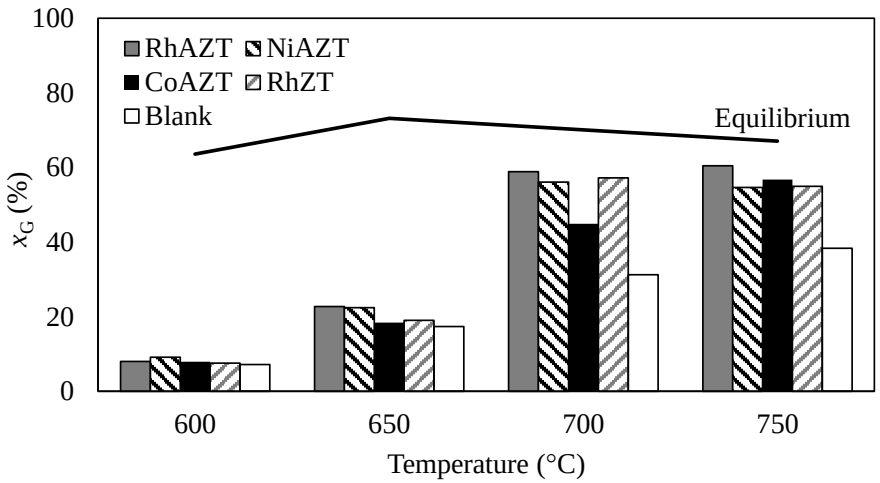

Figure 4.17. Thermodynamic and experimental glycerol conversions with respect to temperature at CO_2/G=4.

It is obvious from Figure 4.17 that glycerol conversion increases with increasing temperature for all catalysts. Though it is worth noting for Ni/AZT and Rh/ZT glycerol conversions at 750 °C are lower than those obtained at 700 °C (for more detailed

results see Table 4.5). This particular trend is similar to the thermodynamic behavior but shifted to higher temperatures. There is a significant jump of more than 30% in glycerol conversions when temperature is increased from 650 to 700 °C for Rh/AZT, Ni/AZT and Rh/ZT, whereas this jump is relatively smaller for Co/AZT with an increase of 26.5%. Rh/AZT showed higher catalytic activity at almost every temperature when compared with other catalysts, but the differences are more significant at higher temperatures when considering both glycerol and carbon dioxide conversions. The highest glycerol conversion of 60.4% is obtained with Rh/AZT at 750 °C followed by 58.9% which is also obtained with Rh/AZT at lower temperature of 700 °C. Thus, it is possible to state that Rh/AZT is catalytically more active than others by means of both glycerol and carbon dioxide conversions as well as H_2 and CO yields.

Product distributions of gaseous effluent of the glycerol dry reforming reactor is crucial in determining the catalytic activity and syngas compositions. Yield values together with H_2/CO ratios, CO_2 and glycerol conversions and selectivity values of H_2, CO, CH_4, C_2H_4 and C_2H_6 are tabuled in Tables 4.5 and 4.6, respectively. Hydrogen and carbon monoxide yields of all catalysts are increased unquestionably with increasing temperature. In fact, increasing temperature of Rh/AZT from 600 °C to 750 °C increased H_2 yield almost ten times from 0.25 to 2.41 and CO yield from 0.22 to 3.09. Since the catalysts showed more or less the same results at 600 °C, increase in product yields of Rh/AZT is reported to be the highest. Increase in syngas yields can possibly be explained with increase in the rates of glycerol decomposition reactions (Equations 2.8, 2.10, 2.11 and 2.12), 2-oxopropanol decomposition (Equation 2.14) as well as dry and steam reforming of methane (Equations 2.18 and 2.17).

Figure 4.18 and Figure 4.19 show temperature dependence of H_2 and CO yields, respectively. Although CO_2 conversions of Rh/AZT at 700 and 750 °C are very close to thermodynamic conversion values, the same thing cannot be said to H_2 and especially CO yields. The higher gap between thermodynamic barrier and CO yield cause an increase in syngas ratio of Rh/AZT sample which is 0.87 and 0.78 at 700 and 750 °C where equilibrium syngas ratios are 0.66 and 0.62, respectively. This difference

Table 4.5. Product yields over mixed support catalysts at different temperatures (CO_2/G=4).

	T (°C)	Y_{H_2}	Y_{CO}	Y_{CH_4}	$Y_{c_2c_4}$	$Y_{c_2c_6}$	H_2/CO	x_{CO_2}	x_G
RhAZT	600	0.25	0.22	0.02	0.01	0	1.13	0	8.0
	650	0.54	0.83	0.13	0.05	0.01	0.65	3.4	22.7
	700	2.32	2.67	0.02	0	0	0.87	25.0	58.9
	750	2.41	3.09	0	0	0	0.78	30.9	60.4
NiAZT	600	0.33	0.19	0	0.01	0	1.68	0	9.1
	650	0.56	0.89	0.11	0.05	0.01	0.63	0	22.4
	700	2.14	1.76	0.04	0	0.01	1.22	12.9	56.1
	750	2.16	2.57	0.01	0	0	0.84	26.3	54.7
CoAZT	600	0.24	0.26	0.02	0.01	0	0.94	0	7.9
	650	0.39	0.75	0.11	0.05	0.01	0.52	0.3	18.4
	700	1.26	1.70	0.21	0.04	0.01	0.74	1.0	44.9
	750	1.72	2.54	0.28	0.01	0.01	0.68	8.7	56.8
RhZT	600	0.23	0.20	0.02	0.01	0	1.14	0	7.5
	650	0.42	0.77	0.11	0.05	0.01	0.54	1.2	19.0
	700	1.95	2.42	0.15	0.01	0.01	0.81	11.4	57.3
	750	1.79	2.53	0.20	0	0	0.71	13.9	55.0

between thermodynamic and experimental CO yields is probably driven by carbon formation reactions that consumes CO which not only reduces the product yields, but also deactivates the catalysts.

Low hydrogen to carbon monoxide ratio (*i.e.* $H_2/CO < 2$) syngas can be used in Fisher-Tropsch synthesis (FTS) and syngas ratio of 1 can be directly used in FTS for liquid fuel production [14,116]. At low temperatures syngas ratio changed between 0.94 and 1.68 whereas at high temperatures it is changed between 0.68 and 0.84 depending on the catalyst. Considering the fact that glycerol dry reforming reaction (Equation

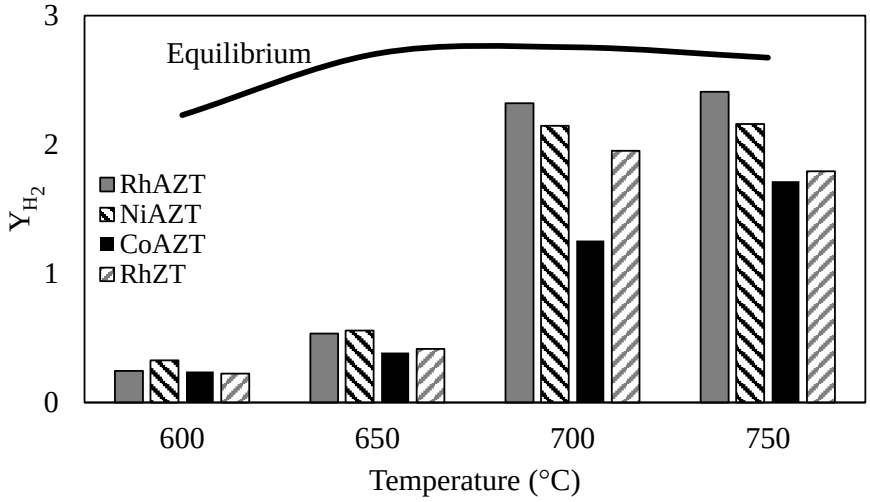

Figure 4.18. Thermodynamic and experimental H_2 yields with respect to temperature (CO_2/G=4).

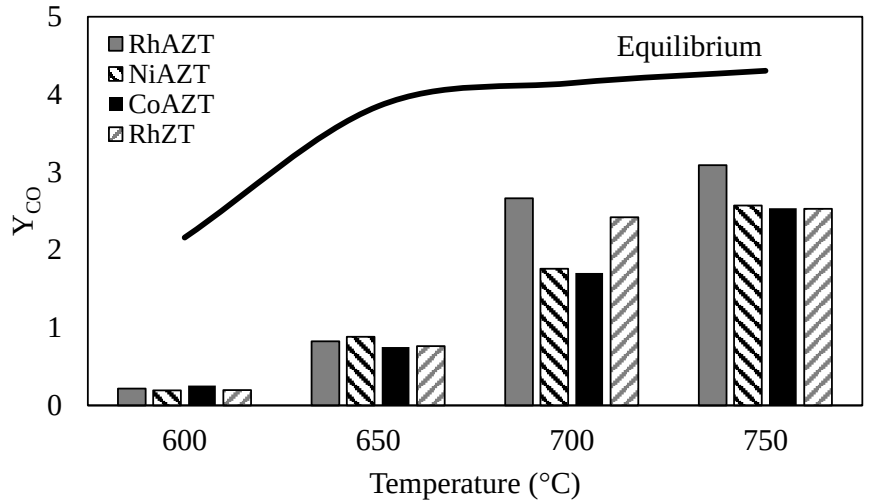

Figure 4.19. Thermodynamic and experimental CO yields with respect to temperature (CO_2/G=4).

Table 4.6. Product selectivity values over mixed support catalysts at different temperatures (CO_2/G=4).

	T (°C)	S_{H_2}	S_{CO}	S_{CH_4}	$S_{c_2c_4}$	$S_{c_2c_6}$
RhAZT	600	3.09	2.74	0.25	0.17	0.03
	650	2.36	3.64	0.55	0.20	0.04
	700	3.94	4.53	0.03	0	0
	750	3.99	5.11	0.01	0	0
NiAZT	600	3.60	2.14	0.02	0.15	0.02
	650	2.48	3.94	0.48	0.20	0.05
	700	3.82	3.14	0.07	0.01	0.01
	750	3.95	4.70	0.03	0	0
CoAZT	600	3.05	3.24	0.29	0.15	0.02
	650	2.12	4.08	0.59	0.25	0.06
	700	2.80	3.79	0.47	0.08	0.03
	750	3.02	4.46	0.48	0.02	0.01
RhZT	600	3.00	2.64	0.25	0.19	0.04
	650	2.18	4.02	0.58	0.25	0.05
	700	3.41	4.23	0.26	0.01	0.01
	750	3.26	4.60	0.36	0	0.01

2.7) produces 3 moles of H_2 and 4 moles of CO for one mole of glycerol, syngas ratio would be 0.75 if only this reaction is occurred inside the reactor. Syngas ratios higher or lower than 0.75 would therefore indicate the existence of side reactions like methanation and RWGS.

In addition to solid carbon, methane, ethane and ethylene, by-products of GDR, can be considered as the indicators of catalyst deactivation. Their existence in the product stream signals progressive deactivation. For instance, first methane is seen in product stream followed by ethylene and ethane meanwhile severe decrease in especially CO_2 conversion is observed. Thermodynamically, no ethylene or ethane is produced at

any temperature and production of solid carbon is not favored at temperatures above 650 °C. Thus, catalyst activation due to accumulation of carbonaceous species on the catalysts is the major reason for losses in catalytic activity specifically at lower temperatures. Methane concentration in the product stream of Rh/AZT and Ni/AZT catalysts first increases then decreases with increasing temperature. Whereas, in Co/AZT and Rh/ZT experiments it is observed that methane yield increase continuously with temperature. At this stage, comparing selectivity values may be more explanatory. For all catalysts, CH_4 selectivities increase between 650 and 700 °C and decrease above 700 °C. The increasing trend is though to be due to methanation and acetaldehyde decomposition reactions that are exothermic and thermodynamically favored at lower temperatures. On the other hand, endothermic steam and dry reforming seem to affect product distribution at higher temperatures, which is in perfect alignment with the thermodynamic analysis made on steam and dry reforming of methane that no reforming reactions observed at temperatures below 620 and 650 °C [34], respectively.

Consequently, higher temperatures are desired for dry reforming of glycerol due to higher catalytic activities and stabilities. The highest CO_2 and glycerol conversions of respectively 30.9% and 60.4% are achieved with Rh/AZT at 750 °C and CO_2/G ratio of 4. The highest syngas yield with ratio of 0.78 is also achieved with this catalyst at the same conditions.

4.2.2. Effect of CO_2/G Ratio

Feed composition of reactant stream has potential influence on the product distributions as well as reactant conversions. In this study, the effect of CO_2 concentration in the feed is observed by changing the CO_2/G ratios between 1 and 4 while keeping glycerol feed constant at 4 NmL min^{-1}. The ratios are adjusted so that total flow rate is 40 NmL min^{-1} and the balance is achieved by inert N_2. Similar to temperature investigations in Section 4.2.1.1, thermodynamic analysis for CO_2/G ratio is made.

4.2.2.1. Thermodynamic Analysis. Thermodynamic limits at different CO_2/G ratios are determined *via* CHEMCAD software (see Section 4.2.1.1 for details). Temperature of the system is kept constant at 750 °C while four distinct CO_2/G ratios are tested. Thermodynamic yields, H_2/CO ratios and CO_2 and glycerol conversions can be seen in Table 4.7 and thermodynamic product selectivities are available in Table 4.8. Products that are used in the simulation but not produced in the reaction simulations are not given in the table, in other words if a product is not available in Table 4.7 or Table 4.8 its yield or selectivity value is equal to zero.

Thermodynamically, increasing CO_2 amount in the feed composition suppresses both CO_2 and glycerol conversions. Yields of H_2 and CH_4 are decreased while CO and CH_4 are increased with increasing CO_2/G ratio. Similarly, in literature CO_2/G ratio of 1 is proposed to be the most suitable value [13, 17, 19, 95]. Although, this ratio is proposed to be the best one, in this study the default ratio is selected to be 4 since at this value it is possible to observe CO_2 conversions at lower temperatures (*i.e.* >650 °C)and more greenhouse gas CO_2 is consumed when inlet and outlet streams are considered.

Increase in CO_2/G ratio promotes syngas selectivity while suppressing H_2 yield. The major reaction dominating is RWGS. Increase in CO_2 amount cause a shift to H_2 and CO side of the reaction. Thus while H_2 is consumed more CO is produced and therefore H_2/CO ratio is decreased from 1.02 to 0.62 when CO_2/G ratio is changed from 1 to 4. Similar relation is also observed in the thermodynamic studies previously [13,95]. Wang *et al.* [95] reported CO_2 conversions of $\sim 35\%$ and $\sim 50\%$ at 727 °C when CO_2/G is 4 and 1, respectively. Those findings are very similar to the thermodynamic analysis results reported in this study.

CO_2/G ratio is another parameter that may affect the catalytic activity and therefore coking. Methane, which is an unwanted product that should be eliminated before Fischer-Tropsch synthesis, is affected by CO_2/G ratio. Increasing the ratio hinders CH_4 formation and therefore preferable. Although no solid carbon formation

is observed thermodynamically at 750 °C regardless of CO_2/G ratio, Freitas *et al.* [13] found that increasing CO_2/G ratio inhibits solid carbon formation. This is attributed to reduction of CO_2 into CO and oxygen which then oxides carbon deposited onto the catalyst surface.

Table 4.7. Thermodynamic product yields at carbon dioxide-to-glycerol ratios (T=750 °C).

CO_2/G	Y_{H_2}	Y_{CO}	Y_{CO_2}	Y_{CH_4}	Y_{H_2O}	H_2/CO	x_{CO_2} (%)	x_G (%)
1	3.49	3.40	0.57	0.03	0.46	1.02	43.0	88.6
2	3.17	3.78	1.22	0.01	0.80	0.84	39.3	80.0
3	2.90	4.07	1.93	0.01	1.08	0.71	35.7	73.0
4	2.67	4.30	2.70	0.01	1.32	0.62	32.7	67.1

Table 4.8. Thermodynamic product selectivities at carbon dioxide-to-glycerol ratios (T=750 °C).

CO_2/G	S_{H_2}	S_{CO}	S_{CO_2}	S_{CH_4}	S_{H_2O}
1	3.94	3.84	0.64	0.03	0.52
2	3.97	4.72	1.52	0.02	1.00
3	3.98	5.57	2.65	0.01	1.48
4	3.98	6.42	4.03	0.01	1.96

4.2.2.2. Activity Tests. CO_2/G ratio effect on CO_2 conversion of Rh/AZT, Ni/AZT/Co/AZT and Rh/ZT along with thermodynamic conversions are given in Figure 4.20. The highest CO_2 conversion of 39.2% is achieved with Rh/AZT at CO_2/G ratio of 2 whereas the lowest conversion of 5.1% is achieved with Rh/ZT at ratio of 1. Although thermodynamics state a linearly decreasing trend, experimental results of all catalysts except Rh/ZT indicated an optimum CO_2/G ratio of 2 whereas the highest conversion is obtained at CO_2/G=3 for the Rh/ZT sample. Most of the other thermodynamics

[13, 95] and experimental [16, 17, 24, 25, 27] studies of glycerol dry reforming reported CO_2/G ratio of 1 as optimal ratio, but in recent studies of Tavanarad *et al.* [29] it is shown that increasing CO_2/G ratio from 0 to 3 increased catalytic activity. Also similar results to that reported in this study is observed in the works of Siew *et al.* [18, 19], in which CO_2 conversion first increases when CO_2/G ratio increases from 0 to 1.68 and then decreases. As also reported in the previous section, in blank tests no CO_2 conversion is observed thus the results are not included in Figure 4.20.

The trend observed in Figure 4.20 can be ascribed to dry reforming of methane. Methane amount in the product stream decreases with increasing CO_2/G molar feed ratio as reported in Table 4.9. Thus, in lower CO_2/G ratio (*i.e.* 1) experiments, methane dry reforming do not proceed to its extent. This in turn results in lower CO_2 conversions and high CH_4 yields. Additionally, produced H_2O in RWGS reaction is probably used in steam reforming of various hydrocarbons, especially CH_4. Thus, as CO_2/G ratio is increased, RWGS (Equation 2.9) reaction proceeds which eventually produce more H_2O. This excess water is then used in steam reforming reactions of hydrocarbons.

Glycerol conversions of binary and ternary support catalysts and blank tests together with thermodynamic conversions with respect to CO_2/G ratios are provided in Figure 4.21. For all catalysts, glycerol conversion decreases with increasing ratio due to RWGS reaction. However, glycerol conversions do not differ with CO_2/G ratio in blank tests. Increase in CO_2 amount shifts the reaction to H_2O side. Since H_2O is not taken into consideration by the definition of glycerol conversion to gaseous products, increase in water yield decreases the glycerol conversion. Moreover, as explained previously methane dry reforming and RWGS reactions may be the route cause of the gap between experimental results and thermodynamics. Depending on glycerol conversions, the catalyst showing the best activity is Rh/AZT with highest conversion of 82.3% at CO_2/G ratio of 1. Glycerol conversion of over 90% of the thermodynamic barrier is achieved over Rh/AZT at every CO_2/G ratio whereas this percentage decreases to 80% over Ni/AZT and Rh/ZT and to 75% over Co/AZT.

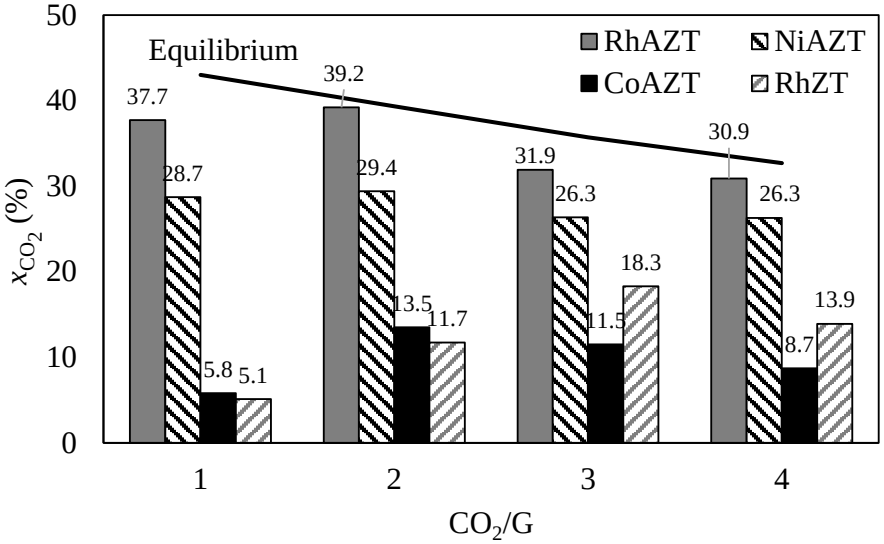

Figure 4.20. Thermodynamic and experimental CO_2 conversions with respect to CO_2/G ratios (T=750 °C).

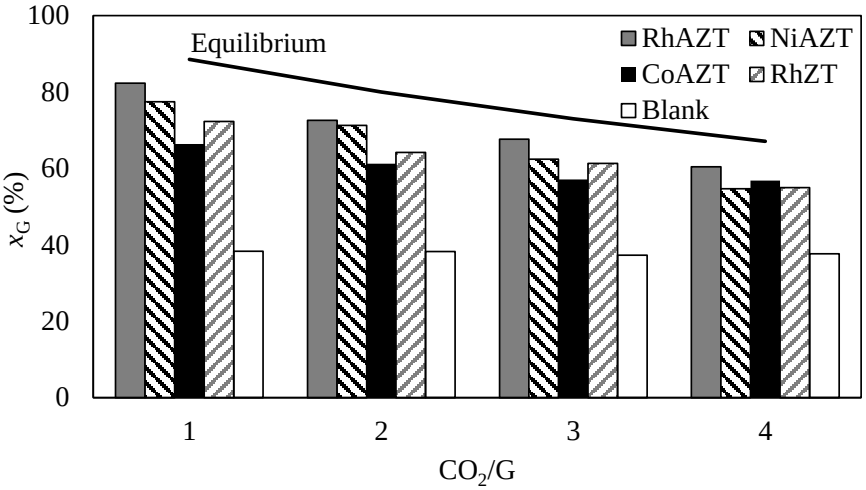

Figure 4.21. Thermodynamic and experimental glycerol conversions with respect to CO_2/G ratios (T=750 °C).

Table 4.9. Product yields over mixed support catalysts at different CO_2/G ratios (T=750 °C).

	CO_2/G	Y_{H_2}	Y_{CO}	Y_{CH_4}	$Y_{c_2c_4}$	$Y_{c_2c_6}$	H_2/CO	x_{CO_2}	x_G
RhAZT	1	3.26	2.48	0.01	0	0	1.32	37.7	82.3
	2	2.90	2.78	0	0	0	1.04	39.2	72.6
	3	2.70	2.99	0	0	0	0.90	31.9	67.7
	4	2.41	3.09	0	0	0	0.78	30.9	60.4
NiAZT	1	3.07	2.20	0.01	0	0	1.39	28.7	77.4
	2	2.82	2.37	0.01	0	0	1.19	29.4	71.2
	3	2.46	2.45	0.02	0	0	1.01	26.3	62.4
	4	2.16	2.57	0.01	0	0	0.84	26.3	54.7
CoAZT	1	2.14	2.05	0.24	0	0.01	1.04	5.8	66.4
	2	1.95	2.29	0.24	0	0.01	0.85	13.5	61.2
	3	1.78	2.27	0.24	0	0.01	0.78	11.5	57.1
	4	1.72	2.54	0.28	0.01	0.01	0.68	8.7	56.8
RhZT	1	2.40	2.17	0.24	0	0.01	1.11	5.1	72.3
	2	2.09	2.19	0.23	0	0.01	0.95	11.7	64.2
	3	2.11	2.57	0.16	0	0	0.82	18.3	61.3
	4	1.79	2.53	0.20	0	0	0.71	13.9	55.0

Blank tests were performed to investigate the extent of homogeneous glycerol conversions. Since no CO_2 conversion is observed when there is almost 40% glycerol conversion; it is possible do state that RWGS reaction is catalytically driven. Whereas, glycerol decomposition reaction takes place in the absence and presence of catalysts. Considering glycerol decomposition reactions are endothermic, increase in the temperature should increase its rate. The findings reported in the previous section (see Figure 4.17) are in perfect alignment with this suggestion.

Product yields and selectivities obtained on Rh/AZT, Ni/AZT, Co/AZT and Rh/ZT with respect CO_2/G ratio is available in Tables 4.9 and 4.10, respectively.

Table 4.10. Product selectivity values over mixed support catalysts at different CO_2/G ratios (T=750 °C).

	T (°C)	$\mathbf{S_{H_2}}$	$\mathbf{S_{CO}}$	$\mathbf{S_{CH_4}}$	$\mathbf{S_{c_2c_4}}$	$\mathbf{S_{c_2c_6}}$
RhAZT	1	3.97	3.01	0.02	0	0
	2	3.99	3.83	0.00	0	0
	3	3.99	4.41	0.01	0	0
	4	3.99	5.11	0.01	0	0
NiAZT	1	3.97	2.84	0.02	0	0
	2	3.96	3.33	0.02	0	0
	3	3.95	3.92	0.03	0	0
	4	3.95	4.70	0.03	0	0
CoAZT	1	3.22	3.09	0.37	0.01	0.01
	2	3.19	3.75	0.38	0	0.01
	3	3.11	3.98	0.42	0.01	0.01
	4	3.02	4.46	0.48	0.02	0.01
RhZT	1	3.32	3.00	0.33	0	0.01
	2	3.25	3.41	0.36	0	0.01
	3	3.45	4.19	0.27	0	0
	4	3.26	4.60	0.36	0	0.01

Both experimental and theoretical H_2 yields are found to decrease monotonically when the ratio is increased from 1 to 4 (see Figure 4.22). On the other hand, CO yields show opposite trend as can be seen in Figure 4.23. The same reasoning proposed for glycerol conversion decrease can also be applied here, due to increase in CO_2 amount Le Chatelier's principle dictate RWGS to shift towards H_2O and CO side. Thus, it is possible to adjust desired syngas ratio by changing CO_2/G ratios. For direct utilization of liquid fuels, CO_2/G ratios close to 1 would be preferable [14, 116].

Methane, ethane and ethylene are unwanted by-products whose existence indicate decrease in catalytic activity. No ethane or ethylene existed in product streams of

both Rh/AZT and Ni/AZT at every CO_2/G ratio and those catalyst showed superior activities to Co/AZT and Rh/ZT. In fact, in reaction test over Rh/AZT, methane is not observed at CO_2/G ratios higher than 2. Therefore, it is possible to state Rh/AZT catalyst is better in catalyzing methane dry and steam reforming reactions and both Rh/AZT and Ni/AZT are more active in ethane and ethylene reforming reactions.

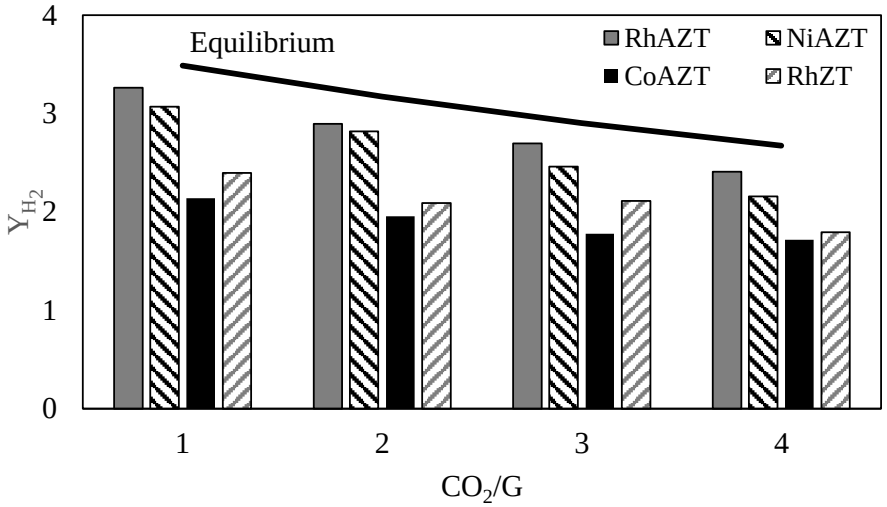

Figure 4.22. Thermodynamic and experimental H_2 yields with respect to CO_2/G ratios at 750 °C.

Finally, lower CO_2/G ratios are preferable in terms of high catalytic activity due to increased conversions but higher ratios are preferable in terms of catalytic stability since it decreases carbonaceous species deposited on catalyst surface. Thus, there is a trade-off between activity and stability when selecting CO_2/G ratio. The highest glycerol conversion of 82.3% is obtained with Rh/AZT at CO_2/G ratio of unity while highest CO_2 conversion of 39.2% is obtained over the same catalyst at ratio of 2. Highest syngas with ratio 1.32 is obtained over Rh supported on AZT.

4.2.3. Effect of Active Metal

In this study three different metals, namely rhodium, nickel and cobalt, are used in dry reforming of glycerol. In Figure 4.24, CO_2 and glycerol conversions over these

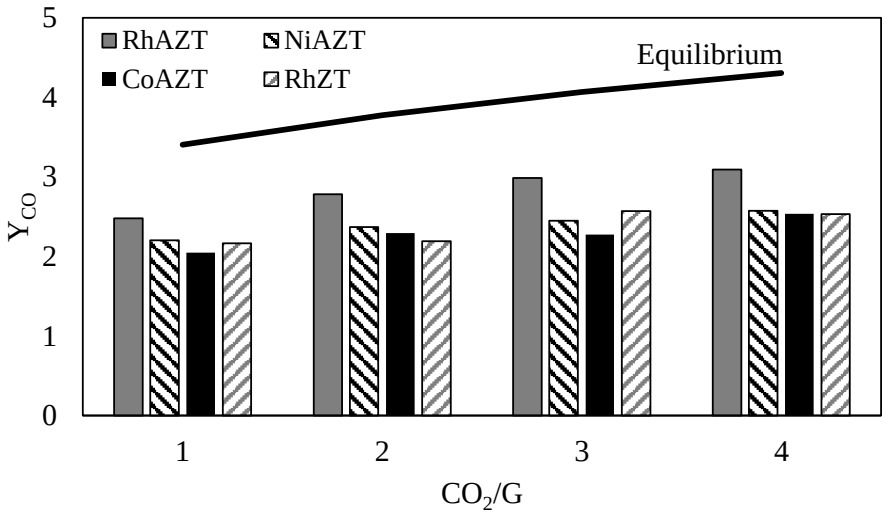

Figure 4.23. Thermodynamic and experimental CO yields with respect to CO_2/G ratios at 750 °C.

three catalysts are compared. The comparison is based on experiments conducted at default conditions, 750 °C with CO_2/G ratio of 4 and W/F ratio of 0.5 mg min NmL^{-1}. Difference between the highest and lowest glycerol conversion is 5.7% while for CO_2 conversion it is 22.9%. Thus, it is possible to state tha the type of active metals plays an important role in CO_2 conversion. In literature, however, it is stated that not only the active metal plays important roles in CO_2 conversion. Strong metal-support interaction is stated as the key determining factor in achieving high catalytic activities especially for CO_2 conversions [137, 138]. Although there is no direct relation between SMSI and good dispersion of catalysts [139], high catalytic activity of Rh/AZT hints Rh particles are better dispersed on AZT than Ni and Co particles. In fact, catalyst characterization studies that will be elaborated in Section 4.2.7 supports the results obtained with activity tests. Rh particles have smaller particle sizes when compared with Ni and Ni crystallite sizes are smaller than Co (consult to Section 4.2.7.2). These findings support the increasing CO_2 conversions in the order of Rh/AZT, Ni/AZT followed by Co/AZT. Moreover Rh particles conserve their particle sizes after GDR. Furthermore, CO adsorption tests made on Rh/AZT and Ni/AZT did not reveal any convenient conclusion. Thus, it is possible to state that there is strong metal-support

interactions within these catalysts [140]. Less catalytic activity of Co/AZT compared to Rh and Ni supported on AZT may be resulted due to acidic nature of cobalt. Acidic sites promote coke deposition which blocks the active sites of the metals [54]. TEM analysis on 72 h spent Co/AZT samples indicate the severe coke deposition on the catalyst (see Section 4.2.7.2 and Figure 4.43). Tavanarad *et al.* [29] also showed in their glycerol dry reforming studies that Rh showed the highest activity compared to other noble metals, namely Ru, Ir, Pd and Pt (details are given in Section 2.2.2).

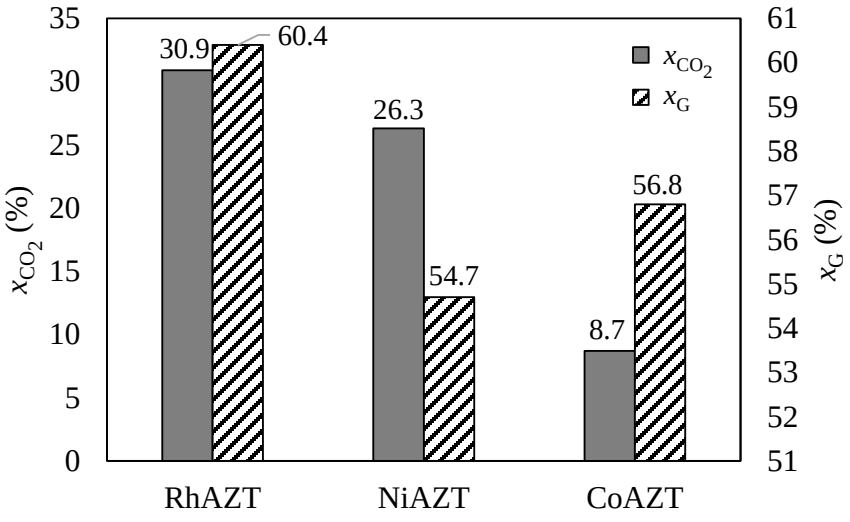

Figure 4.24. Carbon dioxide and glycerol conversions over different active metals supported on AZT (T=750 °C and CO_2/G=4).

It is also important to mention the active metal loadings. Rh/AZT and Rh/ZT samples contain only 1 wt.% of rhodium while Ni/AZT and Co/AZT samples contain 5 wt.% nickel and cobalt, respectively. Thus, improved catalytic activity of Rh/AZT sample should be more emphasized since it is more capable in glycerol dry reforming even it is in lower amounts. Additionally, 1 wt.% Ni/AZT catalyst is also synthesized to make comparison between 1wt.% Rh/AZT but it showed catalytic activity similar to 5 wt.% Co/AZT, therefore no further activity tests are performed on that sample.

Product yields over different active metals supported on ternary support AZT are shown in Table 4.11. As expected, experiments over Rh/AZT yielded higher synthesis gas. The lowest syngas with lowest ratio of 0.68 is obtained over Co/AZT. There is

an opposite relation between methane, ethane and ethylene formation and catalytic activity which indicates Rh/AZT is better in steam and dry reforming of methane as previously mentioned in Section 4.2.1 and Section 4.2.2. Gaur *et al.* [141] reported in their dry methane reforming studies that Rh catalyst is more active than Ni catalyst. Although no ethane or ethylene is present in the product stream of Rh/AZT and Ni/AZT, in literature it is proposed that Rh has more capacity in C–C and C=C bond breakage [142]. Finally, H_2 yield over Rh/AZT is higher than Ni/AZT but its H_2/CO ratio is lower do to the extent of RWGS reaction.

Table 4.11. Product yields over AZT catalysts (T=750 °C and CO_2/G=4).

Catalyst	$\mathbf{Y_{H_2}}$	$\mathbf{Y_{CO}}$	$\mathbf{Y_{CH_4}}$	$\mathbf{Y_{c_2c_4}}$	$\mathbf{Y_{c_2c_6}}$	$\mathbf{H_2/CO}$
RhAZT	2.41	3.09	0	0	0	0.78
NiAZT	2.16	2.57	0.01	0	0	0.84
CoAZT	1.72	2.54	0.28	0.01	0.01	0.68

Considering catalytic activity performances, rhodium would be the best candidate for dry reforming of glycerol. But since its a noble metal, its cost should be considered as well. Therefore, a cheaper metal alternative, Ni attracts attention due to its relatively high catalytic activity to Co both supported on AZT.

4.2.4. Effect of Support

Rh metal is impregnated on four different supports, namely ZrO_2, CeO_2, ZrO_2-TiO_2 and Al_2O_3-ZrO_2-TiO_2, in order to investigate the effect of supporting material on catalytic activity. Glycerol and CO_2 conversions for these four catalysts are provided in Figure 4.25. CO_2 conversions are more responsive to the changes in supporting material than glycerol conversions. For instance, Rh/AZT gave a CO_2 conversion of 30.9% where it is reduce more than half to 13.9% for Rh/ZT sample. However, glycerol conversions measured on Rh/AZT and Rh/ZT are 60.4% and 55%, respectively.

When single, binary and ternary supports (Zr, ZT and AZT, respectively) are compared, it can be stated that the addition of TiO_2 to ZrO_2 hinders while addition of both TiO_2 and Al_2O_3 promotes the activity. Addition of TiO_2 is considered due to its high activity characteristics reported in the methane dry reforming [110, 117, 118]. Therefore, its addition was carried out in the context of an attempt to improve functional properties that can be useful in the catalysis of GDR. The opposite findings can be interpreted by the fact that TiO_2 is an acidic support which is known to promote coke formation. In the literature ZT is reported as a Brønsted acid [115]. Although it is strongly acidic, it can be used as an acid-base bifunctional catalyst [107]. Another disadvantage of TiO_2 is that it may partially migrate and block active sites of the catalysts [109]. On the other hand, Rh supported on ternary oxide (AZT) is found to perform better than Rh/ZT. A similar finding is valid for the comparison of ternary and single oxide (ZrO_2 and CeO_2) supported on Rh catalysts, with AZT favoring better dispersion of Rh nano-particles (see the TEM images provided in Sections 4.1.2.1 and 4.2.7.2). Additionally, AZT promotes RWGS (consult to Section 4.2.5) which may explain improved activity of Rh/AZT compared to other Rh-based catalysts.

BET surface areas of the Rh supported single oxides were reported in the decreasing order as Rh/Al_2O_3 >Rh/TiO_2 >Rh/ZrO_2 by Ruckenstein and Wang [109]. In this work, surface area of AZT (182 m^2 g^{-1}) is found higher than that of ZT (26 m^2 g^{-1}) followed by ZrO_2 (16.3 m^2 g^{-1}) and CeO_2 (10.2 m^2 g^{-1}), in accordance with the literature. As presented in Figure 4.25, however, the decreasing order of specific surface areas is not correlated with the catalytic activities. Thus, there is no straightforward relation between surface area and catalytic activity as also reported by Abate *et al.* [126]. A better way to explain the activity of catalysts would be by interactions between metal and support. When TEM images are considered, no sintering is observed over Rh/AZT (see Section 4.2.7.2) while there is significant increase in the Rh particle sizes in case of RhZr and RhCe (see Section 4.1.2.1). This would indicate AZT is a good support. However, average particle sizes of Ni and Co supported on AZT is found to increase as measured by the comparison of the TEM images of the fresh and aged catalyst samples (see Section 4.2.7.2). Therefore, it is more convenient to state that the strength of

interaction between the metal and the support, which seems to decrease in the order of Rh/AZT >Ni/AZT >Co/AZT, is the key determinant in catalytic activity.

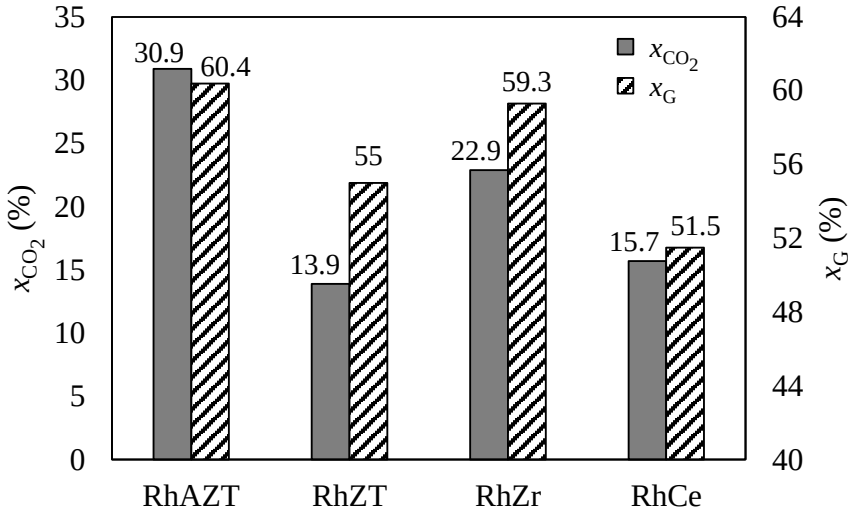

Figure 4.25. Carbon dioxide and glycerol conversions over Rh supported on single, binary and mixed supports (T=750 °C and CO_2/G=4).

Product yields over Rh impregnated single and mixed support catalysts are compared in Table 4.12. Highest syngas yield together with highest H_2/CO ratio is obtained over Rh/AZT, the most active catalyst. Although their syngas ratios are approximately the same, Rh/ZrO_2 sample showed higher H_2 and CO yields compared to Rh/ZT. The lowest synthesis gas and highest CH_4 yields are achieved over Rh/CeO_2 sample which indicates the low catalytic activity. Though, more CO_2 conversion is observed over this catalyst when compared to Rh/ZT. The probable explanation is Rh/ZT catalyst promoted methane steam reforming so that its CO_2 conversion is decreased and glycerol conversion and CH_4 yield is increased.

Support selection for dry reforming of glycerol is highly complex. Metal-support interactions as well as promoting metal dispersion play important role in determining the catalytic activities. Ternary support AZT is proposed to be the most active support in this study while adding TiO_2 to ZrO_2 is found to decrease the activity.

Table 4.12. Product yields over Rh impregnated single and binary support catalysts (T=750 °C and CO_2/G=4).

Catalyst	Y_{H_2}	Y_{CO}	Y_{CH_4}	$Y_{c_2c_4}$	$Y_{c_2c_6}$	H_2/CO
RhAZT	2.41	3.09	0	0	0	0.78
RhZT	1.79	2.53	0.20	0	0	0.71
RhZr	2.01	2.86	0.17	0	0	0.70
RhCe	1.45	2.26	0.29	0	0	0.64

4.2.5. Effect of Residence Time

Residence time is an important parameter determining the extent of reactions occurring inside a reactor. In this study, residence time effect is investigated over Ni/AZT by changing the catalyst amount packed inside the reactor. For this purpose 20, 50, 100 and 150 mg of Ni/AZT that corresponds to respective residence times of 0.5, 1.25, 2.5 and 3.75 mg_{cat} min NmL^{-1} are packed and tested at default operating conditions of 750 °C and CO_2/G=4. Carbon dioxide and glycerol conversion results can be seen in Figure 4.26. As expected, CO_2 conversions progressively increase as catalyst amount is increased. Although glycerol conversions seems to fluctuate, the secondary axis (corresponds to glycerol conversion) spacing is short and therefore corresponding conversions to catalyst amounts are approximately the same. Increasing catalyst amount from 20 to 50 mg increased CO_2 conversion from 26.3% to 31.2%, while further increase to 150 only improve the conversion by 1.1% from 31.2% to 32.3%. Considering the thermodynamic conversion at the same operating conditions is 32.7%, increasing catalyst amount to 0.2 g would not improve CO_2 conversion any further and therefore would be meaningless. In fact, using 50 mg of catalyst is more economical considering the catalyst cost and CO_2 conversion values.

Residence time effects on CO_2 and glycerol conversions over all catalyst are investigated with residence times of 0.5 and 3.75 mg_{cat} min NmL^{-1} and compared in Figure 4.27 and Figure 4.28, respectively together with blank tests obtained over pure

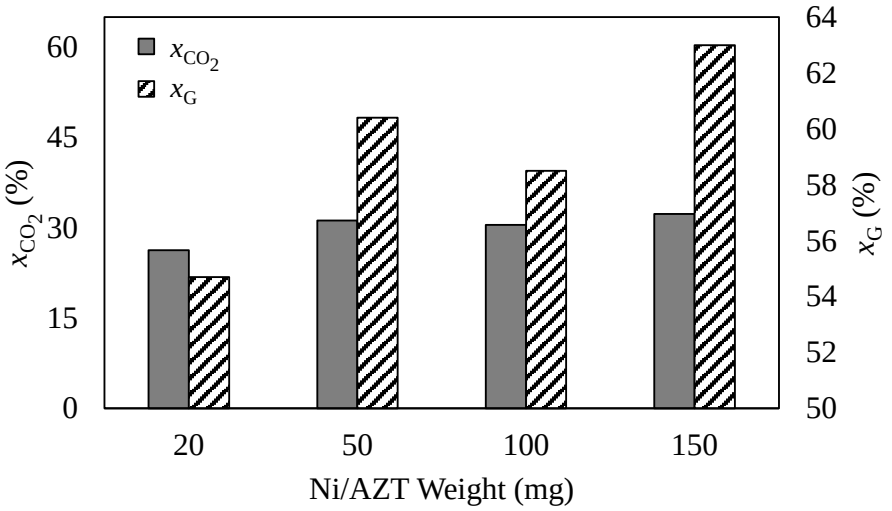

Figure 4.26. Carbon dioxide and glycerol conversions obtained with different amounts of Ni/AZT (T=750 °C and CO_2/G=4).

AZT. The lowest difference between catalytic activities is obtained over Rh/AZT sample considering both CO_2 and glycerol conversions, meaning that Rh/AZT is active even at its lowest amount of 20 mg. Rhodium particles are well-dispersed on the AZT support so that the total active metal area is enhanced. The improved surface area of Rh particles improved the catalytic activity. These findings support smaller crystallite size and better dispersion of Rh particles as proposed in previous Section 4.2.3 and validated in coming Section 4.2.7.2.

Different active metals impregnated on the same support show different metal-support interactions. For instance, good dispersion of Rh particles over AZT support due to SMSI is not the same to that of Ni/AZT catalyst. Ni-AZT interaction is not strong as Rh-AZT which may explain the significant difference between the activity of 20 and 150 mg samples. Active metal sites over 20 mg of Rh/AZT is enough to achieve theoretical CO_2 conversions whereas at least 50 mg of Ni/AZT is necessary to achieve conversions close to thermodynamic limits. Thus, well-dispersion of Rh particles over AZT can be observed. On contrary, poorly dispersed Co over AZT and Rh over ZT may explain the differences between reactant conversions over 20 and 150 mg samples.

Active metals on support surface are prone to coke formation and sintering especially when metal-support interactions are not strong. Previously, in Section 4.2.4 strong metal-support interaction was ascribed to Rh/AZT. SMSI promotes dispersion and hinders sintering of particles under severe conditions. Interactions between Rh particles and ZT support is previously found weak in aforementioned section. This weak interaction between the active metal and the support possibly results in decreased surface area and make catalyst prone to sintering which end up in a dramatic decrease of 16% in CO_2 conversion upon decreasing catalyst amount from 150 to 20 mg.

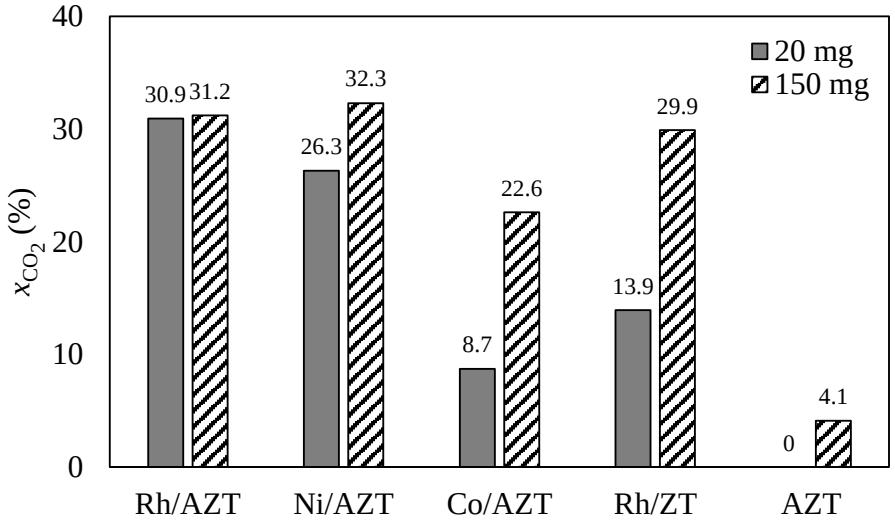

Figure 4.27. Effect of catalyst weight on CO_2 conversion over mixed support catalysts and blank AZT (T=750 °C and CO_2/G=4).

Another interesting finding from the Figures 4.27 and 4.28 is CO_2 and glycerol conversions obtained over pure AZT. First of all, even no CO_2 conversion is observed with 20 mg AZT there is significant glycerol conversion of 31.9%. This demonstrates the significance of glycerol thermal decomposition. Figure 4.27 proves that AZT plays direct role in CO_2 consumption primarily by RWGS reaction. AZT is probably not capable of catalyzing dry reforming of glycerol since glycerol conversion increase between 20 and 150 mg AZT do not compensate the CO_2 conversion increase. More CO_2 is converted than glycerol between these two experiments (note that stoichiometry of GDR is 1:1 for CO_2:glycerol - Equation 2.7), therefore it should be spent in another reaction rather than GDR which is probably reverse water gas shift reaction (Equation

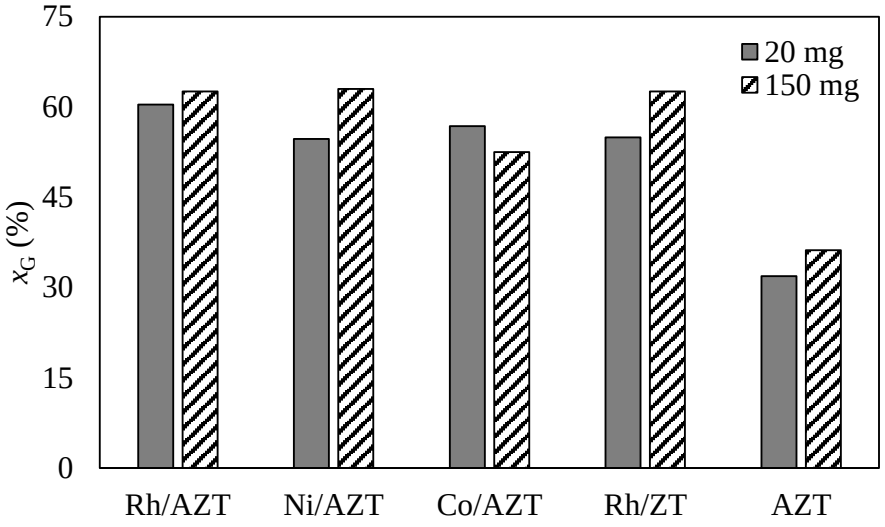

Figure 4.28. Effect of catalyst weight on glycerol conversion over mixed support catalysts and blank AZT (T=750 °C and CO_2/G=4).

2.9). RWGS promotes CO_2 conversion while suppresses glycerol conversion by H_2O production. This may also be supported by blank test done at same operating conditions where no catalyst is used. Under those conditions glycerol conversion of 37.6% is obtained which is higher than both pure AZT results.

To summarize, residence time has significant impact on catalytic activities especially over Co/AZT and Rh/ZT catalysts. For Ni/AZT further increment in catalyst amount after 50 mg found economically not feasible. Finally, 20 mg of Rh/AZT is found to be almost as active as 150 mg thus residence time range investigated in this study has almost no effect on Rh/AZT.

4.2.6. Stability Tests

72 h longevity tests over Rh/AZT, Ni/AZT, Co/AZT and Rh/ZT catalysts are performed at default temperature of 750 °C and CO_2/G ratio of 4 but with residence time of 3.75 mg min NmL^{-1} (catalyst amount = 150 mg). CO_2 conversions with respect to time can be seen in Figure 4.29. Rh/AZT and Ni/AZT demonstrate good stability

with only less than $\sim$ 13% and 8% decrease in CO_2 conversions, respectively at the end of 72 h. *In-situ* FTIR results of fresh and 72 h spent Rh/AZT (see Section 4.2.7.3) showed that there is slight sintering of active metal which explains the minor decrease in CO_2 conversion. On the other hand, CO_2 conversion of Rh/ZT progressively dropped from 31.2% to 20.9%. This 30.3% decrease in conversion shows the deactivation of the catalyst and its trend suggests that deactivation would continue even after 72 h. Co/AZT is the most deactivated catalyst and its CO_2 conversion dropped from 25.2% to 11.0%. Catalyst deactivates very fast in the first 2 hours and deactivation flattens until the end of the experiment around 69th hour where rapid deactivation starts again.

Possible deactivation mechanisms in glycerol dry reforming are metal sintering and coke deposition. In many studies carbon deposition on the catalyst surface is found to be reversible with oxygen treatment [16, 22, 26–29]. The carbonaceous species that are easily removed *via* oxidation are whisker type, encapsulating and filamentous carbon. Sintering occurs at high temperatures as employed in this study and when H_2O is present in the system. Although water does not enter the reactor as reactant, it is produced through RWGS reaction. It is unfortunately not possible to understand the deactivation mechanism by simply observing the catalytic activity. Therefore post-experiment catalyst characterization techniques are performed to identify the deactivation mechanisms in the catalysts. Those results will be further explained in the next Section 4.2.7.

When 72 h stability of Rh supported on single oxide supports ZrO_2 and CeO_2 in Section 4.1.1 are compared with Rh/AZT and Rh/ZT, it is obvious that addition of Al_2O_3 to support structure increased the stability of the catalyst significantly. Although it was reported that addition of Al_2O_3 did not improved stability [118], the opposite is found in this study. On the other hand, addition of TiO_2 slightly improved stability and activity. Please note that in smaller amounts (0.5 mg_{cat} min NmL^{-1}) of catalyst experiments, Rh/ZT gave lower activity compared to RhZr.

ToS glycerol conversions of mixed support catalysts can be seen in Figure 4.30. The results fluctuate since calculation of glycerol conversion is not straightforward.

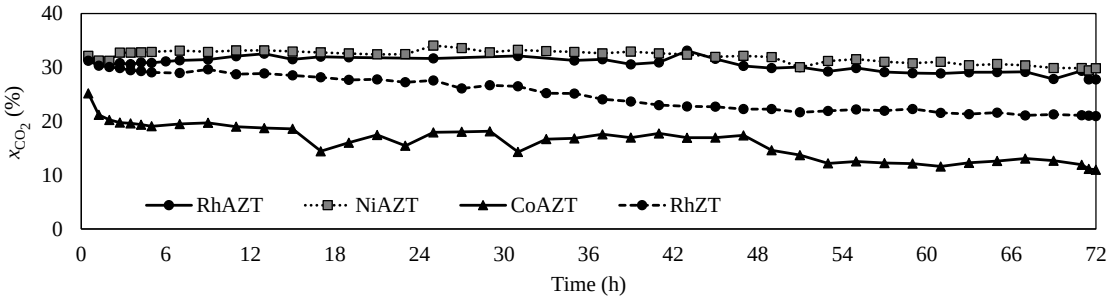

Figure 4.29. 72 h ToS CO_2 conversion of single mixed catalysts (T=750 °C and CO_2/G=4).

In general, opposite to CO_2 conversions, glycerol conversions tend to increase due to activity loss. Activity loss decrease mostly RWGS rate, thus less H_2 and CO_2 is converted to CO and H_2O which is not included in calculation of glycerol conversion. The lowest change is obtained with Ni/AZT from 62.1% to 63.4% which also proves its stability in long run. For Rh/AZT sample, glycerol conversion is increased from 58.7% to 66.4% which may seem much compared to its high stability to CO_2 conversion. Though, percentage decrease (12.6%) and increase (13.1%) of CO_2 and glycerol conversions are basically the same, making RWGS a major factor in determining the activity of Rh/AZT. Decrease in the rate of RWGS also explains the increase in H_2 as well as the decrease in the CO yields. On the other hand, although CO_2 conversion of Co/AZT is drastically dropped, the increase of glycerol conversion from the beginning to end of the experiment is only 1.0%. A similar trend is also observed in Rh/ZT, whose glycerol conversion is dropped from 61.3% to 60.8%. In general, if catalysts showed good stability towards CO_2 conversion, their glycerol conversions are less effected and vise versa.

Product distributions at selected times (0.5^{th}, 13th, 25th, 37th, 49th, 61st and 72nd) are presented in Table 4.13 and Table 4.14. H_2 yields of Rh/AZT and Ni/AZT first increased until 49th h and then started to decrease, while H_2 selectivity values of both catalysts are the same and stay approximately at 4.00. The same thing cannot be said to CO selectivities of both catalysts, they dropped continuously. Considering H_2

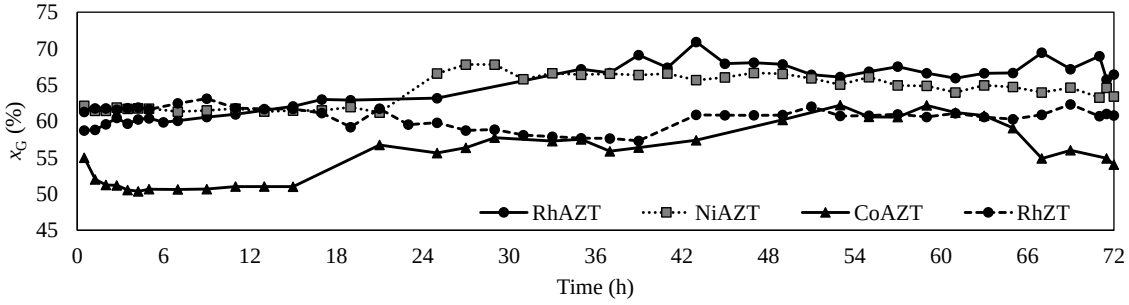

Figure 4.30. 72 h ToS glycerol conversion of mixed support catalysts (T=750 °C and CO_2/G=4).

and CO yields together with CO_2 and glycerol conversions, it is possible to state that ability of catalysts to reform hydrocarbons with steam is decrease with time. Thus, RWGS cannot proceed to its extent due to Le Chatelier's principle. For Co/AZT, both H_2 and CO yields and selectivities fluctuate. Whereas for Rh/ZT, H_2 and CO yields and selectivities progressively drop which indicates the catalytic deactivation.

An indicator of catalytic activity is methane, ethane and ethylene formation. Those compounds are not seen or seen on trace amounts in Rh/AZT and Ni/AZT samples. On the other hand, CH_4 is almost seen at every time over Co/AZT and Rh/ZT samples. CH_4 formation (Equations 2.19, 2.17 and 2.18) decreases glycerol conversion while its effect on CO_2 conversion is unknown since rates of Equations 2.18 and 2.19 are not known. Therefore, methanation can neutralize the increase in glycerol conversion due to deactivation of catalysts, which decreased the rate of RWGS. Thus, it is possible to have an insight about the decreasing CO_2 conversions over Co/AZT and Rh/ZT while their glycerol conversions are not affected as much.

Finally, catalytically most active catalyst Rh/AZT is also found stable for at least 72 hours. Surprisingly, when used in high residence times Ni/AZT slightly surpasses Rh/AZT in both catalytic activity and long run stability. Co/AZT and Rh/ZT are found to deactivate in long run with more than 56% and 33% losses in CO_2 conversions, respectively.

Table 4.13. Product yields over mixed support catalysts.

	t (h)	Y_{H_2}	Y_{CO}	Y_{CH_4}	$Y_{C_2H_4}$	$Y_{C_2H_6}$	H_2/CO	x_{CO_2}	x_G
RhAZT	0.5	2.35	3.19	0	0	0	0.74	31.8	58.7
	13	2.44	3.25	0	0	0	0.75	32.1	61.0
	25	2.52	3.29	0	0	0	0.77	31.7	63.2
	37	2.66	3.39	0	0	0	0.79	31.5	66.6
	49	2.71	3.40	0	0	0	0.80	29.9	67.8
	61	2.63	3.34	0	0	0	0.79	28.9	65.9
	72	2.65	3.33	0	0	0	0.80	27.8	66.4
NiAZT	0.5	2.49	3.16	0	0	0	0.79	32.2	62.2
	13	2.45	3.09	0	0	0	0.79	33.2	61.3
	25	2.66	3.22	0	0	0	0.83	34.1	66.6
	37	2.66	3.18	0	0	0	0.84	32.6	66.5
	49	2.66	3.10	0	0	0	0.86	31.9	66.5
	61	2.55	2.93	0	0	0	0.87	30.0	64.0
	72	2.53	2.83	0	0	0	0.89	29.8	63.4
CoAZT	0.5	2.04	3.00	0.08	0	0	0.68	25.2	55.0
	13	1.73	2.91	0.15	0	0	0.60	18.7	51.0
	25	1.92	3.13	0.15	0	0	0.61	18.0	55.6
	37	1.93	3.02	0.15	0	0.01	0.64	17.6	55.9
	49	2.04	3.39	0.17	0	0.01	0.60	14.6	60.2
	61	2.06	3.29	0.18	0	0.01	0.63	11.6	61.2
	72	1.84	2.99	0.15	0	0.01	0.61	11.0	54.0
RhZT	0.5	2.45	3.29	0	0	0	0.74	31.2	61.3
	13	2.40	3.16	0.03	0	0	0.76	28.9	61.7
	25	2.20	3.05	0.09	0	0	0.72	27.6	59.8
	37	1.99	2.85	0.16	0	0	0.70	24.1	57.6
	49	2.02	2.90	0.20	0	0	0.70	22.3	60.8
	61	2.01	2.87	0.21	0	0	0.70	21.6	61.1
	72	2.00	2.86	0.21	0	0	0.70	21.0	60.8

Table 4.14. Product selectivity values over mixed support catalysts.

	Time (h)	$\mathbf{S_{H_2}}$	$\mathbf{S_{CO}}$	$\mathbf{S_{CH_4}}$	$\mathbf{S_{C_2H_4}}$	$\mathbf{S_{C_2H_6}}$
RhAZT	0.5	4.00	5.42	0	0	0
	13	4.00	5.32	0	0	0
	25	4.00	5.21	0	0	0
	37	3.99	5.09	0	0	0
	49	3.99	5.02	0	0	0
	61	3.99	5.07	0.01	0	0
	72	3.99	5.01	0.01	0	0
NiAZT	0.5	4.00	5.09	0	0	0
	13	4.00	5.05	0	0	0
	25	4.00	4.83	0	0	0
	37	4.00	4.77	0	0	0
	49	3.99	4.66	0	0	0
	61	3.99	4.58	0	0	0
	72	3.98	4.47	0	0	0
CoAZT	0.5	3.71	5.46	0.15	0	0
	13	3.40	5.70	0.29	0	0.01
	25	3.45	5.62	0.26	0	0.01
	37	3.45	5.40	0.26	0	0.01
	49	3.40	5.63	0.28	0	0.01
	61	3.36	5.37	0.30	0	0.01
	72	3.40	5.53	0.28	0	0.01
RhZT	0.5	3.99	5.37	0.01	0	0
	13	3.89	5.13	0.05	0	0
	25	3.68	5.09	0.16	0	0
	37	3.46	4.94	0.27	0	0
	49	3.33	4.77	0.33	0	0
	61	3.29	4.70	0.35	0	0
	72	3.29	4.70	0.35	0	0

4.2.7. Catalyst Characterizations

Catalyst characterizations of fresh (reduced for 2 h under 40 NmL min^{-1} H_2 at 800 °C), 5 h and 72 h spent Rh/AZT, Ni/AZT, Co/AZT and Rh/ZT are reported in this section as well as BET surface area of calcined AZT and ZT samples. Detailed characterizations of AZT and ZT can be found elsewhere [119].

4.2.7.1. BET Analysis. Results of BET surface analysis of prepared supports AZT and ZT are provided in Table 4.15. Specific surface area of AZT is significantly higher than that of ZT. Although not reported here, surface area of AZT is also significantly higher than single oxide supports ZrO_2 and CeO_2 which have BET specific surface areas of 16.3 and 10.2 m^2 g^{-1}, respectively [105]. Thus, introduction of TiO_2 increased the surface area of ZrO_2 and addition of Al_2O_3 to ZT, further improved the surface area. Ruckenstein and Wang [109] reported decreasing specific surface areas of Rh-based support on single oxides as Rh/Al_2O_3>Rh/TiO_2>Rh/ZrO_2. Thus, BET specific surface area results of the supports are in agreement with the literature.

Table 4.15. BET specific surface area of binary and ternary oxide supports.

Support	**BET Specific Surface Area (m^2 g^{-1})**
AZT	182
ZT	26

BET analysis results for Rh/AZT, Ni/AZT, Co/AZT together with AZT are provided in Table 4.16. Those samples are just calcined at 800 °C, *i.e.* they are not reduced under H_2 flow and not used in the reactions. Impregnating metal on the AZT support decreased both BET specific surface area and pore volume as expected due to blockage of the pores. Rh/AZT has the highest surface area within other catalyst which supports the higher activity of the catalyst. Surface area as well as pore volume of Ni/AZT is higher than Co/AZT which follows the order of catalytic activity. The higher specific surface area of the catalyst is, the better the metal is dispersed on

the support. Validity of this statement is confirmed by the same decreasing order of catalytic activity and the specific surface area and also by the TEM analysis of the fresh catalyst samples presented in the following section. On the other hand, no direct relation between average pore size and activity can be found with the current results. Impregnating Rh or Co on AZT decreased average pore size, while impregnation of Ni increased it significantly.

Table 4.16. BET analysis results for mixed oxide and its catalysts.

Catalyst	**BET Specific Surface Area (m^2 g^{-1})**	**Pore Volume (cm^3 g^{-1})**	**Average Pore Radius (Å)**
AZT	182	0.253	25.3
RhAZT	123	0.209	15.5
NiAZT	119	0.156	41.3
CoAZT	100	0.128	16.5

4.2.7.2. TEM and EDX Measurements. Fresh, 5 h and 72 h spent samples of Rh/AZT, Ni/AZT and Co/AZT are investigated through TEM and EDX analyses. Representative HR-TEM images of fresh Rh/AZT can be seen in Figure 4.31, which revealed all Rh particles are covered with support AZT. Rh particles are also well dispersed with an average particle size of $\sim$ 2.5 nm. STEM-EDX results of fresh Rh/AZT provided in Figure 4.32 validate the existence of Rh, Al, Zr and Ti atoms. HR-TEM images with different resolutions of 5 h spent Rh/AZT are given in Figure 4.33. The images show an average particle size of $\sim$ 2.5 nm, which is the same with the fresh sample. This finding supports superior activity and stability of Rh/AZT. Additionally, existences of Rh, Al, Zr, Ti atoms in 5 h spent Rh/AZT are also found (Figure 4.34).

HR-TEM imaging is performed on Ni/AZT for fresh and 5 h spent samples, whereas STEM-EDX analysis is made on fresh, 5 h and 72 h spent samples. When HR-TEM images of fresh (in Figure 4.35) and 5 h spent (in Figure 4.37) samples of Ni/AZT are compared, increase in the average particle sizes can be interpreted. Average particle

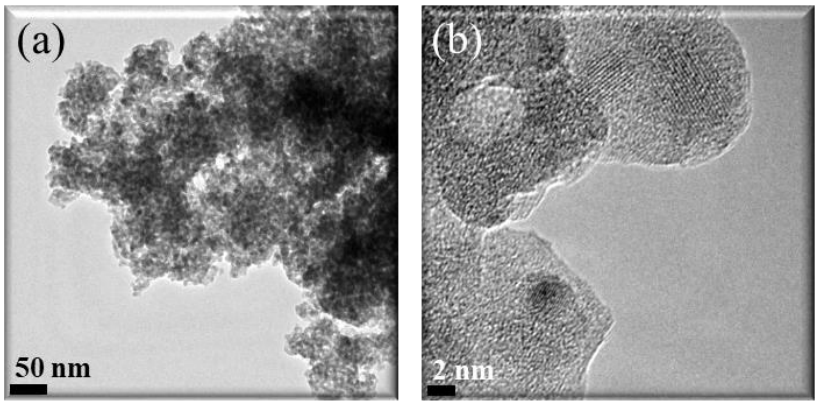

Figure 4.31. HR-TEM images of fresh Rh/AZT with 50 nm (a) and 2 nm (b) resolution.

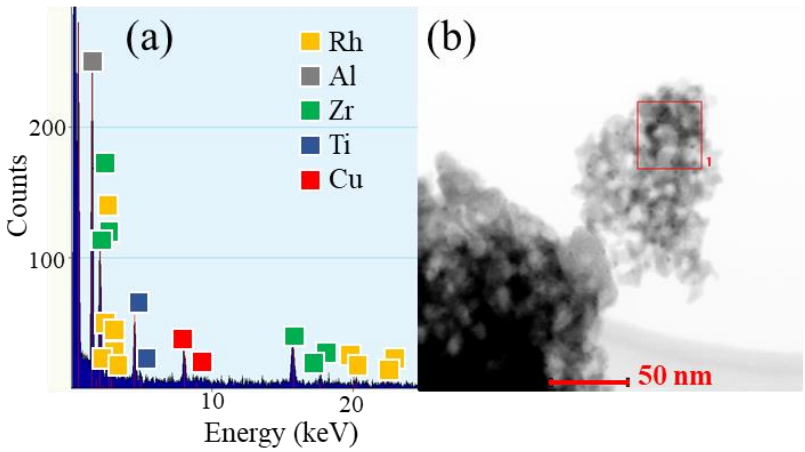

Figure 4.32. STEM-EDX analysis of fresh Rh/AZT.

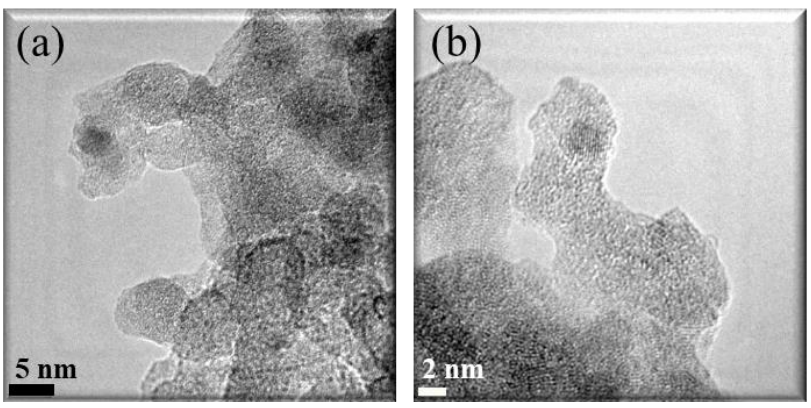

Figure 4.33. HR-TEM images of 5 h spent Rh/AZT with 5 nm (a) and 2 nm (b) resolution.

size of the fresh Ni/AZT is calculated higher than 5 nm. It is almost not possible to find Ni particles that are not covered with support. STEM-EDX analyses on fresh (Figure 4.36), 5 h (Figure 4.38) and 72 h (Figure 4.39) spent samples of Ni/AZT indicate the existence of Ni, Al, Zr and Ti atoms. Additionally, coke is not observed in EDX analyses of Rh and Ni supported on AZT catalysts.

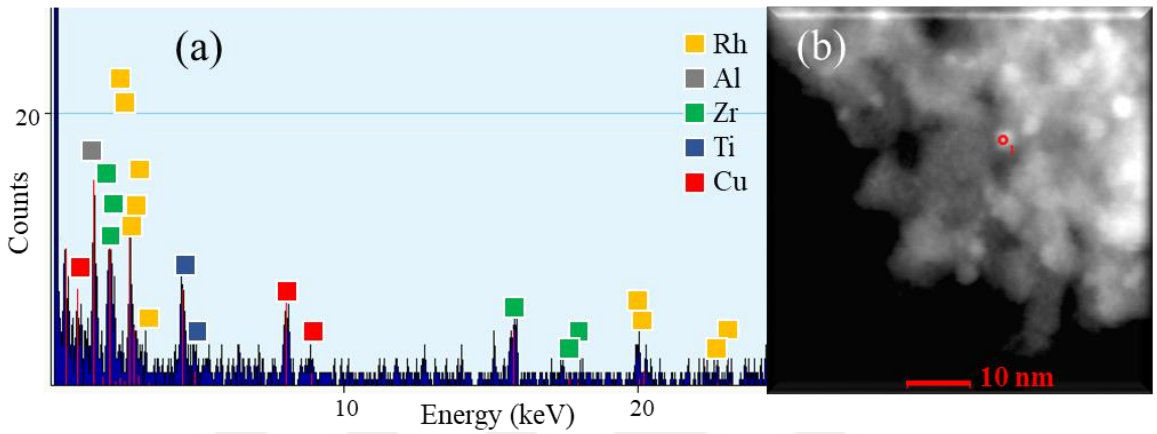

Figure 4.34. STEM-EDX analysis of 5 h spent Rh/AZT.

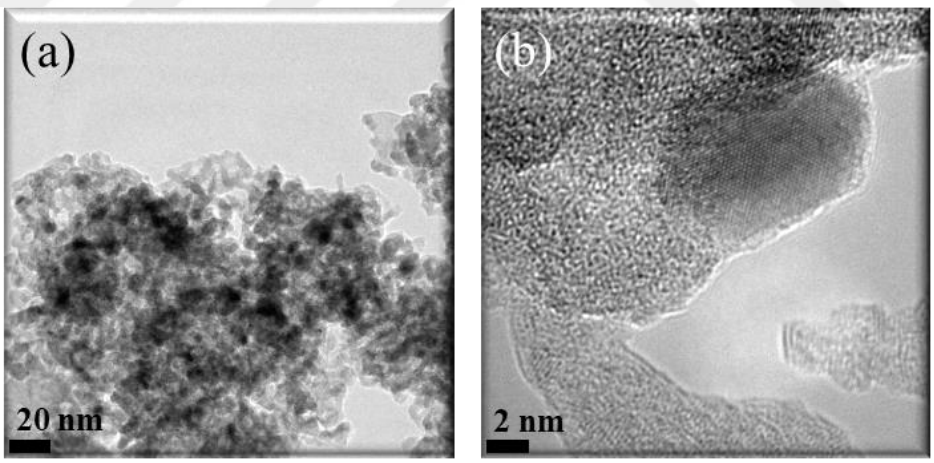

Figure 4.35. HR-TEM images of fresh Ni/AZT with 20 nm (a) and 2 nm (b) resolution.

TEM images of fresh, 5 h and 72 h spent and STEM-EDX analyses of fresh and 72 h spent samples of Co/AZT can be seen in Figures 4.40, 4.42, 4.43, 4.41 and 4.45, respectively. The initial average particle size of Co in fresh sample is higher than 5 nm (*ca.* 10 nm) and grew significantly when used in GDR. Most of the Co particles are covered with either support or coke. In fact, Figure 4.44 suggests graphite layers over

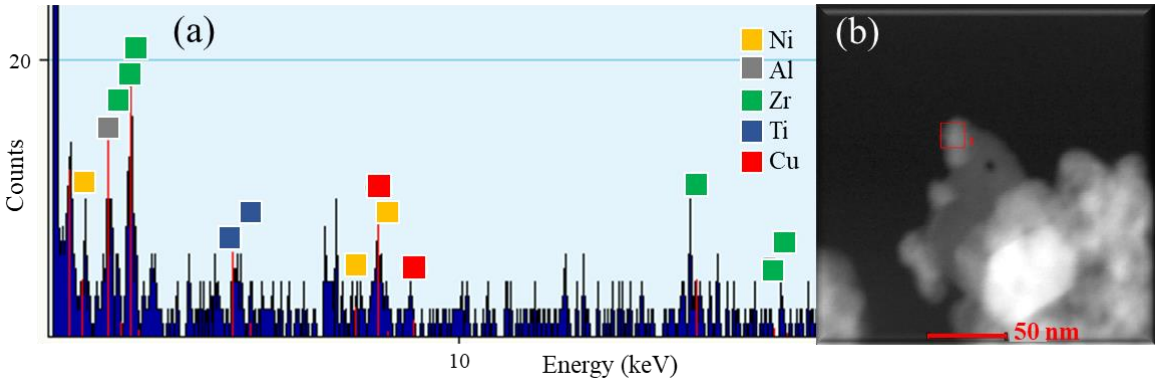

Figure 4.36. STEM-EDX analysis of fresh Ni/AZT.

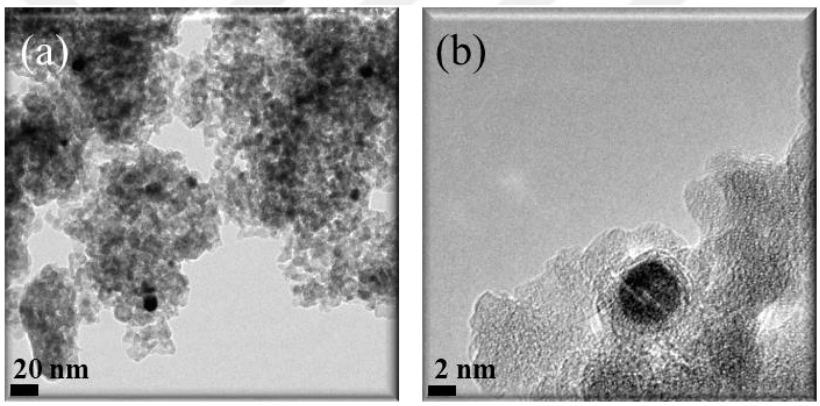

Figure 4.37. HR-TEM images of 5 h spent Ni/AZT with 20 nm (a) and 2 nm (b) resolution.

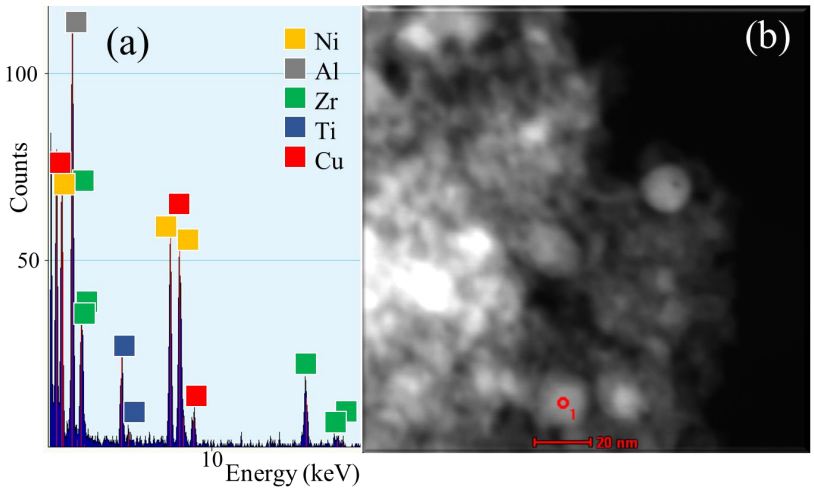

Figure 4.38. STEM-EDX analysis of 5 h spent Ni/AZT.

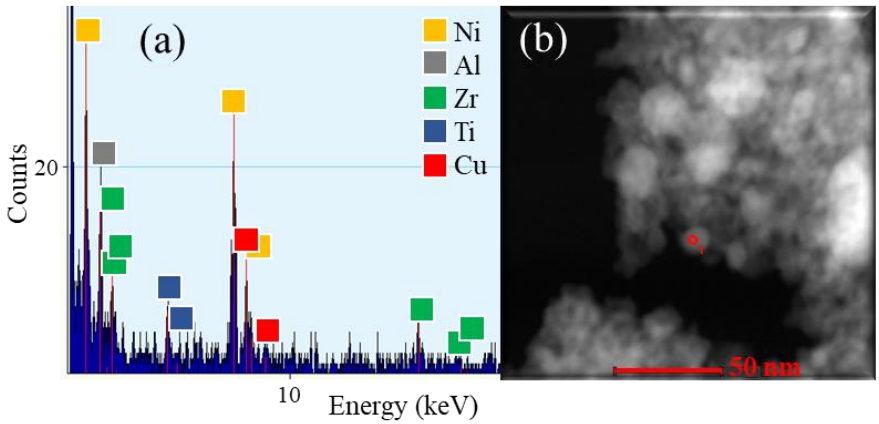

Figure 4.39. STEM-EDX analysis of 72 h spent Ni/AZT used in stability analysis.

the catalyst surface. 0.36 nm of lattice spacing indicates a graphitic type of carbon found *via* TEM analysis. STEM-EDX analyses on both fresh and 72 h spent samples prove the existence of Co, Al, Zr and Ti atoms.

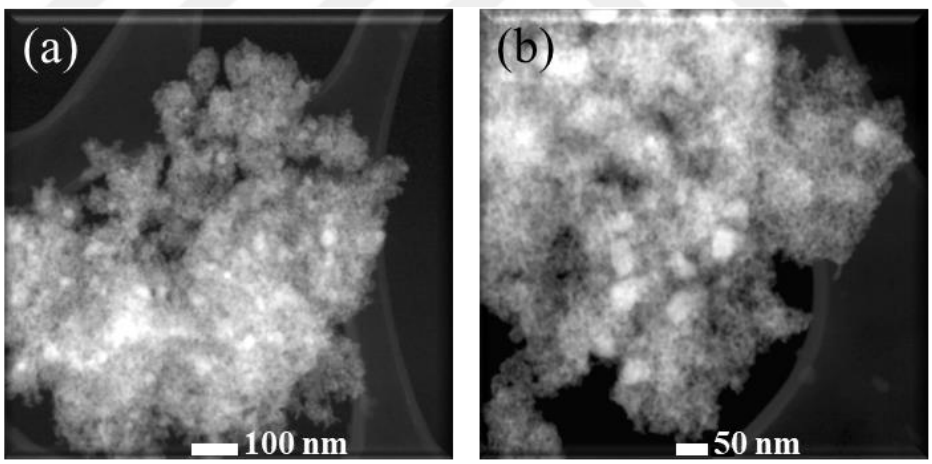

Figure 4.40. TEM images of fresh Co/AZT with 100 nm (a) and 50 nm (b) resolution.

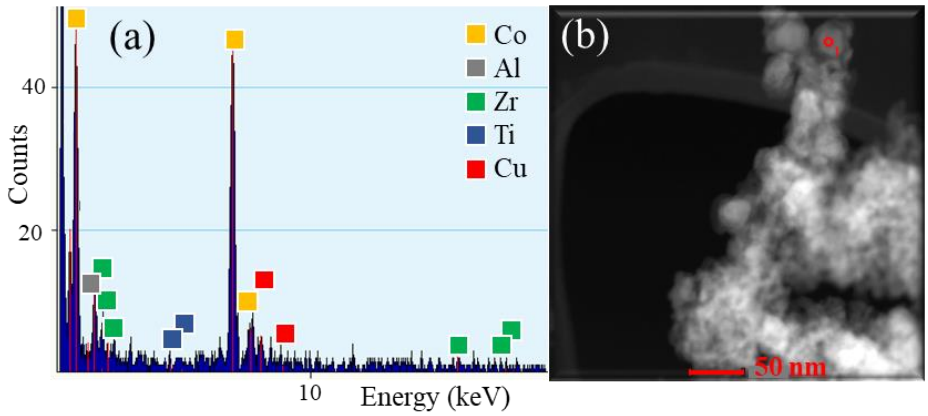

Figure 4.41. STEM-EDX analysis of fresh Co/AZT.

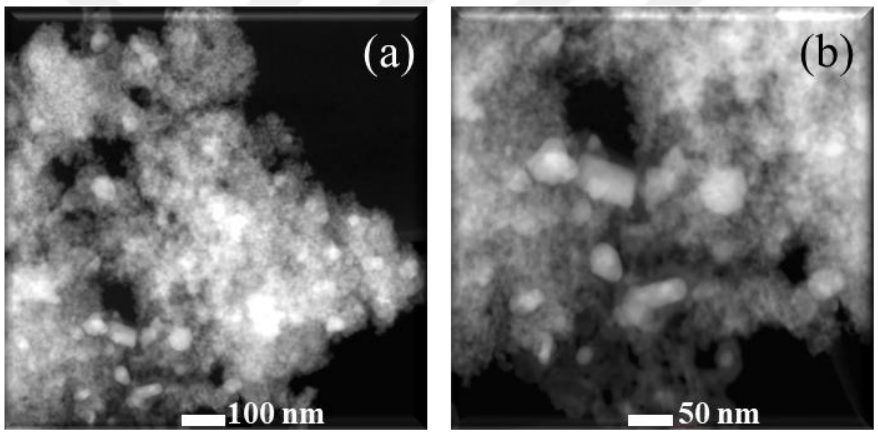

Figure 4.42. TEM images of 5 h spent Co/AZT with 100 nm (a) and 50 nm (b) resolution.

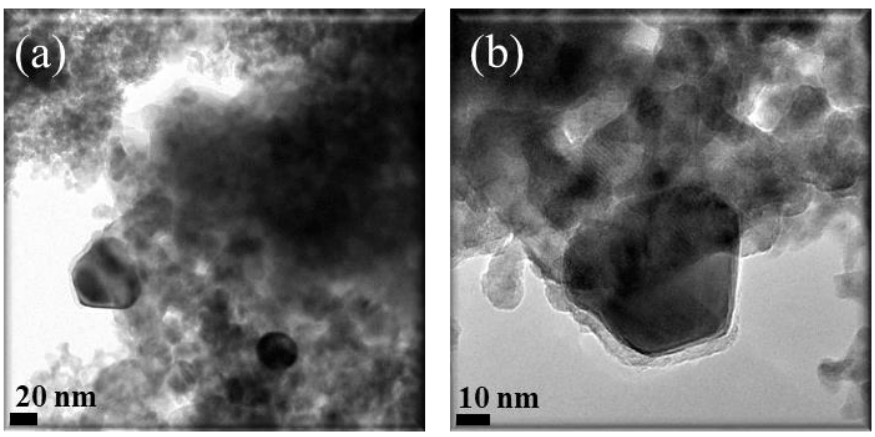

Figure 4.43. TEM images of 72 h spent Co/AZT with 20 nm (a) and 10 nm (b) resolution.

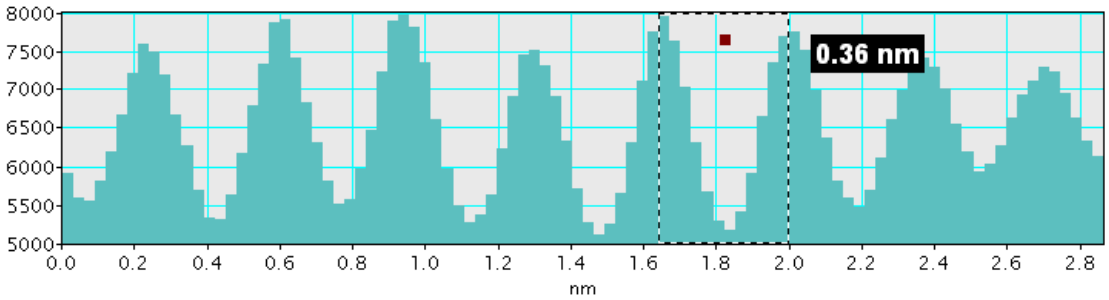

Figure 4.44. TEM result indicating lattice spacing of graphitic carbon over 72 h spent Co/AZT.

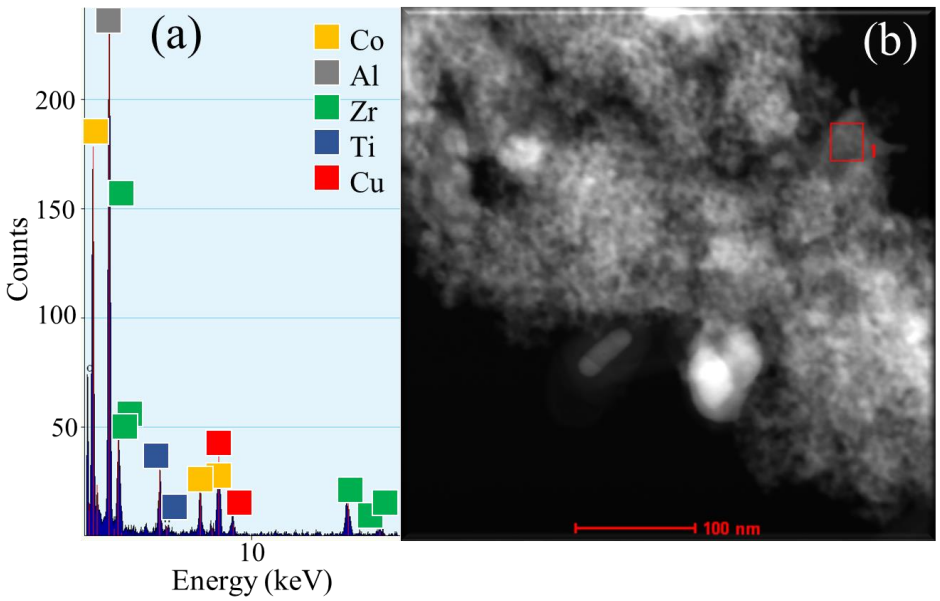

Figure 4.45. STEM-EDX analysis of 72 h spent Co/AZT used in stability analysis.

4.2.7.3. *In-situ* FTIR Spectroscopic Measurements. *In-situ* FTIR spectra of fresh and 72 h spent samples of Rh/AZT is provided in Figure 4.46. The feature seen at 2151 cm^{-1} of fresh sample indicates CO–Rh^{3+} and absence of the same feature after 72 h under reaction conditions suggest Rh^{3+} is partially reduced. Features around 2130 cm^{-1} show these reduced phases of Rh^{2+} or Rh^{+}. Peak at 1904 cm^{-1} of fresh sample indicate two-fold C(*ads*), while in 72 h spent sample it is shifted towards 1873 cm^{-1}. This finding suggests that Rh particles are partially sintered and there is a slight transition from two-fold to three-fold CO adsorption. CO–Rh^{0} signals can be seen around 2032 cm^{-1} in both fresh and 72 h spent samples which have approximately the same intensity. Thus, Rh particles or clusters are durable against GDR operating temperature and long activity tests. Disappearance of signals at 2083 and 2019 cm^{-1} of fresh sample when exposed to 72 h of GDR may suggest that Rh particles are either covered by coke or by the support, with the latter being more likely to occur as the STEM-EDX analysis of 72 h spent Rh/AZT samples did not indicate existence of carbon. Nevertheless, this is subject to further validation by XPS analysis which is on-going.

In-situ FTIR spectroscopic measurements performed over Ni and Co supported on AZT did not revealed any signal, thus are not reported in this study. Ni particles are probably covered by support AZT whereas Co particles may be covered either by support or coke.

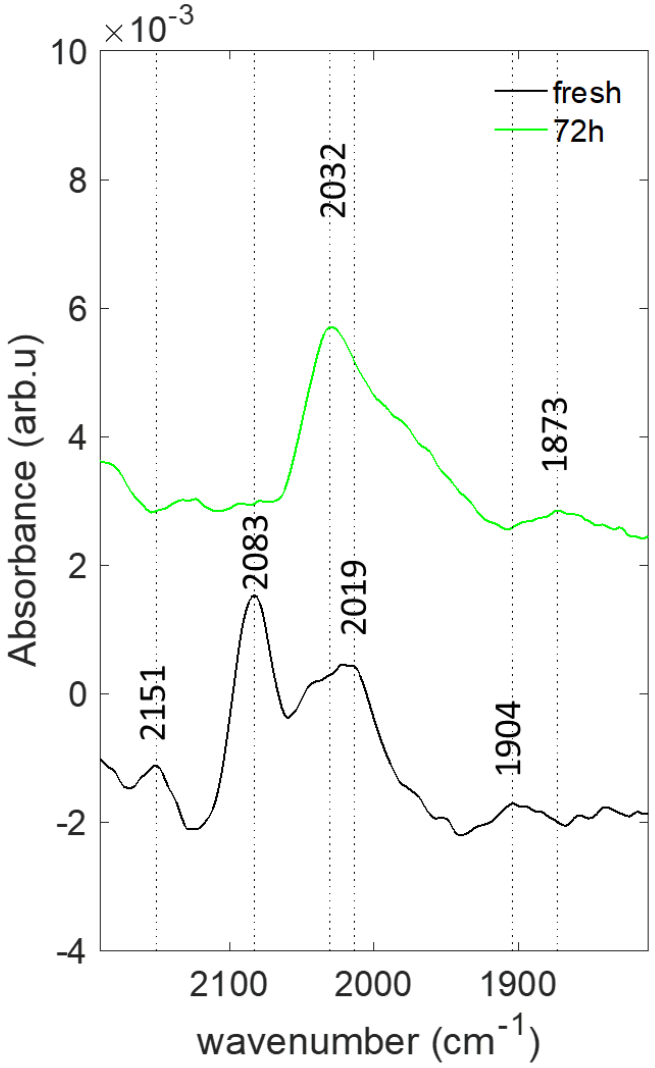

Figure 4.46. *In-situ* FTIR spectra of fresh and 72 h spent Rh/AZT.

5. CONCLUSION

The aim of this study was to develop active and stable catalyst for glycerol dry reforming and to investigate the effects of operational parameters, namely temperature, molar inletCO_2/G ratio and residence time, on glycerol and CO_2 conversions as well as on product distributions. Conclusions drawn from activity and stability tests together with catalyst characterizations are listed in two separate sections below. Finally, recommendations for further improvements are listed in a separate section.

5.1. Conclusions from Rh and Co Catalysts Supported on Single Oxides

- Stability test for 72 h on Rh/ZrO_2, Rh/CeO_2, Co/ZrO_2 and Co/CeO_2 revealed Rh/CeO_2 as the catalyst having the highest stability among the others.
- Although Rh/ZrO_2 exhibited higher CO_2 at the beginning, it deactivated significantly faster than Rh/CeO_2.
- Co catalysts supported on single oxides lost their catalytic activity completely before 45 hours.
- CH_4 yields over all catalyst increased in time indicating their deactivation.
- Average particle size of Rh/ZrO_2 grew from 2.1 nm to 4.1 when exposed to GDR while particle size of Rh/CeO_2 remained almost unchanged which was in alignment with stability results.
- EDX measurements on fresh and 5 h spent samples of Rh/ZrO_2 and Rh/CeO_2 validated existence of Rh and Zr and Rh and Co atoms, respectively.
- Strong metal-support interaction within Rh/CeO_2 was confirmed *via in-situ* FTIR measurements while severe coke formation was determined for 5 h spent Rh/ZrO_2 sample.
- *Ex-situ* Raman spectroscopic measurements validated SMSI between Rh and Ce and severe coke formation in Rh/ZrO_2 catalysts when exposed to GDR reaction.

5.2. Conclusions from Rh, Ni and Co Based Binary and Ternary Oxides

- Rh/AZT showed the best performance among other prepared mixed oxide catalysts as well as single oxide catalysts.
- Ni/AZT showed the best stability together with Rh/AZT under GDR conditions for 72 hours compared to all catalysts.
- Highest CO_2 conversion at default conditions (750 °C, $CO_2/G = 4$, 0.5 mg_{cat} min NmL^{-1}) was recorded as 30.9% over Rh/AZT. This conversion was 94.5% of the corresponding thermodynamic value.
- Activities of the catalysts were found to follow the decreasing order of Rh/AZT >Ni/AZT >Rh/ZT >Co/AZT.
- Reaction temperature had a significant positive effect on extent of GDR in both thermodynamic calculations and experiments.
- No CO_2 conversion is observed at 600 °C over any catalyst whereas approximately the same glycerol conversions ($\sim$ 8%) are noted.
- Increasing CH_4 yield was observed over Co/AZT and Rh/ZT with increasing temperature whereas there was an opposite relation between temperature and CH_4 yield for Rh/AZT and Ni/AZT.
- Based on CO_2 conversion and syngas (H_2 and CO) yields, operating at 750 °C was found to be the optimum.
- Highest CO_2 conversion (39.2%) at residence time of 0.5 mg_{cat} min NmL^{-1} was calculated at 750 °C and CO_2/G ratio of 2 over Rh/AZT. This point was the closest recorded conversion to (*i.e.* 99.5%) thermodynamic limit.
- Increasing CO_2/G feed ratio had negative effect on reactant conversions and H_2 yield predicted by thermodynamic calculations. The experiments, however, have initially resulted in increasing and then decreasing trends.
- Increasing CO_2/G ratio decreased syngas yield and ratio (H_2/CO).
- Support effect was investigated by impregnating Rh over ZrO_2, CeO_2, ZT and AZT and activity of the catalyst followed the decreasing order of Rh/AZT >RhZr >Rh/ZT >RhCe.
- AZT showed superior stability and activity compared to other supports. Includ-

ing TiO_2 to ZrO_2 decreased the activity and did not affect stability.

- Increasing residence time had positive effect on catalytic activity and the highest calculated CO_2 conversion of 32.3% was achieved over Ni/AZT at 750 °C, at CO_2/G ratio of 4 and residence time of 3.75 mg_{cat} min NmL^{-1}.
- Rh/AZT showed approximately the same catalytic activity at residence times of 0.5 and 3.75 mg_{cat} min NmL^{-1} whereas there was significant promotion in catalytic activity (especially for CO_2 conversion) of all other catalysts with residence time.
- Both Rh/AZT and Ni/AZT showed good stability 72 h ToS whereas more than 30 and 50% decrease in catalytic activity was observed over Rh/ZT and Co/AZT within the longevity experiment, respectively.
- BET analysis revealed decreasing specific surface area of only calcined samples as follows: AZT (182 m^2 g^{-1}) >Rh/AZT (123 m^2 g^{-1}) >Ni/AZT (119 m^2 g^{-1}) >Co/AZT (100 m^2 g^{-1}) which is in alignment with catalytic activity of the impregnated catalysts.
- TEM imaging of fresh, 5 and 72 h spent samples of AZT supported catalysts revealed that $\sim$ 2.5 nm Rh particle size was preserved over 5 h operation while Ni and Co average particle sizes grew under GDR conditions.
- EDS measurements on AZT catalysts provided that all catalysts contained Al, Zr and Ti in addition to the corresponding metals.
- *In-situ* FTIR spectroscopic measurements over fresh and 72 h spent Rh/AZT suggested that Rh particles was covered with either coke or AZT after 72 ToS.

5.3. Recommendations

- Longer stability tests can be done over Co/AZT and Rh/ZT to understand whether catalytic activity will be lost completely.
- Metal loading of especially Ni catalysts can be varied to see possible improvements.
- Effect of calcination temperature that changes AZT surface area can be investigated.
- Rh and Ni can be supported on another binary oxide Al_2O_3-ZrO_2 to benefit from

high surface area of Al_2O_3 and oxygen capacity of ZrO_2.

- Residence time investigation over Co/AZT and Rh/ZT can be made similar to Ni/AZT, so that the optimum amount of catalysts necessary can be found for GDR.
- Temperature programmed desorption can be made on AZT samples to investigate the difference between desorbed substances and understand the types of carbonaceous species adsorbed on the catalysts.
- X-ray photoelectron spectroscopy measurements on fresh and spent catalysts can be made in order to investigate the surface concentration of Rh, Ni and Co and their oxidation states before and after GDR.
- *Ex-situ* Raman analysis on metals supported on ternary oxide can reveal metal surface interactions between Rh, Ni, Co and AZT.

REFERENCES

1. Power Generation Research, *The Biofuels Global Market Outlook 2017-2021*, Tech. Rep. April, 2018, https://www.researchandmarkets.com/research/38nzc7/global_biofuels?w=12, accessed at July 2018.

2. Union Zur Förderung Von Oel- Und Proteinpflanzen E.V., *UFOP Report on Global Market Supply*, Tech. rep., 2017, https://www.ufop.de/files/3515/1515/2657/UFOP_Report_on_Global_Market_Supply_2017-2018.pdf, accessed at July 2018.

3. National Biodiesel Board, *Biodiesel, Biodiesel Basics*, Tech. rep., 2016, http://biodiesel.org/what-is-biodiesel/biodiesel-basics, accessed at July 2018.

4. U.S. Energy information administration, *Monthly biodiesel production report with data for April 2018*, Tech. Rep. June, 2018, http://www.eia.gov/biofuels/biodiesel/production/, accessed at July 2018.

5. Schuchardt, U., R. Sercheli and R. M. Vargas, "Transesterification of vegetable oils: A review", *Journal of the Brazilian Chemical Society*, Vol. 9, No. 3, pp. 199–210, 1998.

6. Dou B., C. Wang, H. Chen *et al.*, "Continuous sorption-enhanced steam reforming of glycerol to high-purity hydrogen production", *International Journal of Hydrogen Energy*, Vol. 38, No. 27, pp. 11902–11909, 2013.

7. Quispe, C. A. G., C. J. R. Coronado and J. A. Carvalho, "Glycerol: Production, consumption, prices, characterization and new trends in combustion", *Renewable*

and Sustainable Energy Reviews, Vol. 27, pp. 475–493, 2013.

8. Pagliaro, M. and M. Rossi, *The Future of Glycerol*, Green Chemistry Series, The Royal Society of Chemistry, 2008.

9. Pagliaro, M., R. Ciriminna, H. Kimura *et al.*, "From glycerol to value-added products", *Angewandte Chemie International Edition*, Vol. 46, No. 24, pp. 4434–4440, 2007.

10. Cintas, P., S. Tagliapietra, E. Calcio Gaudino *et al.*, "Glycerol: A solvent and a building block of choice for microwave and ultrasound irradiation procedures", *Green Chemistry*, Vol. 16, No. 3, p. 1056, 2014.

11. Ciriminna, R., C. D. Pina, M. Rossi *et al.*, "Understanding the glycerol market", *European Journal of Lipid Science and Technology*, Vol. 116, No. 10, pp. 1432–1439, 2014.

12. Ma, X., L. Sun and C. Song, "A new approach to deep desulfurization of gasoline, diesel fuel and jet fuel by selective adsorption for ultra-clean fuels and for fuel cell applications", *Catalysis Today*, Vol. 77, No. 1-2, pp. 107–116, 2002.

13. Freitas, A. C. D. and R. Guirardello, "Comparison of several glycerol reforming methods for hydrogen and syngas production using Gibbs energy minimization", *International Journal of Hydrogen Energy*, Vol. 39, No. 31, pp. 17969–17984, 2014.

14. De Klerk, A., *Fischer-tropsch refining*, John Wiley & Sons, 2012.

15. Lee, H. C., K. W. Siew, J. Gimbun *et al.*, "Application of cement clinker as Ni-catalyst support for glycerol dry reforming", *Bulletin of Chemical Reaction Engineering and Catalysis*, Vol. 8, No. 2, pp. 137–144, 2013.

16. Lee, H. C., K. W. Siew, J. Gimbun *et al.*, "Synthesis and characterisation of

cement clinker-supported nickel catalyst for glycerol dry reforming", *Chemical Engineering Journal*, Vol. 255, pp. 245–256, 2014.

17. Lee, H. C., K. W. Siew, M. R. Khan *et al.*, "Catalytic performance of cement clinker supported nickel catalyst in glycerol dry reforming", *Journal of Energy Chemistry*, Vol. 23, No. 5, pp. 645–656, 2014.

18. Siew, K.W., H.C. Lee, J. Gimbun *et al.*, "Characterization of La-promoted Ni/Al_2O_3 catalysts for hydrogen production from glycerol dry reforming", *Journal of Energy Chemistry*, Vol. 23, No. 1, pp. 15–21, 2014.

19. Siew, K. W., H. C. Lee, J. Gimbun *et al.*, "Production of CO-rich hydrogen gas from glycerol dry reforming over La-promoted Ni/Al_2O_3 catalyst", *International Journal of Hydrogen Energy*, Vol. 39, No. 13, pp. 6927–6936, 2014.

20. Kumar, M. A., C. Venumadhav, T. V. Sagar *et al.*, "Catalytic tri-reforming of glycerol for hydrogen generation", *Indian Journal of Chemistry - Section A Inorganic, Physical, Theoretical and Analytical Chemistry*, Vol. 53, No. 4-5, pp. 530–534, 2014.

21. Siew, K. W., H. C. Lee, J. Gimbun *et al.*, "Syngas production from glycerol-dry (CO_2) reforming over La-promoted Ni/Al_2O_3 catalyst", *Renewable Energy*, Vol. 74, No. 3, pp. 441–447, 2015.

22. Siew, K. W., H. C. Lee, M. R. Khan *et al.*, "CO_2 reforming of glycerol over La-Ni/Al_2O_3 catalyst: A longevity evaluative study", *Journal of Energy Chemistry*, Vol. 24, No. 3, pp. 366–373, 2015.

23. Arif, N. N. M., D. N. Vo, M. T. Azizan *et al.*, "Carbon dioxide dry reforming of glycerol for hydrogen production using Ni/ZrO_2 and Ni/CaO as catalysts", *Bulletin of Chemical Reaction Engineering & Catalysis*, Vol. 11, No. 2, pp. 200–209, 2016.

24. Harun, N., J. Gimbun, M. T. Azizan *et al.*, "Characterization of Ag-promoted Ni/SiO_2 catalysts for syngas production via carbon dioxide (CO_2) dry reforming of glycerol", *Bulletin of Chemical Reaction Engineering & Catalysis*, Vol. 11, No. 2, pp. 220–229, 2016.

25. Arif M. N. N., N. Harun, N. Yunus *et al.*, "Reforming of glycerol for hydrogen production over Ni based catalysts: Effect of support type", *Energy Sources, Part A: Recovery, Utilization and Environmental Effects*, Vol. 39, No. 7, pp. 657–663, 2017.

26. Harun, N., S. Z. Abidin, N. N. M. Arif *et al.*, "Characterization of Ni catalyst supported on α-Al_2O_3 and SiO_2 for syngas production via dry reforming of glycerol", *Malaysian Journal of Catalysis*, Vol. 3, No. 2, pp. 48–53, 2018.

27. Harun, N., S. Z. Abidin, O. U. Osazuwa *et al.*, "Hydrogen production from glycerol dry reforming over Ag-promoted Ni/Al_2O_3", *International Journal of Hydrogen Energy*, pp. 1–13, 2018.

28. Tavanarad, M., F. Meshkani and M. Rezaei, "Production of syngas via glycerol dry reforming on Ni catalysts supported on mesoporous nanocrystalline Al_2O_3", *Journal of CO_2 Utilization*, Vol. 24, No. September 2017, pp. 298–305, 2018.

29. Tavanarad, M., F. Meshkani and M. Rezaei, "Synthesis and application of noble metal nanocatalysts supported on $MgAl_2O_4$ in glycerol dry reforming reaction", *Catalysis Letters*, Vol. 148, No. 1, pp. 164–172, 2018.

30. Schulz, H., "Short history and present trends of Fischer–Tropsch synthesis", *Applied Catalysis A: General*, Vol. 186, No. 1-2, pp. 3–12, 1999.

31. Dry, M. E., "The Fischer-Tropsch process: 1950-2000", *Catalysis Today*, Vol. 71, No. 3-4, pp. 227–241, 2002.

32. Rostrup-Nielsen, J., J. Sehested and J. Nørskov, "Hydrogen and synthesis gas by

steam and CO_2 reforming", *Advances in Catalysis*, Vol. 47, pp. 65–139, 2002.

33. Pen, M., J. Gomez, J. G. Fierro *et al.*, "New catalytic routes for syngas and hydrogen production", *Applied Catalysis A: General*, Vol. 144, No. 1-2, pp. 7–57, 1996.

34. Gao, J., Z. Hou, H. Lou *et al.*, "Dry (CO_2) reforming", *Fuel cells: Technologies for Fuel Processing*, pp. 191–221, Elsevier, 2011.

35. Van Hook, J. P., "Methane-steam reforming", *Catalysis Reviews—Science and Engineering*, Vol. 21, No. 1, pp. 1–51, 1980.

36. Rostrup-Nielsen, J. and J. B. Hansen, "Chapter 4 - Steam Reforming for Fuel Cells", D. Shekhawat, J. J. Spivey and D. A. Berry (Editors), *Fuel Cells: Technologies for Fuel Processing*, pp. 49 – 71, Elsevier, Amsterdam, 2011.

37. Van Beurden, P., "On the catalytic aspects of steam-methane reforming", *Energy Research Centre of the Netherlands (ECN), Technical Report I-04-003*, 2004.

38. Barelli, L., G. Bidini, F. Gallorini *et al.*, "Hydrogen production through sorption-enhanced steam methane reforming and membrane technology: A review", *Energy*, Vol. 33, No. 4, pp. 554–570, 2008.

39. Iulianelli, A., P. Ribeirinha, A. Mendes *et al.*, "Methanol steam reforming for hydrogen generation via conventional and membrane reactors: A review", *Renewable and Sustainable Energy Reviews*, Vol. 29, pp. 355–368, 2014.

40. Li, K., H. Wang, Y. Wei *et al.*, "Syngas production from methane and air via a redox process using Ce–Fe mixed oxides as oxygen carriers", *Applied Catalysis B: Environmental*, Vol. 97, No. 3-4, pp. 361–372, 2010.

41. Xu, J. and G. F. Froment, "Methane steam reforming, methanation and water-gas shift: I. Intrinsic kinetics", *AIChE Journal*, Vol. 35, No. 1, pp. 88–96, 1989.

42. Basile, A., L. Di Paola, F. Hai *et al.*, *Membrane reactors for energy applications and basic chemical production*, Woodhead Publishing, 2015.

43. Haryanto, A., S. Fernando, N. Murali *et al.*, "Current status of hydrogen production techniques by steam reforming of ethanol: A review", *Energy & Fuels*, Vol. 19, No. 5, pp. 2098–2106, 2005.

44. Vaidya, P. D. and A. E. Rodrigues, "Glycerol reforming for hydrogen production: A review", *Chemical Engineering and Technology*, Vol. 32, No. 10, pp. 1463–1469, 2009.

45. Contreras, J., J. Salmones, J. Colín-Luna *et al.*, "Catalysts for H_2 production using the ethanol steam reforming (a review)", *International Journal of Hydrogen Energy*, Vol. 39, No. 33, pp. 18835–18853, 2014.

46. Ni, M., D. Y. Leung and M. K. Leung, "A review on reforming bio-ethanol for hydrogen production", *International Journal of Hydrogen Energy*, Vol. 32, No. 15, pp. 3238–3247, 2007.

47. Vaidya, P. D. and A. E. Rodrigues, "Insight into steam reforming of ethanol to produce hydrogen for fuel cells", *Chemical Engineering Journal*, Vol. 117, No. 1, pp. 39–49, 2006.

48. Cavallaro, S., "Ethanol steam reforming on Rh/Al_2O_3 catalysts", *Energy & Fuels*, Vol. 14, No. 6, pp. 1195–1199, 2000.

49. Vizcaíno, A., P. Arena, G. Baronetti *et al.*, "Ethanol steam reforming on Ni/Al_2O_3 catalysts: Effect of Mg addition", *International Journal of Hydrogen Energy*, Vol. 33, No. 13, pp. 3489–3492, 2008.

50. LeValley, T. L., A. R. Richard and M. Fan, "The progress in water gas shift and steam reforming hydrogen production technologies–a review", *International Journal of Hydrogen Energy*, Vol. 39, No. 30, pp. 16983–17000, 2014.

51. Iriondo, A., V. Barrio, J. Cambra *et al.*, "Glycerol steam reforming over Ni catalysts supported on ceria and ceria-promoted alumina", *International Journal of Hydrogen Energy*, Vol. 35, No. 20, pp. 11622–11633, 2010.

52. Adhikari, S., S. Fernando, S. R. Gwaltney *et al.*, "A thermodynamic analysis of hydrogen production by steam reforming of glycerol", *International Journal of Hydrogen Energy*, Vol. 32, No. 14, pp. 2875–2880, 2007.

53. Dou, B., Y. Song, C. Wang *et al.*, "Hydrogen production from catalytic steam reforming of biodiesel byproduct glycerol: Issues and challenges", *Renewable and Sustainable Energy Reviews*, Vol. 30, pp. 950–960, 2014.

54. Pakhare, D. and J. Spivey, "A review of dry (CO_2) reforming of methane over noble metal catalysts", *Chemical Society Reviews*, Vol. 43, No. 22, pp. 7813–7837, 2014.

55. Budiman, A. W., S. H. Song, T. S. Chang *et al.*, "Dry reforming of methane over cobalt catalysts: A literature review of catalyst development", *Catalysis Surveys from Asia*, Vol. 16, No. 4, pp. 183–197, 2012.

56. Colmenares, J. C., R. F. Colmenares Quintero and I. S. Pieta, "Catalytic dry reforming for biomass-based fuels processing: Progress and future perspectives", *Energy Technology*, Vol. 4, No. 8, pp. 881–890, 2016.

57. Morales-Cano, F., L. F. Lundegaard, R. R. Tiruvalam *et al.*, "Improving the sintering resistance of Ni/Al_2O_3 steam-reforming catalysts by promotion with noble metals", *Applied Catalysis A: General*, Vol. 498, pp. 117–125, 2015.

58. Lavoie, J. M., "Review on dry reforming of methane, a potentially more environmentally-friendly approach to the increasing natural gas exploitation", *Frontiers in Chemistry*, Vol. 2, No. November, pp. 1–17, 2014.

59. Ghoneim, S. A., R. A. El-Salamony and S. A. El-Temtamy, "Review on innovative

catalytic reforming of natural gas to syngas", *World Journal Of Engineering and Technology*, Vol. 4, No. February, pp. 116–139, 2016.

60. Abatzoglou, N. and C. Fauteux-Lefebvre, "Review of catalytic syngas production through steam or dry reforming and partial oxidation of studied liquid compounds", *Wiley Interdisciplinary Reviews: Energy and Environment*, Vol. 5, No. 2, pp. 169–187, 2016.

61. Usman, M., W. M. A. Wan Daud and H. F. Abbas, "Dry reforming of methane: Influence of process parameters - A review", *Renewable and Sustainable Energy Reviews*, Vol. 45, pp. 710–744, 2015.

62. Dębek, R., M. Motak, T. Grzybek *et al.*, "A short review on the catalytic activity of hydrotalcite-derived materials for dry reforming of methane", *Catalysts*, Vol. 7, No. 1, p. 32, 2017.

63. Shah, Y. T. and T. H. Gardner, "Dry reforming of hydrocarbon feedstocks", *Catalysis Reviews - Science and Engineering*, Vol. 56, No. 4, pp. 476–536, 2014.

64. Ross, J. R., "Natural gas reforming and CO_2 mitigation", *Catalysis Today*, Vol. 100, No. 1-2, pp. 151–158, 2005.

65. Abdullah, B., N. A. A. Ghani and D. V. N. Vo, "Recent advances in dry reforming of methane over Ni-based catalysts", *Journal of Cleaner Production*, Vol. 162, pp. 170–185, 2017.

66. Carioca, J. and M. Leal, "Ethanol production from sugar-based feedstocks", Vol. 3, 2011.

67. Tsiakaras, P. and A. Demin, "Thermodynamic analysis of a solid oxide fuel cell system fuelled by ethanol", *Journal of Power Sources*, Vol. 102, No. 1-2, pp. 210–217, 2001.

68. Wang, W. and Y. Wang, "Dry reforming of ethanol for hydrogen production: Thermodynamic investigation", *International Journal of Hydrogen Energy*, Vol. 34, No. 13, pp. 5382–5389, 2009.

69. Kale, G. R. and B. D. Kulkarni, "Thermoneutral point analysis of ethanol dry autothermal reforming", *Chemical Engineering Journal*, Vol. 165, No. 3, pp. 864–873, 2010.

70. Kale, G. R. and T. M. Gaikwad, "Thermodynamic analysis of ethanol dry reforming: Effect of combined parameters", *ISRN Thermodynamics*, Vol. 2014, pp. 1–10, 2014.

71. Ortiz, A. L., R. P. Sámano, M. M. Zaragoza *et al.*, "Thermodynamic analysis and process simulation for the H_2 production by dry reforming of ethanol with $CaCO_3$", *International Journal of Hydrogen Energy*, Vol. 40, No. 48, pp. 17172–17179, 2015.

72. Hu, X. and G. Lu, "Syngas production by CO_2 reforming of ethanol over Ni/Al_2O_3 catalyst", *Catalysis Communications*, Vol. 10, No. 13, pp. 1633–1637, 2009.

73. Kumar, A., R. R. Bhosale, S. S. Malik *et al.*, "Thermodynamic investigation of hydrogen enrichment and carbon suppression using chemical additives in ethanol dry reforming", *International Journal of Hydrogen Energy*, Vol. 41, No. 34, pp. 15149–15157, 2016.

74. De Oliveira-Vigier, K., N. Abatzoglou and F. Gitzhofer, "Dry-Reforming of Ethanol in the Presence of a 316 Stainless Steel Catalyst", *The Canadian Journal of Chemical Engineering*, Vol. 83, No. 6, pp. 978–984, 2005.

75. Jankhah, S., N. Abatzoglou and F. Gitzhofer, "Thermal and catalytic dry reforming and cracking of ethanol for hydrogen and carbon nanofilaments' production", *International Journal of Hydrogen Energy*, Vol. 33, No. 18, pp. 4769–4779, 2008.

76. Abatzoglou, N., J. Blanchard, H. Oudghiri-Hassani *et al.*, "The use of catalytic reforming reactions for CO_2 sequestration as carbon nanotubes", *Proceedings of the 2006 IASME/WSEAS International Conference on Energy & Environmental Systems, Chalkida, Greece*, pp. 21–26, 2006.

77. Blanchard, J., H. Oudghiri-Hassani, N. Abatzoglou *et al.*, "Synthesis of nanocarbons via ethanol dry reforming over a carbon steel catalyst", *Chemical Engineering Journal*, Vol. 143, No. 1-3, pp. 186–194, 2008.

78. Bellido, J. D., E. Y. Tanabe and E. M. Assaf, "Carbon dioxide reforming of ethanol over Ni/Y_2O_3–ZrO_2 catalysts", *Applied Catalysis B: Environmental*, Vol. 90, No. 3-4, pp. 485–488, 2009.

79. Da Silva, A. M., K. R. De Souza, G. Jacobs *et al.*, "Steam and CO_2 reforming of ethanol over Rh/CeO_2 catalyst", *Applied Catalysis B: Environmental*, Vol. 102, No. 1-2, pp. 94–109, 2011.

80. Zawadzki, A., J. Bellido, A. F. Lucrédio *et al.*, "Dry reforming of ethanol over supported Ni catalysts prepared by impregnation with methanolic solution", *Fuel Processing Technology*, Vol. 128, pp. 432–440, 2014.

81. Hou, T., Y. Lei, S. Zhang *et al.*, "Ethanol dry reforming for syngas production over Ir/CeO_2 catalyst", *Journal of Rare Earths*, Vol. 33, No. 1, pp. 42–45, 2015.

82. Drif, A., N. Bion, R. Brahmi *et al.*, "Study of the dry reforming of methane and ethanol using Rh catalysts supported on doped alumina", *Applied Catalysis A: General*, Vol. 504, pp. 576–584, 2015.

83. Bahari, M. B., N. H. H. Phuc, B. Abdullah *et al.*, "Ethanol dry reforming for syngas production over Ce-promoted Ni/Al_2O_3 catalyst", *Journal of Environmental Chemical Engineering*, Vol. 4, No. 4, pp. 4830–4838, 2016.

84. Bahari, M. B., B. C. Goo, T. L. Pham *et al.*, "Hydrogen-rich syngas production

from ethanol dry reforming on La-doped Ni/Al_2O_3 catalysts: Effect of promoter loading", *Procedia Engineering*, Vol. 148, pp. 654–661, 2016.

85. Bej, B., S. Bepari, N. C. Pradhan *et al.*, "Production of hydrogen by dry reforming of ethanol over alumina supported nano-NiO/SiO_2 catalyst", *Catalysis Today*, Vol. 291, pp. 58–66, 2017.

86. Lin, Y. C., "Catalytic valorization of glycerol to hydrogen and syngas", *International Journal of Hydrogen Energy*, Vol. 38, No. 6, pp. 2678–2700, 2013.

87. Liu, B. and J. Greeley, "Decomposition pathways of glycerol via C–H, O–H, and C–C bond scission on Pt (111): A density functional theory study", *The Journal of Physical Chemistry C*, Vol. 115, No. 40, pp. 19702–19709, 2011.

88. Valliyappan, T., N. N. Bakhshi and A. K. Dalai, "Pyrolysis of glycerol for the production of hydrogen or syn gas", *Bioresource Technology*, Vol. 99, No. 10, pp. 4476–4483, 2008.

89. Shekhar, R. and M. A. Barteau, "Decarbonylation and hydrogenation reactions of allyl alcohol and acrolein on Pd (110)", *Surface Science*, Vol. 319, No. 3, pp. 298–314, 1994.

90. Wang, Z., X. M. Cao, J. Zhu *et al.*, "Activity and coke formation of nickel and nickel carbide in dry reforming: A deactivation scheme from density functional theory", *Journal of Catalysis*, Vol. 311, pp. 469–480, 2014.

91. Wang, S., Q. Wang, X. Song *et al.*, "Dry autothermal reforming of glycerol with in situ hydrogen separation via thermodynamic evaluation", *International Journal of Hydrogen Energy*, Vol. 42, No. 2, pp. 838–847, 2017.

92. Gaddalla, A. M. and M. E. Sommer, "Carbon dioxide reforming of methane on nickel catalysts", *Chemical Engineering Science*, Vol. 44, No. 12, pp. 2825–2829, 1989.

93. de Araujo, G. C., S. M. de Lima, J. M. Assaf *et al.*, "Catalytic evaluation of perovskite-type oxide $LaNi_{1-x}Ru_xO_3$ in methane dry reforming", *Catalysis Today*, Vol. 133, pp. 129–135, 2008.

94. Zhang Z. L., V. A. Tsipouriari, A. M. Efstathiou *et al.*, "Reforming of methane with carbon dioxide to synthesis gas over supported rhodium catalysts: I. Effects of support and metal crystallite size on reaction activity and deactivation characteristics", *Journal of Catalysis*, Vol. 158, No. 1, pp. 51–63, 1996.

95. Wang, X., M. Li, M. Wang *et al.*, "Thermodynamic analysis of glycerol dry reforming for hydrogen and synthesis gas production", *Fuel*, Vol. 88, No. 11, pp. 2148–2153, 2009.

96. Knifton, J. F., "Ethylene glycol from synthesis gas via ruthenium melt catalysis", *Journal of the American Chemical Society*, Vol. 103, No. 13, pp. 3959–3961, 1981.

97. Ross, J. R. H., A. N. J. Van Keulen, M. E. S. Hegarty *et al.*, "The catalytic conversion of natural gas to useful products", *Catalysis Today*, Vol. 30, No. 1-3, pp. 193–199, 1996.

98. Kale, G. R. and B. D. Kulkarni, "Thermodynamic analysis of dry autothermal reforming of glycerol", *Fuel Processing Technology*, Vol. 91, No. 5, pp. 520–530, 2010.

99. Zakaria, Z. Y., M. Jusoh, A. Johari *et al.*, "Thermodynamic analysis of hydrogen production from ethanol-glycerol mixture through dry reforming", *Energy Procedia*, Vol. 61, pp. 2391–2394, 2014.

100. Zakaria, Z. Y., M. Jusoh, A. Johari *et al.*, "Thermodynamic analysis of hydrogen production from ethanol-glycerol mixture through steam and dry reforming", *Procedia Manufacturing*, Vol. 2, No. February, pp. 92–96, 2015.

101. Saimon, N. N., M. Jusoh, M. J. Kamarudin *et al.*, "Thermodynamic analysis

of hydrogen production from methanol-ethanol-glycerol mixture through dry reforming", *Chemical Engineering*, Vol. 56, 2017.

102. Fernández, Y., A. Arenillas, J. M. Bermúdez *et al.*, "Comparative study of conventional and microwave-assisted pyrolysis, steam and dry reforming of glycerol for syngas production, using a carbonaceous catalyst", *Journal of Analytical and Applied Pyrolysis*, Vol. 88, No. 2, pp. 155–159, 2010.

103. Fernández, Y., A. Arenillas, M. A. Díez *et al.*, "Pyrolysis of glycerol over activated carbons for syngas production", *Journal of Analytical and Applied Pyrolysis*, Vol. 84, No. 2, pp. 145–150, 2009.

104. Reddy, B. M., B. Chowdhury and P. G. Smirniotis, "An XPS study of the dispersion of MoO_3 on TiO_2–ZrO_2, TiO_2–SiO_2, TiO_2–Al_2O_3, SiO_2–ZrO_2, and SiO_2–TiO_2–ZrO_2 mixed oxides", *Applied Catalysis A: General*, Vol. 211, No. 1, pp. 19–30, 2001.

105. Bulutoglu, P. S., *Parametric investigation of catalytic dry reforming of glycerol to synthesis gas*, Master's Thesis, Boğaziçi University, Turkey, 2017.

106. Ho, S. M., "On the structural chemistry of zirconium oxide", *Materials Science and Engineering*, Vol. 54, No. 1, pp. 23–29, 1982.

107. Tanabe, K., "Surface and catalytic properties of ZrO_2", *Materials Chemistry and Physics*, Vol. 13, No. 3-4, pp. 347–364, 1985.

108. Fornasiero, P., R. Dimonte, G. R. Rao *et al.*, "Rh-loaded CeO_2-ZrO_2 solid-solutions as highly efficient oxygen exchangers: Dependence of the reduction behavior and the oxygen storage capacity on the structural-properties", *Journal of Catalysis*, Vol. 151, No. 1, pp. 168–177, 1995.

109. Ruckenstein, E. and H. Wang, "Effect of support on partial oxidation of methane to synthesis gas over supported rhodium catalysts", *Journal of Catalysis*, Vol.

187, No. 1, pp. 151–159, 1999.

110. Kim, S. S., S. M. Lee, J. M. Won *et al.*, "Effect of Ce/Ti ratio on the catalytic activity and stability of Ni/CeO_2–TiO_2 catalyst for dry reforming of methane", *Chemical Engineering Journal*, Vol. 280, pp. 433–440, 2015.

111. Seo, H. O., J. K. Sim, K. D. Kim *et al.*, "Carbon dioxide reforming of methane to synthesis gas over a TiO_2–Ni inverse catalyst", *Applied Catalysis A: General*, Vol. 451, pp. 43–49, 2013.

112. Bradford, M. C. and M. A. Vannice, "The role of metal–support interactions in CO_2 reforming of CH_4", *Catalysis Today*, Vol. 50, No. 1, pp. 87–96, 1999.

113. Bradford, M. C. and M. A. Vannice, "CO_2 reforming of CH_4 over supported Ru catalysts", *Journal of Catalysis*, Vol. 183, No. 1, pp. 69–75, 1999.

114. Yan, Q. G., W. Z. Weng, H. L. Wan *et al.*, "Activation of methane to syngas over a Ni/TiO_2 catalyst", *Applied Catalysis A: General*, Vol. 239, No. 1-2, pp. 43–58, 2003.

115. Matsuda, S. and A. Kato, "Titanium oxide based catalysts-a review", *Applied Catalysis*, Vol. 8, No. 2, pp. 149–165, 1983.

116. Vannice, M., "The catalytic synthesis of hydrocarbons from carbon monoxide and hydrogen", *Catalysis Reviews—Science and Engineering*, Vol. 14, No. 1, pp. 153–191, 1976.

117. Tada, S., T. Shimizu, H. Kameyama *et al.*, "Ni/CeO_2 catalysts with high CO_2 methanation activity and high CH_4 selectivity at low temperatures", *International Journal of Hydrogen Energy*, Vol. 37, No. 7, pp. 5527–5531, 2012.

118. Kumar, P., Y. Sun and R. O. Idem, "Comparative study of Ni-based mixed oxide catalyst for carbon dioxide reforming of methane", *Energy & Fuels*, Vol. 22, No. 6,

pp. 3575–3582, 2008.

119. Say, Z., M. Tohumeken and E. Ozensoy, "NO_x storage and reduction pathways on zirconia and titania functionalized binary and ternary oxides as NO_x storage and reduction (NSR) systems", *Catalysis Today*, Vol. 231, pp. 135–144, 2014.

120. Takahashi, N., A. Suda, I. Hachisuka *et al.*, "Sulfur durability of NO_x storage and reduction catalyst with supports of TiO_2, ZrO_2 and ZrO_2-TiO_2 mixed oxides", *Applied Catalysis B: Environmental*, Vol. 72, No. 1-2, pp. 187–195, 2007.

121. Imagawa, H., T. Tanaka, N. Takahashi *et al.*, "Synthesis and characterization of Al_2O_3 and ZrO_2–TiO_2 nano-composite as a support for NO_x storage–reduction catalyst", *Journal of Catalysis*, Vol. 251, No. 2, pp. 315–320, 2007.

122. Imagawa, H., N. Takahashi, T. Tanaka *et al.*, "Improved NO_x storage-reduction catalysts using Al_2O_3 and ZrO_2–TiO_2 nanocomposite support for thermal stability and sulfur durability", *Applied Catalysis B: Environmental*, Vol. 92, No. 1-2, pp. 23–29, 2009.

123. Say, Z., *Investigation of NO_2 and SO_2 adsorption/desorption properties of advanced ternary and quaternary mixed oxides for $Deno_x$ catalysis*, Ph.D. Thesis, Bilkent University, Turkey, 2015.

124. Trueba, M. and S. P. Trasatti, "γ-Alumina as a support for catalysts: A review of fundamental aspects", *European Journal of Inorganic Chemistry*, Vol. 2005, No. 17, pp. 3393–3403, 2005.

125. Maciver, D., H. Tobin and R. Barth, "Catalytic aluminas I. Surface chemistry of eta and gamma alumina", *Journal of Catalysis*, Vol. 2, No. 6, pp. 485–497, 1963.

126. Abate, S., C. Mebrahtu, E. Giglio *et al.*, "Catalytic Performance of γ-Al_2O_3–ZrO_2–TiO_2–CeO_2 composite oxide supported Ni-based catalysts for CO_2 methanation", *Industrial & Engineering Chemistry Research*, Vol. 55, No. 16, pp. 4451–

4460, 2016.

127. Karakaya, M., *Experimental and quantitative analysis of multiphase catalytic reactions under microfluidic conditions and geometries*, Ph.D. Thesis, Bogazici University, Turkey, 2014.

128. Kayhan, E., S. M. Andonova, G. S. Şentürk *et al.*, "Fe promoted NO_x storage materials: Structural properties and NO_x uptake", *The Journal of Physical Chemistry C*, Vol. 114, No. 1, pp. 357–369, 2009.

129. Simsek, E., M. Karakaya, A. K. Avci *et al.*, "Oxidative steam reforming of methane to synthesis gas in microchannel reactors", *International Jjournal of Hydrogen Energy*, Vol. 38, No. 2, pp. 870–878, 2013.

130. Wang, X., S. Li, H. Wang *et al.*, "Thermodynamic analysis of glycerin steam reforming", *Energy & Fuels*, Vol. 22, No. 6, pp. 4285–4291, 2008.

131. Adhikari, S., S. Fernando and A. Haryanto, "A comparative thermodynamic and experimental analysis on hydrogen production by steam reforming of glycerin", *Energy & Fuels*, Vol. 21, No. 4, pp. 2306–2310, 2007.

132. Campbell, C. T., "Catalyst–support interactions: Electronic perturbations", *Nature Chemistry*, Vol. 4, No. 8, pp. 597–598, 2012.

133. Farmer, J. A. and C. T. Campbell, "Ceria maintains smaller metal catalyst particles by strong metal-support bonding", *Science*, Vol. 329, No. 5994, pp. 933–936, 2010.

134. Lin, W., A. A. Herzing, C. J. Kiely *et al.*, "Probing metal- support interactions under oxidizing and reducing conditions: in situ Raman and infrared spectroscopic and scanning transmission electron microscopic- X-ray energy-dispersive spectroscopic investigation of supported platinum catalysts", *The Journal of Physical Chemistry C*, Vol. 112, No. 15, pp. 5942–5951, 2008.

135. Say, Z., E. I. Vovk, V. I. Bukhtiyarov *et al.*, "Influence of ceria on the NO_x reduction performance of NO_x storage reduction catalysts", *Applied Catalysis B: Environmental*, Vol. 142, pp. 89–100, 2013.

136. Doornkamp, C. and V. Ponec, "The universal character of the Mars and Van Krevelen mechanism", *Journal of Molecular Catalysis A: Chemical*, Vol. 162, No. 1-2, pp. 19–32, 2000.

137. Bitter, J., K. Seshan and J. Lercher, "On the contribution of X-ray absorption spectroscopy to explore structure and activity relations of Pt/ZrO_2 catalysts for CO_2/CH_4 reforming", *Topics in Catalysis*, Vol. 10, No. 3-4, pp. 295–305, 2000.

138. Guo, J., H. Lou, L. Mo *et al.*, "The reactivity of surface active carbonaceous species with CO_2 and its role on hydrocarbon conversion reactions", *Journal of Molecular Catalysis A: Chemical*, Vol. 316, No. 1-2, pp. 1–7, 2010.

139. Tauster, S. J., S. C. Fung, R. T. K. Baker *et al.*, "Strong interactions in supported-metal catalysts", *Science*, Vol. 211, No. 4487, pp. 1121–1125, 1981.

140. Vannice, M. A., C. Twu and S. Moon, "SMSI effects on CO adsorption and hydrogenation on Pt catalysts: I. Infrared spectra of adsorbed CO prior to and during reaction conditions", *Journal of Catalysis*, Vol. 79, No. 1, pp. 70–80, 1983.

141. Gaur, S., D. J. Haynes and J. J. Spivey, "Rh, Ni, and Ca substituted pyrochlore catalysts for dry reforming of methane", *Applied Catalysis A: General*, Vol. 403, No. 1-2, pp. 142–151, 2011.

142. Chiodo, V., S. Freni, A. Galvagno *et al.*, "Catalytic features of Rh and Ni supported catalysts in the steam reforming of glycerol to produce hydrogen", *Applied Catalysis A: General*, Vol. 381, No. 1-2, pp. 1–7, 2010.

APPENDIX A: CALIBRATION OF MASS FLOW CONTROLLERS

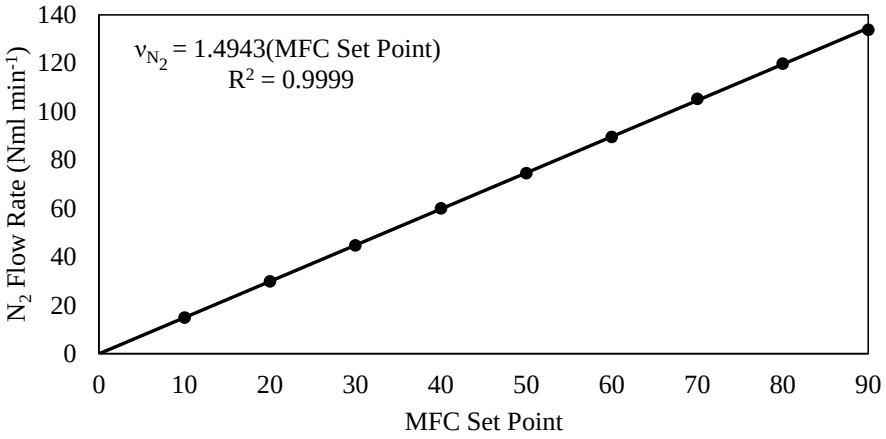

Figure A.1. Calibration curve of MFC for N_2

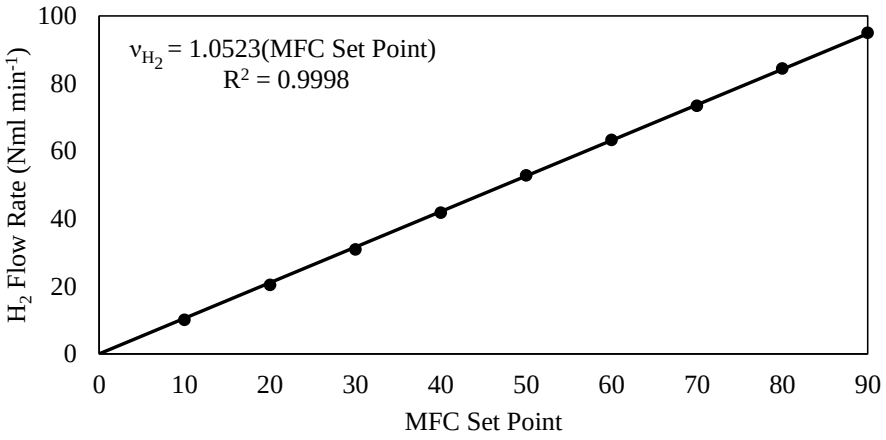

Figure A.2. Calibration curve of MFC for H_2

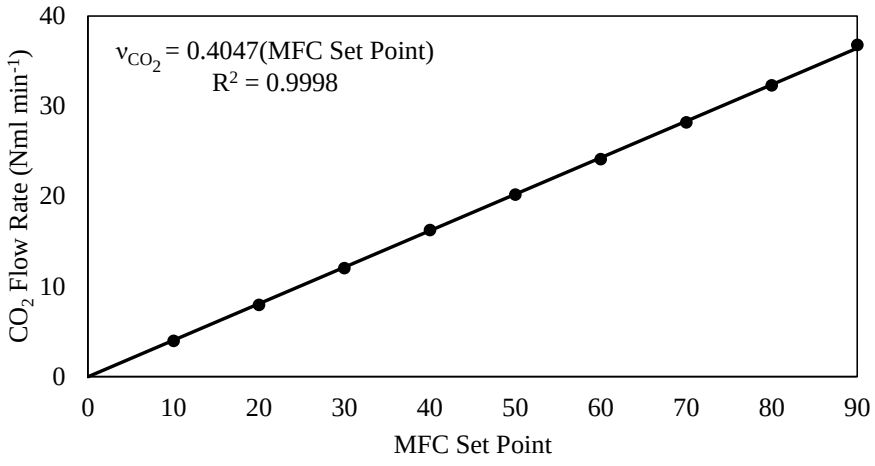

Figure A.3. Calibration curve of MFC for CO_2

APPENDIX B: CALIBRATION OF GAS CHROMATOGRAPHS

B.1. Calibration Curves for Schimadzu GC-2014

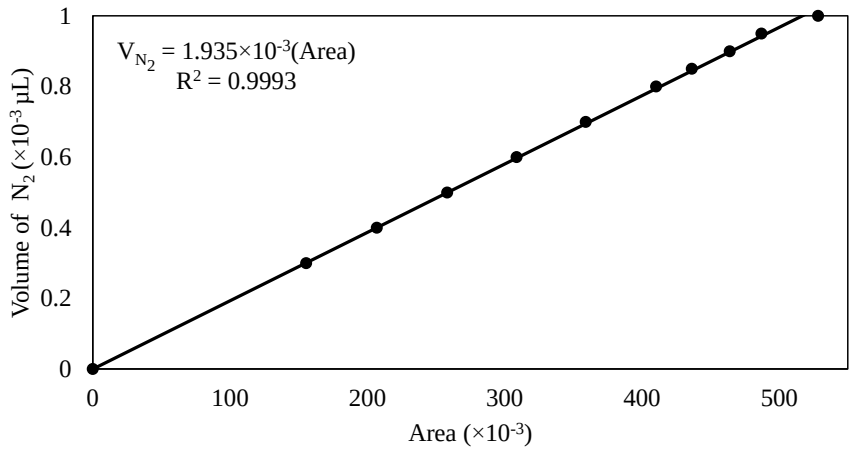

Figure B.1. GC1 calibration curve for N_2

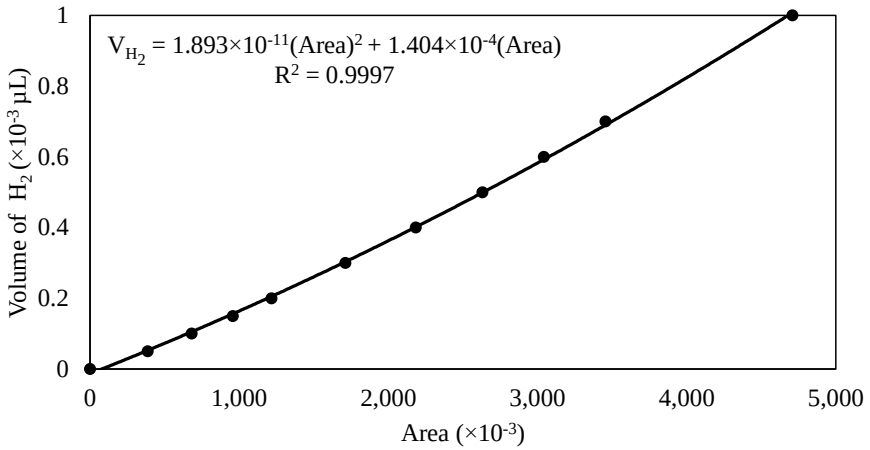

Figure B.2. GC1 calibration curve for H_2

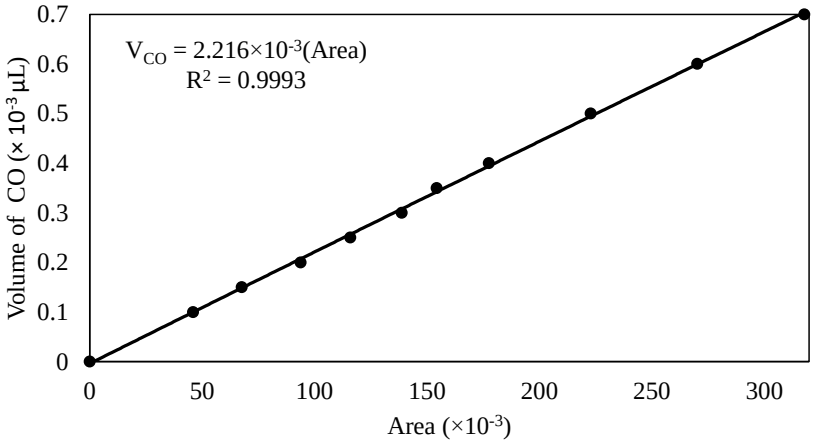

Figure B.3. GC1 calibration curve for CO

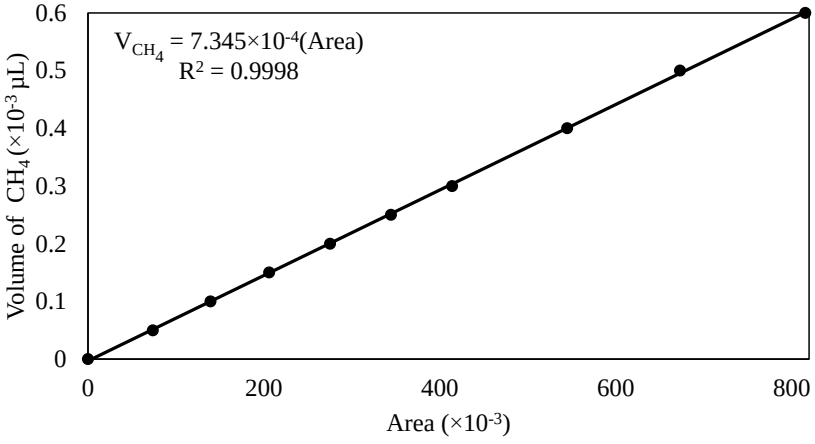

Figure B.4. GC1 calibration curve for CH_4

B.2. Calibration Curves for Agilent GC-6850

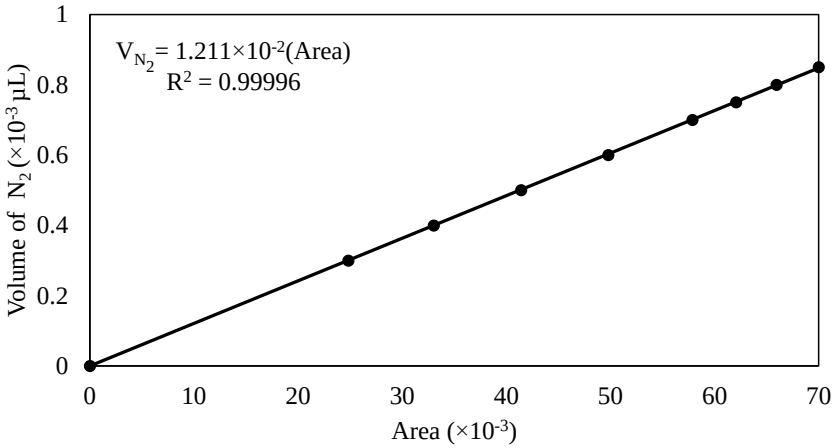

Figure B.5. GC2 calibration curve for N_2

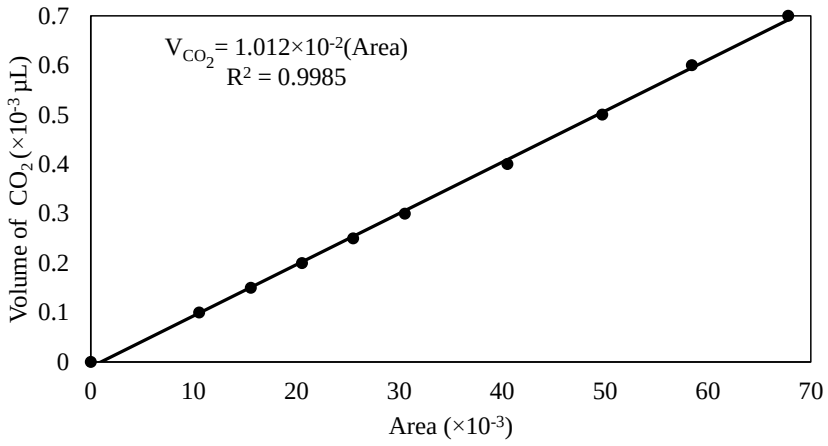

Figure B.6. GC2 calibration curve for CO_2

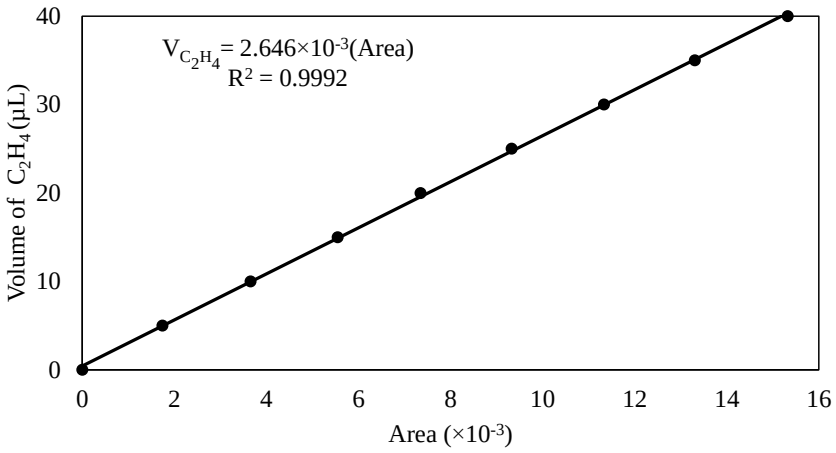

Figure B.7. GC2 calibration curve for C_2H_4

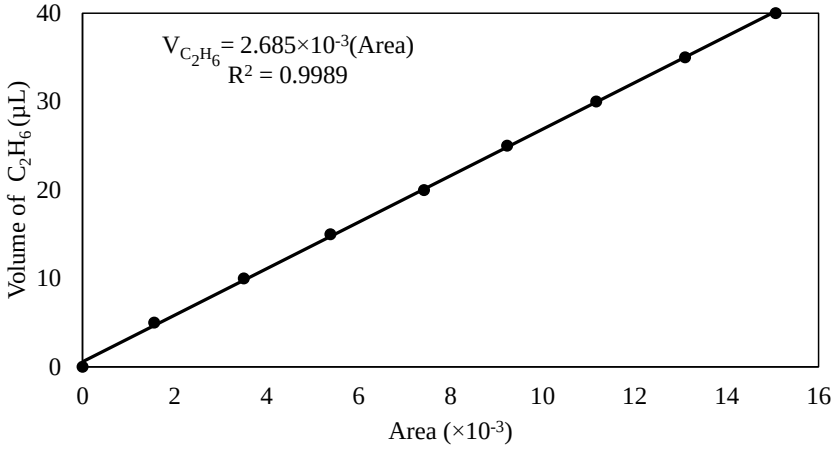

Figure B.8. GC2 calibration curve for C_2H_6